Modeling the Dynamics and Depositional Patterns of Sandy Rivers

by

Douglas J. Jerolmack

B.S., Environmental Engineering, Drexel University, 2001

Submitted to the Department of Earth, Atmospheric and Planetary Sciences, in partial fulfillment of the requirements for the degree of

Doctor of Philosophy

at the

MASSACHUSETTS INSTITUTE OF TECHNOLOGY

June 2006

Author.....
Geophysics, Department of Earth, Atmospheric and Planetary Sciences
May 26, 2006

Certified by.....
David Mohrig
Associate Professor of Geology
Thesis Supervisor

Accepted by.....
Maria T. Zuber
E.A. Griswold Professor of Geophysics
Head of the Department of Earth, Atmospheric and Planetary Sciences

Modeling the Dynamics and Depositional Patterns of Sandy Rivers

by

Douglas J. Jerolmack

Submitted to the Department of Earth, Atmospheric and Planetary Sciences on April 24, 2006, in partial fulfillment of the requirements for the degree of

Doctor of Philosophy

Abstract

This thesis seeks to advance our understanding of the dynamic nature, spatial organization and depositional record of topography in sand-bedded rivers. I examine patterns and processes over a wide range of scales, on Earth and Mars. At the smallest scale, ripples and dunes (bedforms) arise spontaneously under most natural flow conditions, acting as the primary agents of sediment transport and flow resistance in sandy rivers. I use physical modeling in a laboratory flume to explore the feedbacks among bedform geometry, fluid flow and sediment transport. Field observations of dunes in the North Loup River, Nebraska, show that bed roughness displays a statistical steady state and robust scaling. Motivated by these data, I develop a nonlinear stochastic surface evolution model for the topography of sandy rivers which captures the essence of bedform evolution in space and time. I then use a simplified kinematic model for bedform evolution to simulate the production of stratigraphy from migrating dunes, allowing a more accurate reconstruction of river flow conditions from preserved bedform remnants in rocks. At the channel scale I examine the conditions that lead to avulsion, the rapid abandonment of a river channel in favor of a new course at lower elevation. Simple scaling arguments and data from 30 natural systems reveal that anastomosing (multi-branch) rivers and distributary deltas are morphologies that arise when avulsion is the dominant mechanism of channel adjustment. I apply these arguments to the Niobrara River, Nebraska, which has experienced rapid in-channel deposition due to base level rise. I show that the planform pattern of the Niobrara is dominated by base-level-driven avulsions, and is decoupled from the smaller-scale sediment transport. At the largest considered scale are depositional fans, which are constructed by avulsing rivers. The evolution of a fan profile may be modeled at long time- and space-averaged scales as a diffusive process. I use such a model to invert topographic and volumetric data from a fluvial fan on Mars, producing an estimate of the time required to build the fan out of channel and overbank deposits.

Thesis Supervisor: Dr. David Mohrig
Title: Associate Professor

Matrix of Acknowledgement. Displays people and places that have contributed somehow to my happiness and modest success, along with their attributes. Attribute categories are ill-defined and arbitrary – some people may have contributed qualities not included on this list. This list is by no means complete, but simply represents people and places present in the author's mind at the time of writing.

	Mentoring	Friendship	Groovin'	Gurgling Cod	Wardrobe	Best Advisor Ever	Coffee (time)	Technical help	Mental help	Patience	Home	Escape from Boston	Best girl ever
Mom	X	X			X					X			
Dad	X	X								X			
Colin Jerolmack		X			X		X		X			X	
Ian Jerolmack		X			X		X		X			X	
Grandparents		X							X			X	
David Mohrig	X	X	X		X	X	X	X	X	X			
Chris Paola	X							X					
Dan Rothman	X							X					
Kelin Whipple	X							X					
Maria Zuber	X							X					
John Grotzinger	X		X					X					
Kyle Straub		X	X					X					
Joel Johnson		X						X					
Wes Watters		X						X					
Brandon McElroy		X						X		X			
Chiu-Mi Lai		X			X				X				
Roberta Bennett-Calorio		X			X				X	X			
Felix Ng		X						X	X				
Homero Flores		X							X				
Roberta Allard		X		X	X				X				
Claire Welty	X							X		X			
Aaron Packman	X							X		X			
Ben Crosby (and family)		X							X				
Laurent Husson		X					X						
New York Crew		X					X					X	
Nessy		X			X				X	X		X	X
Philadelphia											X	X	
The entire 8th floor	X	X						X	X	X			
The entire 9th floor		X							X	X			

Contents

List of Figures

List of Tables

The evidence

Judgement, condemnation
Trial and tribulation
Locks and keys and one way streets
Schedules and game plans
Mouth to mouth and hand to hand

These systematic disciplines
Of expressing understanding
Are all that were offered me

Here are my findings
This is the evidence
This song bears witness
To the total science
Hard to soft or soft to gone

If you're outside the lingo
If you're outside the jargon
You talk beyond a system
You're talking out of turn

I've got my calculus
I've got my calipers
I've got my scopic monitor
I've got my own
I've gone figuring
I've gone deciphering
I've gone recording and reporting

The covered tracks
Of an invisible regime
Perhaps they tell me
What to sing

-Daniel Higgs

Chapter 1

Introduction

Rivers in depositional environments create their own bed and bank geometry through the interaction of fluid flow, surface topography and sediment transport. The complex feedbacks at the interface of fluid and sediment produce a bewildering array of patterns, from ripples at the centimeter scale to alluvial fans and deltas at a basin scale. Advancing our understanding of the temporal and spatial evolution of these patterns, and the traces they leave behind in the sedimentary record, is the motivation behind this thesis. In order to sensibly relate patterns to the processes that generate them, models are required.

Scaled-down physical models of natural systems allow isolation of variables in a well-controlled environment, and are employed here to build intuition about the evolution of sandy river bottoms. Mathematical models can range from simple, exploratory numerical experiments to detailed simulations that attempt to incorporate physics at the smallest possible scales (Murray, 2003). In this thesis I develop the use of simple models to elucidate the minimum number of ingredients that are required to explain physical phenomena. Mathematical and kinematic models are also employed to explore the connection between migrating surface topography and depositional patterns preserved in rock. A conceptual model and scaling analysis are used to better understand the conditions leading to the existence of multiple channels in depositional rivers.

To focus on the relationships between scale and process in depositional river systems, it is useful to consider a specific example (Fig. 1.1). At the largest scale considered in this thesis are river deltas, which are constructed through deposition by river channels undergoing continuous avulsion – the rapid abandonment of a channel in favor of a new path at lower elevation – over geologic time. At long time and space scales the stochastic nature of avulsing channels averages out such that fan evolution may be modeled as a deterministic, diffusive process (Parker et al., 1998). The Mississippi River delta evolved over the Holocene primarily in response to sea level rise (Aslan and Autin, 1999), and to first order its form and size have been determined principally by boundary conditions. At the intermediate time and space scales of channel planform pattern, the multiple active distributaries of the lower Mississippi erode laterally by bank erosion and avulse due to in-channel deposition. Patterns at this scale are determined by both the mean and fluctuating magnitudes of fluid and sediment discharge, and by boundary conditions such as changing sea level. Sediment in the lower Mississippi channels moves in large sand dunes, representing the smallest-scale pattern of interest. These dunes respond quickly to changes in fluid and sediment transport conditions. Two important questions arising from this example are: (1) which physical processes are most important in determining pattern at a certain scale?; and (2) how are patterns at one scale coupled (or not) to patterns at larger and smaller scales? This thesis seeks to provide at least a partial answer to these questions.

Ripples and dunes (collectively bedforms) arise spontaneously under most sediment transport conditions, representing a fundamental instability at the sediment-fluid interface. These bedforms determine the flow resistance in sandy rivers because they are

the principle roughness elements on the bed. The manner in which bedforms adjust in space and in time determines, to a large extent, the cross-sectional geometry of a sand-bedded channel, because bottom roughness adjusts much more rapidly than channel width. Further, bedform deposits preserved in rock are one of the most common features used to reconstruct flow conditions associated with ancient channels. Chapters 2 through 4 explore these topics. In Chapter 2 I present results from the laboratory showing how subtle changes in bedform geometry can have a strong influence on fluid turbulence, which in turn affects local sediment transport rates. Existing models for bedform evolution do not capture the strong coupling between bedform shape and sediment transport observed in these experiments.

Chapter 3 examines the evolution of bedforms in the braided North Loup River, Nebraska. High resolution topography maps generated from low-altitude aerial photography allow quantification of the time- and space-varying nature of bottom roughness. These data, combined with previously published results in the literature, show that bottom roughness exhibits a statistical steady state with robust spatial and temporal scaling, despite the fact that individual bedforms continually change their shape. The self-organizing nature of bedform evolution suggests that the details of fluid flow may not be important for a first-order description of the bed dynamics. By parameterizing the sediment flux over bedforms in terms of the local elevation and slope of the bed itself, I derive a nonlinear stochastic surface evolution model that quantitatively reproduces the observed scaling and dynamical behavior characteristic of natural sandy bedforms.

Sediment scouring and deposition by migrating bedforms produce sets of partially preserved bedforms that may be preserved in rock, recording the dynamical behavior of the

sediment-fluid interface. Existing models relating stratigraphy to formative bedform geometry assume that trains of bedforms do not change their shape or migration speed through time (Bridge and Best, 1997; Leclair, 2002). In Chapter 4 I use a kinematic model of bedform evolution to explore how the time- and space-varying nature of bedform migration imparts a signature on the stratigraphy. Results from the model compare well to distributions of preserved beds measured from two outcrops. I present new relationships between stratigraphic bed thickness and formative bedform geometry that allow more accurate estimation of river flows that formed ancient channel deposits.

In Chapter 5 I move to a larger scale, that of planform pattern in depositional rivers, to examine the importance of river avulsion in determining channel pattern. A compilation of field and laboratory data demonstrates that avulsion frequency is determined by the time required for a river to deposit one channel-depth above the floodplain – this result confirms and extends the findings of Mohrig et al. (2000), who found a similar condition for river avulsions in a study of ancient channel deposits. A simple scaling analysis of characteristic process times demonstrates that anastomosing (multiple channel belts) rivers and distributary channels on deltas are morphologies that arise when avulsion is the dominant mechanism of channel adjustment. Chapter 6 examines the relationships among channel planform pattern, changing boundary conditions and small-scale sediment transport. Rapid in-channel deposition has been driven by base-level rise in the lower Niobrara River, Nebraska, and has led to avulsions and channel pattern change. Despite large spatial variations in planform geometry, data from the field show that sediment flux and bed stress are the same in almost all river reaches. Results indicate that the river is dynamically adjusted by sediment continuity so that planform

geometry has little effect on the routing of flow and sediment through the river. I use the scaling arguments from Chapter 5, along with field and historical observations of the Niobrara River, to develop a conceptual model for the formation and maintenance of bifurcations by avulsions.

Finally, in Chapter 7 I change scale and scope, moving to the interpretation of a depositional fan on the surface of Mars. With few exceptions, putative fluvial features identified on Mars have been erosional in nature. The recent discovery of a large fan deposit (Malin and Edgett, 2003) has, therefore, significant implications for both the history of flowing water in the region, and the persistence of liquid water on early Mars (Moore et al., 2003). Previous authors argued that the presence of this fluvial fan was evidence for stable liquid water over thousands of years or longer (Malin and Edgett, 2003; Moore et al., 2003). I adapt a terrestrial model for riverine fan construction from avulsing channels (Parker et al., 1998) to Martian conditions, and use it to invert topographic and volumetric data from the Martian surface. This allows an estimate of the minimum formation time and water discharge needed for fan construction. My results show that the entire deposit could have formed in less than a century, and therefore it does not necessarily provide evidence for persistent liquid water over long periods of time.

A wide variety of problems and scales are explored in this thesis, with an equally diverse set of methods. The two uniting themes are channels, which act as the conduits of fluid and sediment from eroding landscapes to depositional basins, and models, which guide interpretation of physical data, test hypotheses and build intuition. The evolution of complex spatial patterns at the sediment-fluid interface is an alluring problem in its own right, but takes on special significance because this interface is the template for human and

ecological communities. In this thesis I strive to convey my enthusiasm for basic research in these fundamental problems, while outlining the implications of my results for river management, prediction of river evolution, and climate interpretation.

References

Aslan, A., and Autin, W.I., 1999, Evolution of the Holocene Mississippi River floodplain, Ferriday, Louisiana: Insights on the origin of the fine-grained floodplains: *J. Sedimentary Res.*, *69*, 800-815.

Bridge, J., and Best, J., 1997, Preservation of planar laminae due to migration of low-relief bed waves over aggrading upper-stage plane beds: Comparison of experimental data with theory: *Sedimentology*, *44*, 253–262.

Leclair, S.F., 2002, Preservation of cross-strata due to the migration of subaqueous dunes: An experimental investigation: *Sedimentology*, *49*, 1157–1180.

Malin, M.C. and K.S., Edgett, 2003, Evidence for persistent flow and aqueous sedimentation on early Mars: *Science*, *302*, 1931-1934.

Mohrig, D., Heller, P.L., Paola, C., and Lyons, W.J., 2000, Interpreting avulsion process from ancient alluvial sequences: Guadalope-Matarranya system (northern Spain) and Wasatch Formation (western Colorado): *GSA Bulletin*, *112*, 1787-1803.

Moore, J.M., A.D. Howard, W.E. Dietrich., and P.M. Schenk, 2003, Martian layered fluvial deposits: Implications for Noachian Climate Scenarios: *Geophys. Res. Lett.*, *30*(24), 2292, doi:10.1029/2003GL019002.

Murray, A.B., 2003, Contrasting the goals, strategies, and predictions associated with simplified numerical models and detailed simulations. In: Wilcock, P.R., and Iverson, R.M., *Prediction in Geomorphology*: Geophysical Monograph 135. American Geophysical Union, 151-168.

Parker, G., C. Paola, K.X. Whipple, and D. Mohrig, 1998, Alluvial fans formed by channelized fluvial and sheet flow. I: Theory: *J. Hydraul. Eng.*, *124*(10), 985-995.

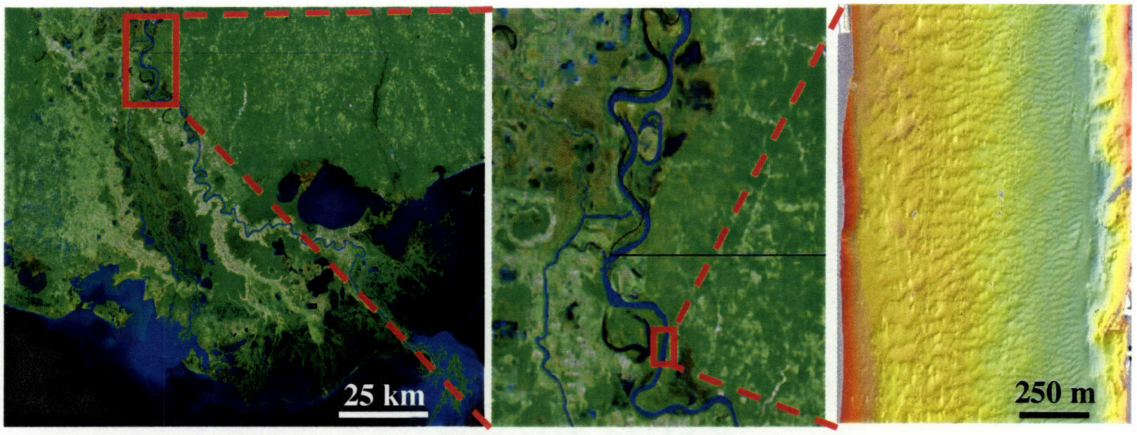

Figure 1.1. (Color) Prevalent patterns on the lower Mississippi River at various spatial scales considered in this thesis. At left is the delta, while center shows the bifurcation of the Mississippi (right channel) at the Atchafalaya River (left channel) – both images are from http://visibleearth.nasa.gov. Right is a bathymetric map of the Mississippi River bottom at New Orleans, from http://weather.lumcon.edu/weatherdata/audubon/map.html.

Chapter 2

Interactions between bedforms: Topography, turbulence and transport[1]

D.J. Jerolmack and D. Mohrig

Department of Earth, Atmospheric and Planetary Sciences, Massachusetts Institute of Technology, Cambridge, Massachusetts 02139, USA

Abstract

Results are presented examining the interaction between two sandy bedforms under low sediment transport conditions in a small laboratory flume. The initial artificially-made bedforms were out of equilibrium with the flow field. Temporal evolution of bedforms was monitored using time-lapse photography in order characterize bedform adjustment to the imposed flow. Velocity measurements were collected using an Acoustic Doppler Velocimeter to characterize both mean flow and turbulence associated with different bedform geometries. Sandy bedforms all had identical initial geometries, however the initial distance between bedform crests was varied between experiments. Overall deformation of the bed varied as a function of initial bedform spacing, however bedforms evolved unpredictably as periods of relatively slow change were punctuated by periods of rapidly changing geometry. Subtle changes in bedform trough geometry were found to

[1] From Jerolmack, D., and D. Mohrig, Interactions between bed forms: Topography, turbulence, and transport, *J. Geophys. Res.*, *110*, F02014, doi:10.1029/2004JF000126, 2005.

have a strong influence on turbulence, and therefore sediment transport. Comparison with field studies suggests the mechanisms described herein are active in natural systems.

2.1. Introduction

As techniques improve for collecting topographic data at higher temporal and spatial resolutions, evidence is mounting for the persistence of locally variable topography and sediment fluxes under steady or slowly varying hydraulic conditions. For example, a recent laboratory study of dunes by Leclair (2002) documented continuously adjusting geometries for individual bedforms and continuously adjusting rates of migration even after the system had been allowed to interact with a constant hydraulic forcing for as long as 24 hours. The exhaustive field study on bedforms of the River Rhine by Carling et al. (2000a, b) produced a comparable result. Measured bedform topography there could not be linked to river stage in a simple way. Laboratory data by Ditchfield and Best (1992) have shown that migration rate for individual bedforms can depart significantly from values predicted using the channel-averaged measurement of sediment flux. These results and others (e.g. river studies by van den Berg (1987), Mohrig (1994), Harbor (1998) and Prent and Hickin (2001)) lead us to conclude that persistent variability in geometry and migration rates are not the exception, but are in fact the hallmark of natural bedforms developing under and interacting with unidirectional shear flows.

Bedforms are created and modified by variations in the sediment flux. Their presence induces flow accelerations, which, in turn, modulate the sediment flux (Nelson et al., 1993). Fortunately, careful work on pieces of these interactions provides a framework for understanding the feedbacks. Particularly useful are the detailed

measurements defining spatial heterogeneity in the flow field over static two-dimensional (Engel, 1981; Wiberg and Nelson, 1992; Nelson et al., 1993; McLean et al., 1994) and three-dimensional (Maddux et al., 2003a, b) bedforms in the laboratory, and over quasi-static dunes in large rivers (Kostaschuk, 2000). Laboratory measurements have mapped out the zones of turbulence production and dissipation over bedforms, and have defined the associated variability in turbulence intensities. These measurements provide critical information as to why natural topography continuously evolves even under steady flow conditions: local values of turbulence intensity are sensitive to local accelerations in the flow and these accelerations are sensitive to local slopes of the bedform surface. In addition, local rates of bedload transport have been shown to be sensitive to high velocity bursts (Schmeeckle and Nelson, 2003; Best et al., 1997). Taken together, these conditions are the ingredients of a recipe for topographic evolutions that are extremely sensitive to boundary conditions. The geometries of an individual bedform will always be evolving in response to its previous form, as well as in response to the structure of the surrounding bed.

Several simple numerical models of subaqueous (e.g. Tufillaro, 1993; Niño et al., 2002) and subaerial (e.g. Prigozhin, 1999; Csahók et al., 2000) bedforms have succeeded in capturing aspects of bedform development from an initially flat surface, such as amplitude growth and merging of bedforms, however in these formulations bedform evolution is governed by irreversible merger of individual topographic elements (see also Werner and Gillespie, 1993) such that bedform wavelength can only increase it time. Werner and Kocurek (1999) suggested the spacing of bedforms is controlled by the dynamics of defects (crestline terminations), however the creation and annihilation of

defects is a natural consequence of spatial variation in sediment flux, which was not considered in their model. Although recent numerical (Hersen et al., 2004) and experimental (Endo et al., 2004) work suggests that individual barchan dunes are dynamically unstable, we are far from understanding the source of bedform instability and its contribution to the maintenance of trains of bedforms.

The goal of the experiments reported here was to examine how bedforms interact when forced to adjust to an imposed flow field, and to describe the interaction among spatially varying flow and sediment transport and changes in bedform geometry.

The geometric variability of bedforms themselves confounds the proper choice of length and time scales for use in generating accurate descriptions of bed evolution. To minimize these complications, we have run a set of experiments using very simple initial geometries. Bedforms were artificially created that were out of equilibrium with the flow field. The importance of small-scale interactions between bedforms was brought to the fore in these 'extreme conditions'. The bed geometries have allowed us to unambiguously identify the influences of one bedform on another. Results presented here summarize the control of initial spacing between two sandy bedforms on subsequent bed evolution in a two-dimensional channel. To do this the bedform spacing was systematically varied while all other parameters were held constant. Adjustments of individual bedforms directly affected many aspects of the bed configuration, highlighting the need to collect both high-resolution spatial and temporal data when characterizing river bottom topography. Periods of rapid local deformation for individual bedforms are connected to subtle changes in local topography, and to the changes in turbulence intensities and sediment transport that they produced.

Throughout this paper, 'bed configuration' and 'bed profile' will be used interchangeably to refer to the entire channel bottom topography, while' bedform' always refers to an individual topographic element, as defined in the Methods section below.

2.2. Methods

2.2.1. Experimental Setup

The initial size and shape for all bedforms was held constant in our experiments. The height and length of each was 0.070 m and 0.395 m, respectively. Each bedform had no topographic variation in the cross-stream direction. The stoss side of each form was inclined at 13° from the horizontal, while inclination of the lee side was 35°. These bedforms were constructed out of two very different materials; aluminum plate and sand. Bedforms made from bent aluminum plate produced a fixed bed, necessary for sampling the velocity structure of the flow field. The aluminum forms also served as the moulds for generating the sandy bedforms. In these cases the channel was first filled with water and then water-saturated-sand was pressed into forms of the equivalent shape and size using the moulds. These experiments were carried out with bedforms constructed from two different sands having median particle diameters of 350 μm and 770 μm, respectively (Table 2.1).

Experiments were conducted in the middle third of a straight flume, 10 m long, 0.16 m wide and 0.25 m deep, with zero slope. The flume recirculated both water and sediment and a valve on the flume return line controlled discharges through the test channel. The narrow width of the flume may have influenced bed evolution, but no attempt has been made to quantify this effect. Four different configurations of the bed

were studied in the test section (Fig. 2.1). In the first case (Fig. 2.1a) a single bedform was placed in the upstream position of the test reach. Results from this single-form case served as a baseline for comparison to the other configurations. A single bedform composed of medium and then coarse sand was used to set the water discharges applied to all of the other runs. Specifically, water discharges were adjusted until transport conditions were slightly above thresholds of initial particle motion for the two sands. The vertically averaged flow velocities associated with this transport stage are listed in Table 2.2. Under these conditions there was almost no translation and/or deformation of the single sandy bedform. Experimental runs having the same discharge, but with two bedforms in the channel, experienced different kinematic behaviors that are reported below.

Three different bedform spacings were used (Fig. 2.1, Table 2.2). These were selected based on velocity measurements collected over a single rigid form in the channel. These measurements characterized the structure of the flow field downstream of an obstruction (i.e., zones 1, 2 and 3 of Fig. 2.1). In the first case two bedforms were positioned end to end, producing a configuration where part of the downstream form (Bedform 2) was situated within the recirculation eddy that developed because of flow separation at the crest of Bedform 1 (Fig. 2.1b). In the second case the bedforms were sufficiently separated such that all of Bedform 2 resided downstream from the point of flow reattachment (Fig. 2.1c). For the final configuration the two forms were placed such that Bedform 2 lay outside of the detectable range of disturbance of the flow field produced by a single upstream bedform (Fig. 2.1d), as determined by measured mean and

turbulent fluid velocity statistics. Our goal was to place the downstream bedform in three very different flow regimes using the three chosen spacings.

2.2.2. Measurement of sandy bedforms

The kinematic histories for the experimental bedforms were recorded using a digital camera taking pictures through a clear plexiglass sidewall. These photographs were taken every 120 s for approximately 3 hours. Selected photographs were digitized using ImageJ, a public domain image processing and analysis program developed at the National Institutes of Health. Resulting digital images were then used to quantify both the translation and deformation of individual bedforms by measuring changes in height, H, length, L, cross-sectional area, A, and downstream position. The migration rate or celerity, c, of individual bedforms was calculated by measuring streamwise changes in the positions of bedform crests over short time intervals. Definitions for all of these properties are shown in Figure 2.2. Measurement precision was limited by the resolution of our photographs. Changes in bed elevation of $<5\times10^{-3}$m could not be resolved. In addition, our method of data collection did not capture cross-stream variability in topography and migration rate. Such variability occurred in cases with medium-sand bedforms (Tables 2.1 and 2.2), but was nearly absent in the coarse-sand runs. Visual inspection of all bedforms led us to conclude that behaviors measured in cross-section near the sidewall were representative of the overall kinematics despite some cross-stream variability associated with bedforms made of medium sand.

The evolving topography in our experiments included the emergence and destruction of individual bedforms. Acknowledging that any definition of first

appearance or disappearance of a discrete bedform is somewhat arbitrary, we decided on the following criteria: 1) the obtuse angle, θ, between the lee face of a new form and the adjacent downstream surface must be less than 150°; and 2) the height of a new form must be >⅓ the height of the bedform from which it developed (Fig. 2.2). This definition separated bedforms from swales and hummocks, and separated smaller-scale superimposed topography from primary bedforms themselves. The smaller topographic elements, including ripples on the stoss sides of bedforms, were not considered separate entities (Fig. 2.2) and were treated as simply contributing to the massiveness of the bedforms on which they resided. With this definition we mapped temporal change in bedform size, shape and number. In each trial run, values of H, L, H/L, A, and c were collected for all bedforms as a function of time. Average values for these parameters were then calculated in two different ways. A system average was calculated at each time step using all of the data from the run, and local averages were determined using only those measurements from bedforms sharing a common original parent (Bedform 1 or Bedform 2, Fig. 2.1). These local measurements allowed us to evaluate how bedform kinematics varied as a function of position in the system. Statistics describing the deformation of individual bedforms as well as the overall evolution of the bed configuration were compiled for each trial, allowing us to assess the relative importance of initial bedform spacing, s, on developing local topography.

At the beginning of each trial the only sand within the channel was that making up the bedforms. The channel floor both upstream and downstream from the bedforms consisted of smooth plexiglass. This immobile surface was also exposed between bedforms in those cases where the spacing, s, was greater than the bedform length, L

(Fig. 2.1c-d). We limited the amount of sand in the system in an attempt to isolate and highlight the interactions between two original bedforms. In cases with only a single bedform made from medium sand (case 6a) and two forms separated by 1.40 m (case 6d), only one run was used to characterize bed evolution. However, in order to assess reproducibility and sensitivity to boundary conditions, three runs were conducted for each of the highly variable scenarios of s = 0.40 m (case 6b) and s = 0.67 m (case 6c). Only these two configurations of the bed were rerun using the coarse sand; cases 7b and 7c, respectively (Fig. 2.1, Table 2.1 & 2.2). Successive profiles of the bed for selected runs using medium sand are shown in Figure 2.3.

Changes in bed topography during the first 1920 s of every trial were used to estimate local values for the streamwise sediment discharge, q_s. These values were calculated using the following equation

$$q_s = \Delta a(1 - k)/\Delta t \qquad (1)$$

where Δa is newly created bedform area (Fig. 2.4), k is porosity, and Δt is the time interval over which the new area was created. Equation 1 was used to estimate the streamwise sediment flux at three locations in the system: 1) the stoss side of Bedform 1; 2) the stoss side of Bedform 2; and, when appropriate, 3) the trough separating Bedform 1 from Bedform 2 (Fig. 2.4). This calculation assumes that no grains bypassed the bedforms completely (i.e. suspension was negligible) in the study region. Values of q_s for trough filling are negative, representing the upstream transport of sediment associated with the recirculation eddy that developed behind Bedform 1 (Fig. 2.1). Trough-filling

values of q_s were only measured for cases where an immediate source of sediment was available for trough filling, i.e. the stoss side of Bedform 2 (cases 6b and 7b, Table 2.2). Sediment flux calculations were not performed using data from the last 2.5 hours of each run because the splitting and merging of bedforms made it difficult to integrate Δa over intervals of time sufficient in duration to produce representative measures of sediment discharge.

2.2.3. Measurement of flow field

All velocity measurements were collected using a Sontek Acoustic Doppler Velocimeter (micro-Lab ADV) running at a sampling frequency of 10 Hz. The sampling volume for this device was small, 10^{-6} m^3, so the flow fields for specific runs were characterized by measuring successive vertical profiles in the streamwise direction down the centerline of the channel. These flow field data were only collected over rigid bedforms to ensure steady topography, as the ADV probe locally perturbed sandy bed topography. In order to determine the range of disturbance due to the presence of a single rigid bedform, the downstream flow field (Fig. 2.1a) was measured at 0.01 m, 0.03 m and 0.06 m above the bed, and every 0.05 m in the streamwise direction. The mean velocity data showed that the reattachment point for the separated flow was located at 0.28 m or $4H$ downstream from the bedform crest and that a measurable momentum deficit associated with the bedform wake had fully dissipated by a distance of 1.05 m or $15H$ downstream from the crest (Fig. 2.1a). These data were used for selection of bedform spacing, s, of sandy bedforms (Fig. 2.1).

Denser sets of measurements were collected over bed configurations defining cases 6b and 7b (Fig. 2.1b). This denser grid of data was used to resolve the effects of small changes in bed topography, particularly trough shape, on flow-field structure. Velocity profiles were assembled using measurements collected at several elevations, z, above the bed; at 0.005 m, and 0.01 m increments from 0.01 m to 0.07 m above the bed. The separation between adjacent profiles was 0.03 m in the streamwise (x) direction.

Velocity at each point was sampled for 15 s based on two lines of reasoning. First, the raw velocity data collected with the ADV can be deconvolved into three potential signals; mean, periodic and deviatoric variations (Lyn et al., 1995). For these experiments we were particularly interested in comparing the mean and deviatoric velocities between cases, so we needed to ensure that sinusoidal variations in velocity associated with the shedding of vortices at the crests of bedforms were not biasing our measurements. This was accomplished by making the sampling interval at each grid point longer than the characteristic period for vortex shedding. The duration of this period was determined by two methods. In one case the non-dimensional Strouhal number, St, was used to estimate the characteristic frequency of vortex shedding. This parameter is

$$St = fD/V \tag{2}$$

where f is the characteristic frequency, D is the characteristic length and V is the characteristic velocity. Reported values of St for round and square cylinders at the appropriate Reynolds numbers (Table 2.2) are 0.2 (Allen, 1968) and 0.13 (Lyn et al.,

1995; Kolár et al., 1997), respectively. Both cylinder geometries are considered here because they bracket the possible range of angularities associated with bedform crests. Using eq. (2) a characteristic period, $1/f$, for the round and square cylinder was found by setting D equal to the original bedform height of 0.07 m and V equal to a characteristic flow velocity of 0.29 m/s (Table 2.2). The respective periods of 1.2 s and 1.9 s are small relative to the 15 s sampling window used at each point.

Second, spectral analyses of several 120 s time series did not reveal any dominant frequency, suggesting that the actual period of vortex shedding was in fact shorter than estimated values from eq. (2) and not resolvable with our experimental setup. That is, a sampling interval of 120 s detected no longer-term oscillatory component to the flow field and produced nearly identical velocity statistics compared to a 15 s sampling interval.

Mean values for the streamwise, u, and vertical, w, components of the velocity field were determined at each grid point by averaging over each 15 s sample and are denoted by $\overline{u}$ and $\overline{w}$, respectively. Deviatoric velocities associated with the streamwise and vertical components of the flow field are $u'(t) = \left(\overline{u} - u\right)$ and $w'(t) = \left(\overline{w} - w\right)$, respectively. Turbulence at any point in the flow is represented by the root mean square (RMS) of the instantaneous streamwise (RMS(u)) and vertical (RMS(w)) velocities, respectively, over the measured time interval.

2.3. Experimental Results

2.3.1. Change in mean bed topography

The only trend common to all runs was a reduction in mean height, the magnitude of which was similar for all runs but one (Fig. 2.5). The outlier was case 6a, the only run with an original topography consisting of a single bedform. Change in mean height with time was not sensitive to the grain size of the original bedforms. Bedforms composed of coarse sand (cases 7b and 7c, Fig. 2.5g) showed both the same rate of change and total height reduction as observed for all cases of two medium sand bedforms (Fig. 2.5a, 2.5d, and 2.5g).

The values for mean length either increased or decreased with time (Fig. 2.5b, 2.5e, and 2.5h) depending on the degree to which bedform splitting occurred during a run. The average reduction in mean length for cases 6b1, 6b3, 6c1, 6c2, and 6c3 (Fig. 2.5b and 2.5e) was 44%. Nearly the opposite change in mean length was observed for those cases where bedform number remained the same, in which case bedform length increased by an average of 40% from start to finish. Unlike mean height, temporal change in mean length was affected by the grain composition of the bed. All three trials with an intermediate spacing between original bedforms composed of medium sand (case 6c) experienced a substantial increase in bedform number and the correlative reduction in mean length. This trend was not observed during the trial using coarse sand and the same original bed configuration (case 7c, Fig. 2.5h and 2.5i). Almost no bedform splitting occurred in case 7c and mean length systematically increased through time. No splitting was observed for the coarse sand bedforms comprising case 7b (Fig. 2.5i); the increase in

grain size evidently suppressed bedform splitting during our runs at these low transport conditions, as discussed below.

The mean steepness (H/L) of bed topography decreased from the start to finish of each run by an amount that depended on the history of bedform splitting and length reduction. During the first ten minutes of runs 6c1, 6c2 and 6c3 the mean steepness decreased from an initial value of 0.17 to an average value of 0.14. Bedform splitting arrested this rapid drop in the overall steepness so that by the end of these three runs its average value was 0.13 (Fig. 2.5f). Little change in steepness occurred over the rest of these runs because the smaller lengths associated with splitting offset the reductions to mean bedform height. In cases where no bedform splitting occurred, the mean steepness continued to drop throughout the runs. The special case of a single original bedform (case 6a) experienced a reduction in steepness from 0.16 to 0.13.

Bedform splitting and merging are reflected in plots of bedform number (Fig. 2.5c, 2.5f, and 2.5i). Figure 2.5c and 2.5f are particularly relevant to any consideration of the variability inherent to the bedform interface. Each figure summarizes the results of three runs having the same initial and boundary conditions and the plots of number versus time show significant differences.

2.3.2 Variability in bedform evolution

2.3.2.a. Temporal variability in bedform activity

Figures 2.3b and 2.3c illustrate increments of time associated with relatively rapid bed developments that are separated by intervals of relative stagnation (e.g., 80-100 minutes, Fig. 2.3b: 90-110 minutes, Fig. 2.3c). In these two series, as in all of the other

experimental runs, intervals of rapid bed evolution are correlated with the splitting of pre-existing bedforms. Splitting generally occurred by a process where the very front of a bedform detached from the parent bedform. The detached element typically moved forward as a new bedform while a new crestline developed near the site of the breakaway, increasing the overall number of bedforms in the system. Bedforms that emerged through the splitting process shared a height similar to that of their parent form, but a shorter length, making them steeper. Bedform celerity through time was also found to be variable. Low rates of migration were punctuated by intervals with higher rates of bedform translation (Fig. 2.6).

2.3.2.b. Local and spatial variability in bedform celerity

Measurements of celerity document three main characteristics for the bedforms in our experiments: 1) celerities of individual bedforms are independent of bedform height (Fig. 2.7); 2) celerities are variable; and 3) higher rates of bedform migration are associated with the downstream position in the channel. Individual values for celerity (Fig. 2.7) have been assembled to generate histograms for Bedform 1 and Bedform 2 (Fig. 2.8, Table 2.3). Differences between the two histograms for any particular case quantify variation with streamwise position. All histograms of celerity in Figure 2.8 are positively skewed, and the average value for the coefficient of variation (standard deviation/mean) is greater than one. Some histograms possess negative values of celerity, which arise because any section of crestline is capable of moving backwards for a short interval of time in response to minor, cross-stream variability in the transport system.

Histograms (Fig. 2.8) illustrate the influence of the original spacing between bedforms on their subsequent celerities. Measurements of celerity collected from the widely spaced bedforms in case 6d (Fig. 2.8c) showed essentially no change between the upstream and downstream positions. Indeed, from the value of the Chi-squared parameter calculated from these two histograms we cannot reject the null hypothesis that they are indistinguishable from one another. In contrast, the histograms in Figure 2.8a and 8b are statistically different at the 5% confidence level. Significantly higher and more variable values of celerity were recorded in the downstream position. The closely and intermediately spaced bedforms of cases 6b and 6c lead to an overall increase in celerity from the upstream to downstream location. Maximum values of celerity in the closely and intermediately spaced configurations were always greater than those observed in the case with widely spaced bedforms.

2.3.2.c. Spatial variability in sediment transport rate

Time-averaged values for the sediment transport (eq. 1) associated with various configurations of Bedform 1 and Bedform 2 define further the range in transport associated with the variable bed topography (Fig. 2.9). Bed deformation and sediment transport was minimal in the case of a single bedform (case 6a). The presence of two bedforms in the system increased sediment transport even though there was no change in water discharge between all trials using the medium sand (Fig. 2.9). Previously described measurements of the flow field suggested that the two bedforms in case 6d (Fig. 2.1d) were placed far enough so that interaction between them might be negligible. This clearly was not the case. Water surface slope increased from 6×10^{-4} for case 6a, to 1×10^{-3} for the case 6d, which would cause an increase in spatially averaged bed stress, and

likely caused increased sediment flux. Another cause could be a change in the structure of the flow field at a resolution finer than our coarse measurements of velocity could resolve.

The enhanced transport associated with multiple bedforms was not evenly distributed down the channel. Fluxes of sediment over the crests of Bedform 2 were always greater than those over Bedform 1. The magnitude of this spatial difference was a function of the spacing between forms. Larger differences were measured when the two forms were placed near each other (cases 6b, 6c, 7b, 7c). Little difference was measured in the case where the two bedforms had the greatest separation between them (case 6d, Fig. 2.9). Sediment fluxes associated with the same bed configuration but a different grain size, medium versus coarse sand, are indistinguishable from each other.

Measurements collected during trials with bed configurations 6b and 7b (Fig. 2.1b) allowed us to compare relative magnitudes of bedform translation versus deformation. In all of these cases, the transport associated with modifying the shape of the trough separating the two bedforms was of the same order of magnitude as the transport contributing to the downstream advancement of Bedform 1 (Fig. 2.9). Visual inspection showed that sediment involved in trough filling was supplied from the stoss side of the downstream bedform, as grains ejected by turbulent bursting were swept upstream by the recirculation eddy and deposited in the trough. These comparable magnitudes highlight an intrinsic difficulty associated with measuring active bedforms. Shape changes are often large over migration distances shorter than one bedform length. Accurate characterization of bedform topography therefore requires numerous rapidly collected profiles.

2.3.3. Variability in the flow field

The rapid rates of change in bedform topography illustrated in Figures 2.3 and 2.6 were preceded by relatively subtle changes in bedform shape, particularly modifications to the troughs separating adjacent bedforms. These adjustments in trough shape (Fig. 2.4) were typically produced by sedimentation from upstream-directed transport within recirculation eddies (Fig. 2.9). Because trough adjustments appeared to be linked to rapid deformations of the bed, we were interested in determining what modifications to the flow field were associated with different trough geometries. Three geometries were selected (Fig. 2.10), and trough filling was characterized by first measuring the flow field over two rigid bedforms (Fig. 2.10a and 2.10d). An aluminum plate was then placed in the trough and the measurements were repeated. In one case the orientation of the plate was horizontal (Fig. 2.10b and 2.10e) and in another case the plate was inclined (Fig. 2.10c and 2.10f). The profiles for mean velocity are remarkably similar between all three setups (Fig. 2.10a, 2.10b, and 2.10c), whereas profiles of turbulence (RMS(u)) are different. Higher values of RMS(u) were measured for both cases with a partially filled trough (Fig. 2.10e and 2.10f) compared to the original configuration (Fig. 2.10d). Relatively small adjustments in bedform geometry produced almost no change in the mean flow field but considerable change in its turbulence structure. The largest fluctuations of u and w occurred in the bedform trough (Fig. 2.10), and we expect these events could sweep or eject sand out of this region. Data indicate that turbulent velocity fluctuations would be much less effective at lifting coarse sand grains. Calculated settling velocity, w_s, (Dietrich, 1982) for d_{50} of the coarse sand (9.9 cm/s) is substantially

larger than that for d_{50} of the medium sand (4.6 cm/s, Fig. 2.11). Instantaneous vertical velocity , w, exceeds w_s of medium sand for 5% of the sample time, while never exceeding w_s of coarse sand. Although mean sediment fluxes for medium and coarse grain runs were indistinguishable (Fig. 2.9), small but significant entrainment of grains for medium sand experiments may explain why those bedforms underwent significant splitting with large variability, whereas coarse grained bedforms simply became longer and flatter (Fig. 2.5h).

2.4. Interpretation of experimental results

Results from our experiments indicate a varied response in bedform evolution to a simple set of initial conditions. Initial bedforms were out of equilibrium with the flow field. While this situation is quite different from naturally-formed topography, it allows us to amplify modes of bedform interaction that likely also operate in natural systems. The average decrease in bedform height, and the increase in length for cases where bedform splitting did not occur, is a direct result of these tall, steep bedforms responding to the imposed flow field. Two aspects of observed bedform development should be relevant to natural rivers: 1) the connection between turbulence-induced sediment transport and rapid rates of bedform evolution; and 2) the influence of one bedform on adjacent bedforms.

After the initiation of splitting began, the subsequent behavior of daughter bedforms appeared to depend strongly on local topography (Fig. 2.3). We found that bedforms close in proximity can merge or split and that a bedform in the wake of an upstream form will migrate and deform more rapidly. Initial spacing of bedforms had a strong influence on subsequent evolution. Bedforms spaced very close together interacted in both

upstream and downstream directions, as significant trough filling appeared to trigger splitting cascades. The process of trough filling was capable of increasing turbulent velocity fluctuations, leading to enhanced and more variable sediment transport. Although mean sediment transport rates were similar for medium and coarse grained bedforms, medium grained bedforms underwent significant splitting while coarse grained bedforms did not. We propose that the local suspension of particles in the medium sand runs produced spatial divergences in the sediment flux, driving the erosion necessary in bedform splitting. Since the threshold for suspension was never exceeded in the coarse sand runs (Fig. 2.11), there exists a substantial difference in morphological evolution compared to the medium sand cases.

Another phenomenon explained by spatial variation in turbulence is the observed downstream increase in the sediment flux. In every case, sediment flux of Bedform 2 was greater than that of Bedform 1 (Fig. 2.9), which has to do with the influence of the upstream bedform on the flow and transport field experienced by the downstream bedform. Measured RMS velocity values were larger downstream of bedform crests (see also Nelson et al., 1995), and the associated developing boundary layer (Fig. 2.1) also produced a shear stress gradient (Nelson et al., 1993; McLean et al., 1994), both of which enhance sediment flux. For cases 6b and 6c, this enhanced sediment flux is reflected in mean values of celerity for Bedform 2, which were greater than those of Bedform 1 (Fig. 2.8 and Table 2.3). A surprising result is the apparent effect downstream forms have on their upstream relatives. Sediment flux of Bedform 1, for every case in which two bedforms were present, is greater than that for the case of a single bedform, case 6a. Variation in celerity of the upstream bedform decreased with increasing spacing,

although the differences were not statistically significant (Chi-square test, see section 3.2.2).

Measurements of water depth over bedforms verified that drawdown of the water surface elevation due to acceleration over topography was small ($<10^{-3}$ m), and more importantly was equal for all bedforms for all runs. Water surface slope, however, varied by about a factor of two over the range of runs, and was not well-controlled. We believe the main differences in bedform behavior among experimental runs were caused by changes in the relative position of bedforms in the turbulent flow field, but cannot rule out that small changes in water surface slope may have had an effect. Changes in water surface slope may explain observed differences in evolution of the upstream bedform under various initial conditions.

2.5. Conclusions

We have presented results from a laboratory setup that was purposely simplified to provide unambiguous measures of how bedform dynamics are influenced by the position of an adjacent bedform. In all cases the initially tall and steep bedforms deformed rapidly in response to the imposed flow, and the manner in which bedforms adjusted was strongly influenced by the initial spacing. These measurements reveal that rates of change in bedform size and shape are sensitive to local topography. The simple initial geometry of the bed and the steady hydraulic discharge imposed on the experiments require that this variability, manifest as broad distributions in celerity and bedform geometry, was produced by the bedforms themselves.

The artificial initial condition was chosen to more easily facilitate the study of bedform interaction in the laboratory. It is reasonable to question whether any results here may be generalized to the case of naturally-formed bedforms. The simple fact that migration speeds of individual bedforms in a train are not equal means that interactions of the type observed here will always occur, as bedforms move in and out of the wakes induced by other bedforms. The implication is that, in sandy rivers, a bedform may be an intrinsically transient feature, as suggested by Hersen et al. (2004) in a model of a barchan dune field.

Rapid local adjustment of bottom topography may occur where upward directed instantaneous velocity exceeds the settling velocity of grains. The interaction between bedforms depends strongly on both topography-induced flow variations and grain size. Placing this study in the context of previous work, a view emerges that the bed configuration in sandy systems is strongly influenced by smaller scale interactions. Coleman and Melville (1994) observed occasional coalescence cascades where one bedform merger triggered others and suggested that this process was controlled by spacing and geometry of the bedforms involved. A similar type of behavior was observed occurring at the onset of bedform initiation from a flat bed where ripples did not develop uniformly, but rather grew fastest in the vicinity of other ripples until the entire bed surface was covered (Coleman and Melville, 1996). Gabel (1993) found that local values of flow velocity, bed shear stress and sediment transport were highly variable, and that bed topography caused this local variability. As a result, correlations of geometry and celerity with discharge were poor.

Our results bear qualitative similarities to the studies of naturally-formed bedforms just described. It is difficult to quantify, however, the degree to which bedform adjustment in our experiments was driven by interactions that also occur in nature, compared to behavior driven by bedforms being out of equilibrium with the flow field. A benefit of our 'extreme condition' setup is that it focused attention squarely on how small scale interactions influence the bed configuration. These results motivate questions such as "how erratic is bedform evolution in a river?", and "how does a river bed attain an 'equilibrium' under an imposed flow regime, and how does it adjust to a changing flow regime?". The mechanism responsible for the apparent noise in bedform behavior is a strong nonlinear feedback between sediment transport and topography, and further exploration of the small scale dynamics may motivate a deterministic mathematical description of river bottom self-organization. A physically realistic model describing bedform dynamics cannot be produced by averaging over the length scales of individual bedforms or time scales associated with rapid adjustment. Physical data can, however, guide development of a phenomenological model: bedforms split and merge, local adjustments act to organize the bed configuration, and all with magnitudes that may scale to mean flow properties.

Our results highlight the connection between evolving topography, turbulence and sediment transport. While detailed flow measurements around static bedforms helped us to understand some of the behaviors observed in this study, we feel that topographic data are the most important information for defining the behavior of the sediment-fluid interface. To make further progress in understanding the evolution of sandy river-bottom topography, field measurements must be made with a temporal and spatial resolution fine

enough to resolve rapid deformation and interaction of individual bedforms. Bedforms mantling the bottoms of alluvial channels are the major source of bed roughness and help set the stage/discharge relationship for a channel at any time. Rates and styles of bedform adjustment control the evolution of the bed roughness, and hence change in stage/discharge relationships. Previous studies have, over the decades, cataloged mean bedform geometries under a wide range of flow conditions. We suggest that future field campaigns document the lifespan, deformation rates and variability of bedforms under these same conditions. While our study does not yield any predictions for bedform evolution, it provides a motivation for examining adjustments at a finer resolution, which should contribute to more accurate predictions of their evolution. In a discussion of the effects of defects on eolian bedform dynamics, Werner and Kocurek (1997) posed the provocative question "does the tail wag the dog?". In the context of subaqueous bedform geometry and sediment flux, the tails of the distributions may do a lot of the wagging.

Notation

A	Area of bedforms, cm^2
c	Bedform celerity, cm min^{-1}
cr	Bedform crest
d	Representative grain diameter, μm
D	Characteristic length, m
f	Characteristic vortex shedding frequency, s^{-1}
Fr	Froude number = $\bar{u}(gh)^{-0.5}$
g	Gravitational acceleration, m s^{-2}
h	Water depth, m
H	Bedform crest height, m
L	Bedform length, m
k	Porosity = 0.35
n	Number of bedforms
N	Number of celerity measurements
p	Peak, but not a bedform
Q_f	Width-averaged fluid discharge, m^2 s^{-1}
q_s	2D Sediment flux, cm^2 s^{-1}

Re	Reynolds number
s	Spacing of bedforms, m
St	Strouhal number = fD/V
t	Time, s
T	Characteristic vortex shedding period, s
t_0	Initial time, s
t_1	Arbitrary later time, s
t_f	Final time for sed. flux calculations = 1920, s
tr	Bedform trough
u	Instantaneous streamwise velocity at a point, m s^{-1}
$\bar{u}$	Average streamwise velocity, m s^{-1}
u'	Deviatoric streamwise velocity = ($\bar{u} - u$), m s^{-1}
u_0	Velocity upstream of bedform at a point, m s^{-1}
V	Characteristic velocity, m s^{-1}
w	Instantaneous vertical velocity at a point, m s^{-1}
$\bar{w}$	Average vertical velocity, m s^{-1}
w'	Deviatoric vertical velocity = ($\bar{w} - w$), cm s^{-1}, m s^{-1}
w_s	Particle settling velocity, cm s^{-1}
x	Streamwise direction, and horizontal position, m
y	Cross stream direction
z	Vertical direction, and position above bed, m
θ	Inclination angle between bedforms, °
Δa	Area of displaced sediment, cm^2
Δt	Time between chosen photographs, s
Δx	Change in x over Δt, cm

Acknowledgements

Support for our research was provided by a Presidential Fellowship to D.J. from the Massachusetts Institute of Technology, and by the STC program of the National Science Foundation via the National Center for Earth-surface Dynamics under the agreement Number EAR- 0120914. We extend our gratitude to Ole Madson, who stimulated development of several ideas presented here. Thanks also to Chris Paola, Wes Watters and Joel Johnson for helpful and encouraging discussions along the way. Thorough reviews by Peter Wilcock and Jonathon Nelson greatly sharpened the focus of this paper.

References

Allen, J.R.L., *Current Ripples*, North-Holland Pub. Co., Amsterdam, 1968.

Best, J., S. Bennett, J. Bridge and M. Leeder, Turbulence modulation and particle velocities over flat sand beds at low transport rates, *J. Hydraul. Div. Am. Soc. Civ. Eng., 123*, 1118-1129, 1997.

Carling, P.A., E. Gölz, H.G. Orr and A. Radecki-Pawlik, The morphodynamics of fluvial sand dunes in the river Rhine, near Mainz, Germany. I. Sedimentology and morphology, *Sedimentology, 47,* 227-252, 2000.

Carling, P.A., E. Gölz, H.G. Orr and A. Radecki-Pawlik, The morphodynamics of fluvial sand dunes in the river Rhine, near Mainz, Germany. II. Hydrodynamics and sediment transport, *Sedimentology, 47,* 253-278, 2000.

Coleman, S.E., and B.W. Melville, Bed-form development, *J. Hydraul. Div. Am. Soc. Civ. Eng.*, *120*, 544–559, 1994.

Coleman, S.E., and B.W. Melville, Initiation of bed forms on a flat sand bed, *J. Hydraul. Div. Am. Soc. Civ. Eng.*, *122*, 301-310, 1996.

Csahók, Z., C. Misbah, F. Rioual, an d A. Valance, Dynamics of aeolian sand ripples, *Euro. Phys. J. E*,, *3*, 71-86, 2000.

Dietrich, W. E., Settling velocity of natural particles, *Water Resour. Res., 18,* 1615-1626, 1982.

Ditchfield, R. and J. Best, Development of bed features, Discussion, *J. Hydraul. Div. Am. Soc. Civ. Eng., 118*, 647-650, 1992.

Endo, N., K. Taniguchi, and A. Katsuki, Observation of the whole process of interaction between barchans by flume experiments, *Geophys. Res. Lett.*, *31*, L12503, doi: 10.1029/2004GL020168, 2004.

Engel, P., Length of flow separation over dunes, *J. Hydraul. Div. Am. Soc. Civ. Eng., 107*, 1133–1143, 1981.

Gabel, S.L., Geometry and kinematics of dunes during steady and unsteady flows in the Calamus River, Nebraska, USA, *Sedimentology, 40*, 237-269, 1993.

Harbor, D.J., Dynamics of bedforms in the Lower Mississippi River, *J. Sedim. Res., 68*, 750-762, 1998.

Hersen, P., K.H. Anderson., H. Elbelrhiti, B. Andreotti, P. Claudin and S. Douady, Corridors of barchan dunes: Stability and size selection, *Phys. Rev. E*, *69*, 011304, 2004.

Kolár, V., D.A. Lyn and W.Rodi, Ensemble-averaged measurements in the turbulent near wake of two side-by-side square cylinders, *J. Fluid Mech., 346*, 201-237, 1997.

Kostaschuk, R., A field study of turbulence and sediment dynamics over subaqueous dunes with flow separation, *Sedimentology, 47*, 519-531, 2000.

Leclair, S.F., Preservation of cross-strata due to the migration of subaqueous dunes: an experimental investigation, *Sedimentology, 49*, 1157-1180, 2002.

Lyn, D.A., S. Einav, W. Rodi and J.H. Park, A laser-Doppler velocimetry study of ensemble-averaged statistics of the turbulent near wake of a square cylinder, *J. Fluid Mech., 304*, 285-320, 1995.

Maddux, T. B., J. M. Nelson, and S. R. McLean, Turbulent flow over three-dimensional dunes: 1. Free surface and flow response, *J. Geophys. Res., 108*(F1), 6009, doi:10.1029/2003JF000017, 2003.

Maddux, T. B., S. R. McLean, and J. M. Nelson, Turbulent flow over three-dimensional dunes: 2. Fluid and bed stresses, *J. Geophys. Res., 108*(F1), 6010, doi:10.1029/2003JF000018, 2003.

McLean, S.R., J.M. Nelson and S.R. Wolfe, Turbulence structure over two-dimensional bed forms: Implications for sediment transport, *J. Geophys. Res., 99* (C6), 12729-12747, 1994.

Mohrig, D., Spatial evolution of dunes in a sandy river, Ph. D. dissertation, 119pp, Univ. of Wash., Seattle, 1994.

Nelson, J.M., S.R. McLean, and S.R. Wolfe, Mean flow and turbulence fields over two-dimensional bed forms, *Water Resour. Res., 29* (12), 3935–3953, 1993.

Nelson, J.M, R.L. Shreve, S.R. McLean and T.G. Drake, Role of near-bed turbulence structure in bed load transport and bed form mechanics, *Water Resour. Res., 31* (8), 2071-2086, 1995.

Niño, Y., A. Atala, M. Barahona and D. Aracena, Discrete particle model for analyzing bedform development, *J. Hydraul. Div. Am. Soc. Civ. Eng., 128*, 381-389, 2002.

Prent, M.T.H. an E.J. Hickin, Annual regime of bedforms, roughness and flow resistance, Lillooet River, British Columbia, BC, *Geomorphology, 41*, 369-390, 2001.

Prigozhin, L., Nonlinear dynamics of Aeolian sand ripples, *Phys. Rev E.*, *60*(1), 729-733, 1999.

Schmeeckle, M.W. and J.M. Nelson, direct numerical simulation of bedload transport using a local, dynamic boundary condition, *Sedimentology, 50*, 279-301, 2003.

Tufillaro, N.B., Discrete dynamical models showing pattern formation in subaqueous bedforms, *Int. J. Bifurcations and Chaos*, *3*(3), 779-784, 1993.

van den Berg, J.H., Bedform migration and bed-load transport in some rivers and tidal environments, *Sedimentology, 34*, 681-698, 1987.

Werner, B.T., and D.T. Gillespie, Fundamentally discrete stochastic model for wind ripple dynamics, *Phys. Rev. Lett.*, *71*(19), 1993.

Werner, B.T., and G. Kocurek, Bed-form dynamics: Does the tail wag the dog?, *Geology*, *25* (9), 771–774, 1997.

Werner, B.T., and G. Kocurek, Bedform spacing from defect dynamics, *Geology*, *25*(8), 727-730, 1999.

Wiberg, P.L. and J.M. Nelson, Unidirectional flow over asymmetric and symmetric ripples, *J. Geophys. Res.*, *97* (C8), 12745– 2761, 1992.

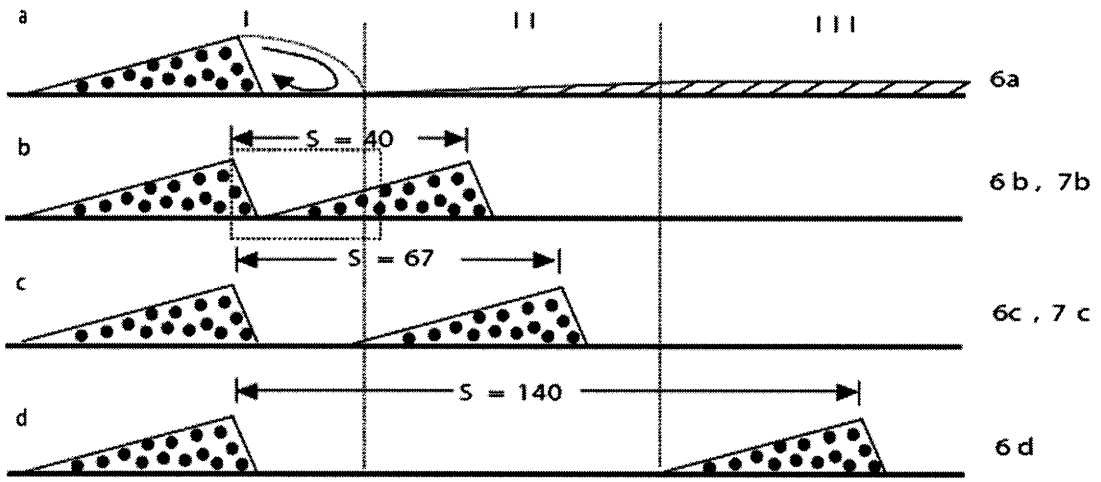

Figure 2.1. Bed configurations used in reported experiments. Labels at right of each plot indicate names of experimental runs with the given bed configuration; see also Table 2.2. (a), Single bedform. The flow field downstream from this single form is divided into three zones, as described in the text. (b), Back-to-back bedforms with crests separated by a spacing, *s*, equal to the bedform length. The dashed-line box demarcates the area where flow measurements were made (see Fig. 2.10). (c), Two identical forms separated by a spacing of 0.67 m. (d), Two identical forms separated by a spacing of 1.40 m. Direction of flow is from left to right in this and all figures.

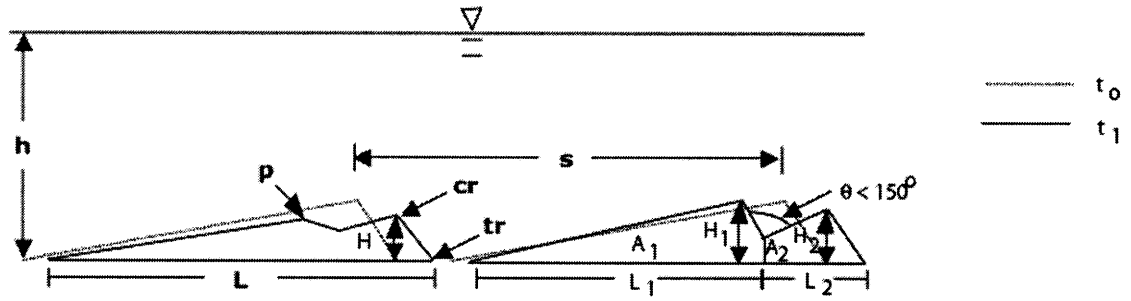

Figure 2.2. Definition sketch for experimental measurements. The bedform configuration is shown both at the beginning of an experiment (t_0) and at some later time (t_1). Bedform features include crest, *cr*, trough, *tr*, and peak (a local topographic high that is not a bedform crest), *p*. A_1 and A_2 are the cross-sectional areas associated with two separate bedforms originating from a single parent form. All other parameters are defined in the text.

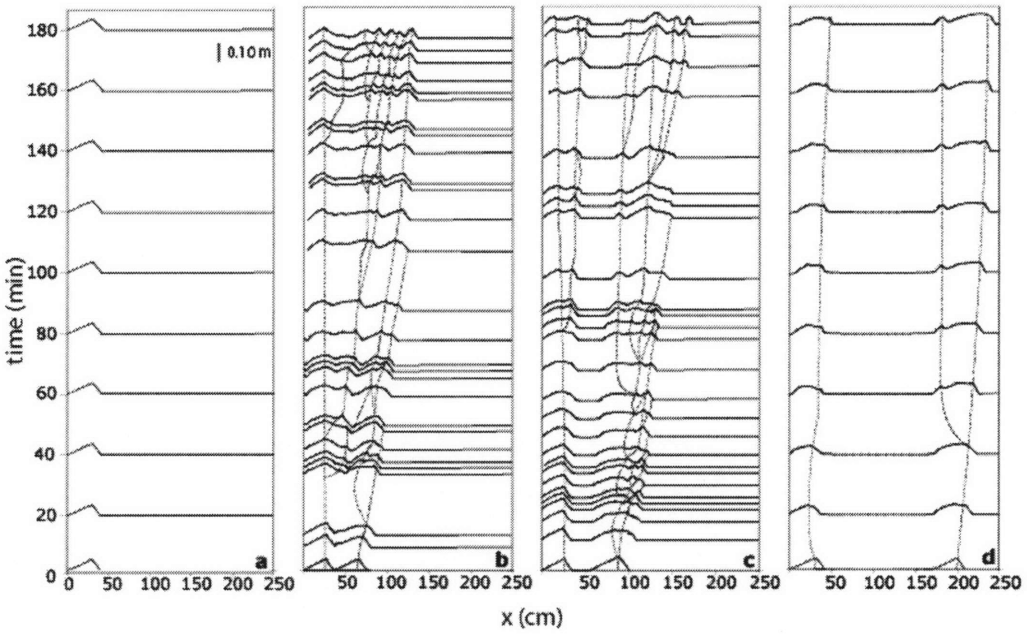

Figure 2.3. Profiles of bedforms as a function of time for (a), run 6a, (b), run 6b3, (c), run 6c3, and (d), run 6d. Each time series is built using the smallest number of profiles necessary to capture significant change in both the positions of crests and bedform number. Dashed lines connect the same crest on successive profiles. The beginning and ending of dashed-lines mark the splitting and merging of individual bedforms, respectively. Vertical scale bar is in (a).

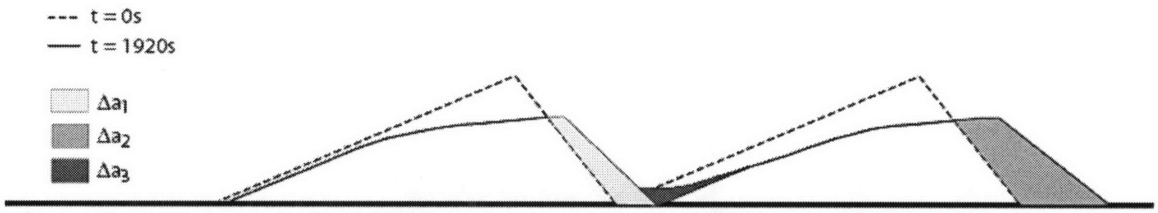

Figure 2.4. Changes in bed topography through time used to calculate local values for streamwise sediment discharge, q_s (Equation 1). The newly generated cross-sectional areas used to determine q_s at the crests of Bedform 1 and Bedform 2 are Δa_1 and Δa_2, respectively. The cross-sectional area used to determine the upstream transport filling in the trough of Bedform 1 is Δa_3.

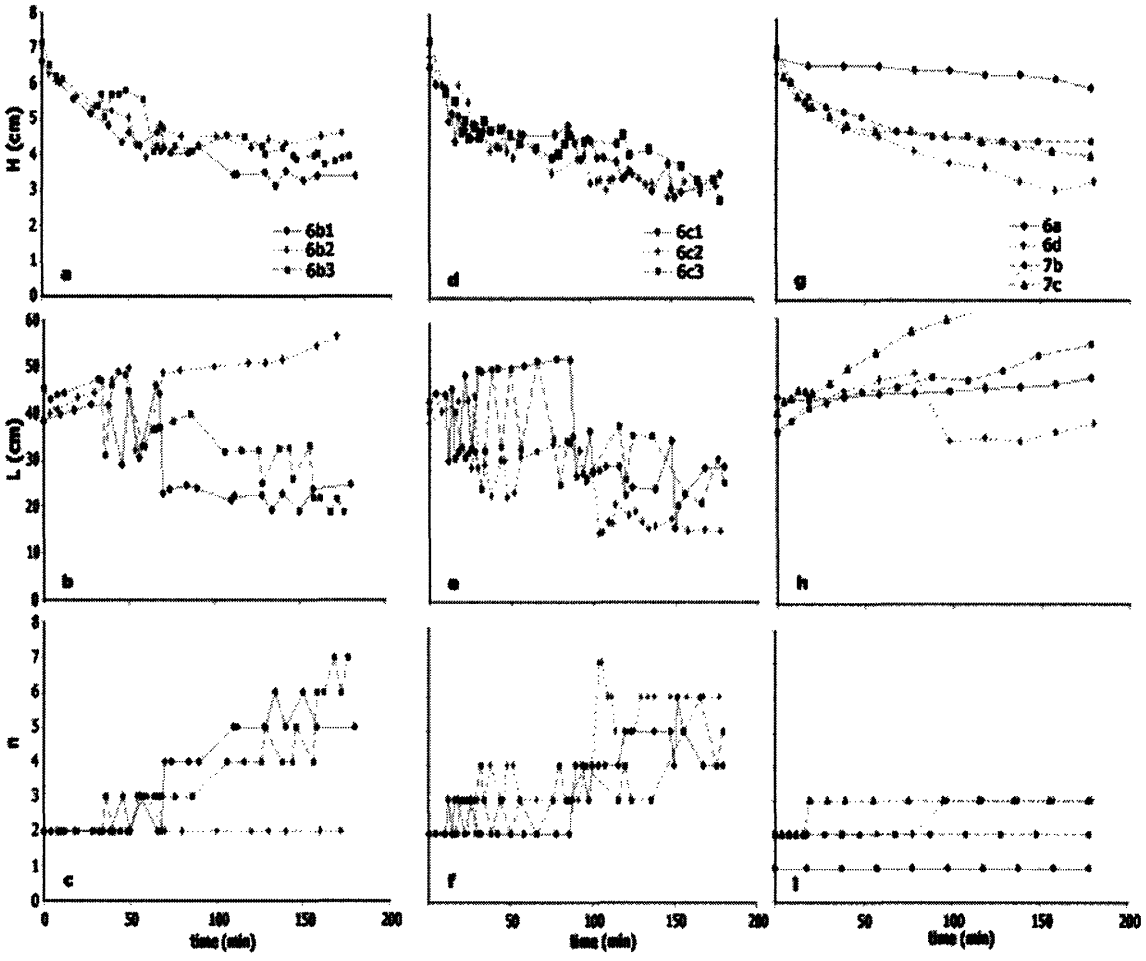

Figure 2.5. Time series of bedform statistics. Top, middle, and bottom rows represent average bedform height, average bedform length, and total number of bedforms, respectively, for all experimental runs. Legends at the top of each column (a, d, g) indicate the run, and apply to all other plots in the respective columns.

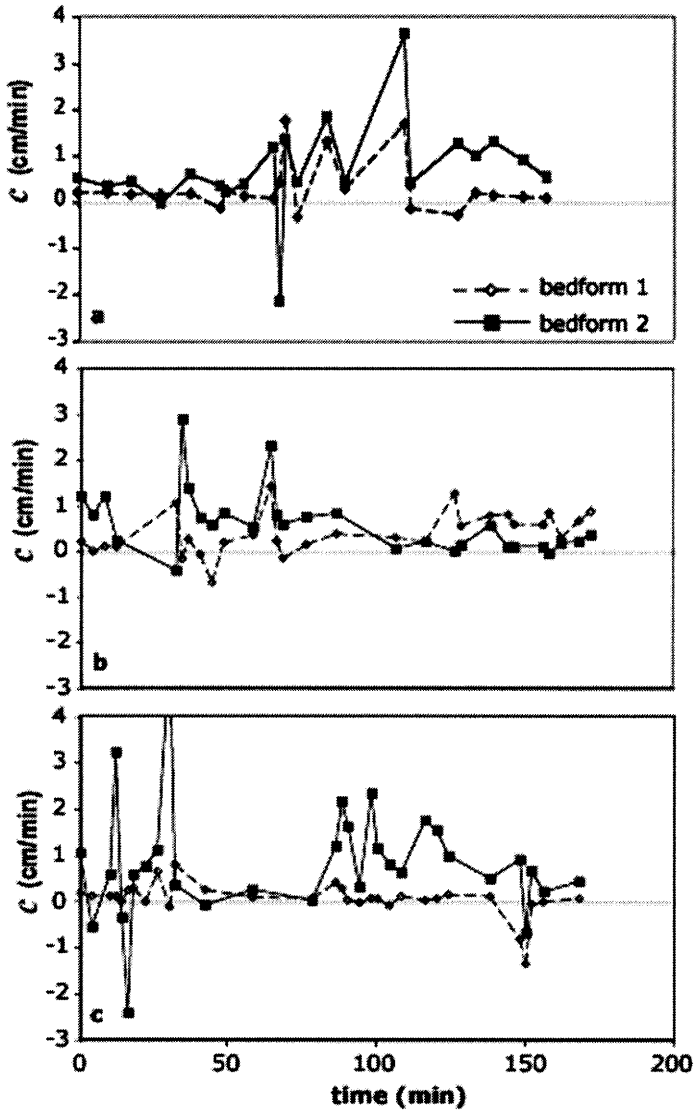

Figure 2.6. Episodic character of bed evolution as shown by time series of bedform celerity for runs (a), 6b1, (b), 6b2 and (c), 6c1.

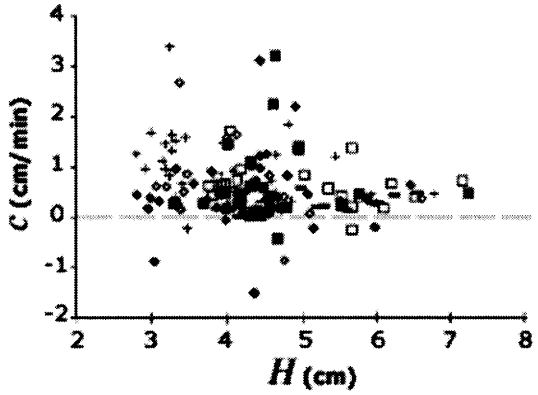

Figure 2.7. Bedform celerity plotted against height using all measurements from individual bedforms in all trials of cases 6b and 6c.

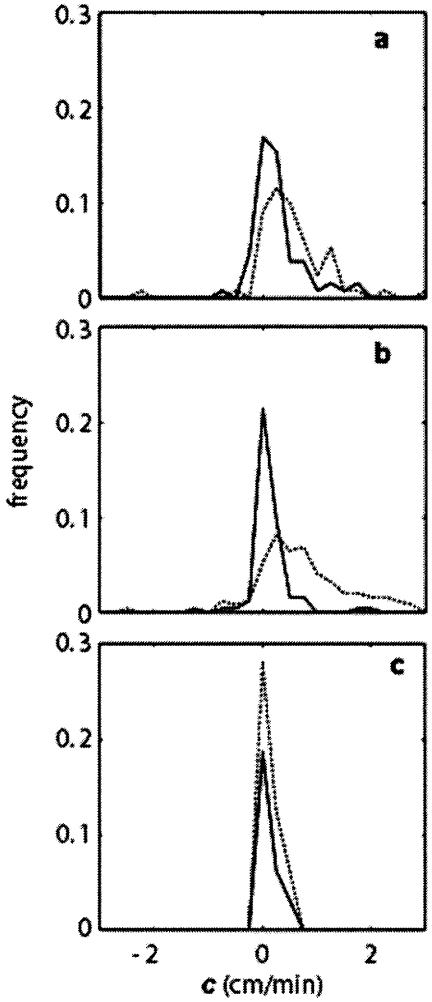

Figure 2.8. Histograms of bedform celerity for all forms that originated from Bedform 1 (solid line) or Bedform 2 (dashed line); (a), runs 6b, (b), runs 6c and (c), run 6d. The bin interval for every histogram is 0.25 cm/min. See Table 2.3 for statistics.

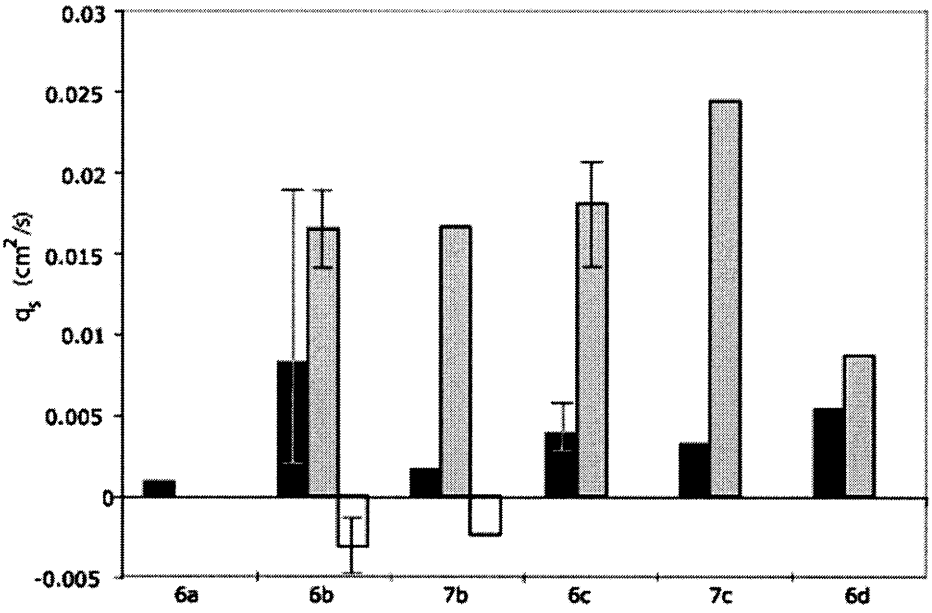

Figure 2.9. Local streamwise fluxes of sediment, q_s, associated with the first 1920 s of every experiment (see Fig. 2.1 for naming convention). Black, grey and white bars indicated sediment flux of Bedform 1, Bedform 2 and trough filling, respectively. Bars for runs 6b and 6c are each averages from 3 runs, where whiskers bracket minimum and maximum values for each case.

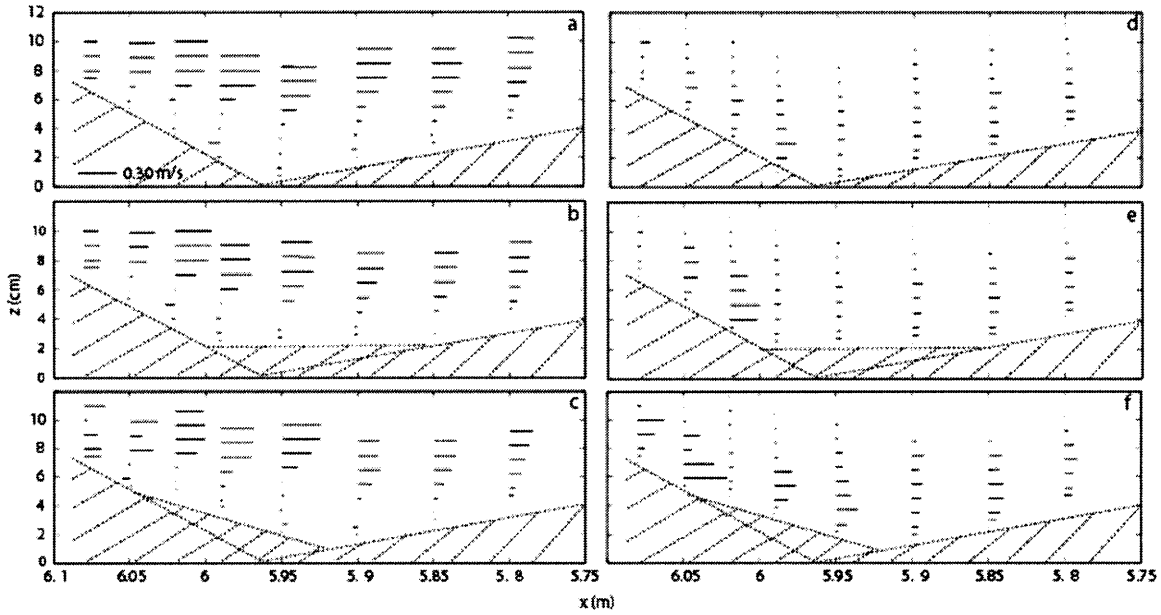

Figure 2.10. Flow measurements collected over two rigid bedforms placed end to end; location is indicated in Fig. 2.1b. Dashed lines outline the rigid bottom topography. Stick profiles defining the mean streamwise velocity values are presented in the left-hand column, while streamwise RMS velocity profiles are in the right-hand column. The vertically averaged value for mean streamwise velocity in each case is 0.27 m/s. (a, d), Mean velocity and RMS(u) associated with a simple unfilled triangular trough, (b, e), a horizontal plate in the trough and (c, f), an inclined plate in the trough. Scale bar is in (a).

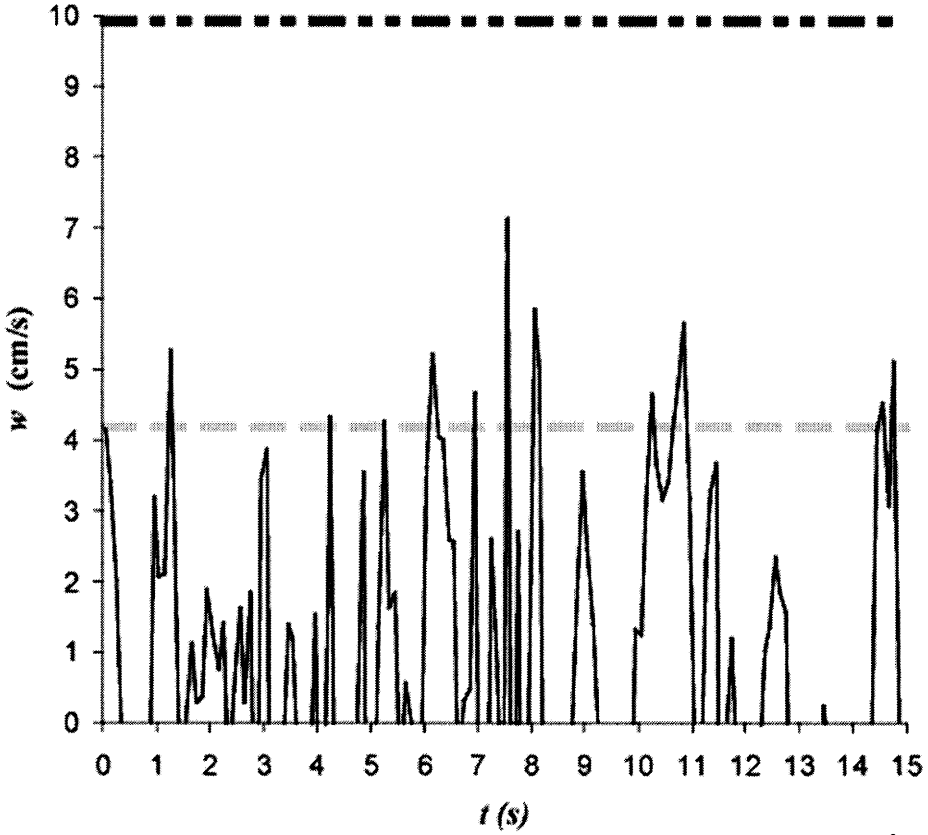

Figure 2.11. Upward directed instantaneous velocity, w, at $z = 5\times10^{-3}$m above the bed and x = 5.85 m, measured for the rigid bedform case shown in Figure 2.10f. Also plotted are fall velocities, w_s, for medium (gray dashed line) and coarse (black dash-dot line) sands.

Table 2.1. Grain size of the medium and coarse sand.

Class	Medium Sand	Coarse Sand
d_{10}	270 μm	475 μm
d_{50}	350 μm	770 μm
d_{90}	510 μm	945 μm

d_{10}, d_{50}, and d_{90} refer to the 10, 50 and 90 cumulative percentile, respectively.

Table 2.2. Initial conditions for all experimental runs.

Run #	d_{50} (μm)	s (m)	$\bar{u}$ (m/s)	h (m)	Q_f (m^2/s)	Fr	Re
6a	350	-	0.27	0.191	5.2×10^{-2}	0.20	1.5×10^4
6b1	350	0.40	0.27	0.191	5.2×10^{-2}	0.20	1.5×10^4
6b2	350	0.40	0.27	0.192	5.2×10^{-2}	0.20	1.5×10^4
6b3	350	0.40	0.27	0.192	5.2×10^{-2}	0.20	1.5×10^4
6c1	350	0.67	0.27	0.191	5.2×10^{-2}	0.20	1.5×10^4
6c2	350	0.67	0.28	0.191	5.3×10^{-2}	0.21	1.6×10^4
6c3	350	0.67	0.27	0.191	5.2×10^{-2}	0.20	1.5×10^4
6d	350	1.40	0.27	0.189	5.1×10^{-2}	0.20	1.5×10^4
7b	770	0.40	0.32	0.192	6.1×10^{-2}	0.22	1.7×10^4
7c	770	0.67	0.32	0.192	6.1×10^{-2}	0.22	1.7×10^4

Flow depth is h, width-averaged fluid discharge is Q_f, and calculated Froude and Reynolds numbers are Fr and Re, respectively. All other parameters defined in text.

Table 2.3. Statistics of time step averaged bedform celerity for cases 6b, 6c and 6d: see figure 2.8 for histograms.

Measure	Case 6b	Case 6c	Case 6d
N	130	246	24
Bedform 1 c (cm/min)	0.15, 0.28 (0.46)	0.10, 0.13 (0.37)	0.08, 0.14 (0.13)
Bedform 2 c (cm/min)	0.43, 0.57 (0.77)	0.66, 0.94 (1.19)	0.06, 0.13 (0.18)
System c (cm/min)	0.23, 0.43 (0.65)	0.26, 0.59 (1.01)	0.08, 0.14 (0.16)

N = total number of celerity readings for each case; the low number of case 6d is due to a smaller number of crests generated due to less activity, and also because only one trial was performed. Celerity values for each case are as follows: median, mean (standard deviation).

Chapter 3

A unified model for subaqueous bedform dynamics[2]

D.J. Jerolmack and D. Mohrig

Department of Earth, Atmospheric and Planetary Sciences, Massachusetts Institute of Technology, Cambridge, Massachusetts 02139, USA

Abstract

Bedform evolution remains dynamic even in the special case of steady, uniform flow. Data from the sandy, braided North Loup River, Nebraska, USA, show that roughness features on the channel bottom display a statistical steady-state and robust scaling that are maintained through the collective interactions of transient (short-lived) bedforms. Motivated by such field data, and laboratory observations of bedform growth, we develop a nonlinear stochastic surface evolution model for the topography of bedload-dominated sandy rivers in which instantaneous sediment flux explicitly depends on local elevation and slope. This model quantitatively reproduces laboratory observations of initial growth and saturation of bedforms from a flat surface, and also generates long-term dynamical behavior characteristic of natural systems. We argue that the variability in geometry and kinematics of bedforms in steady flow, and the existence of roughness at all wavelengths up to the largest dunes, are a consequence of the nonlinear relationship between sediment flux and topography, subject to noise.

---

[2] From Jerolmack, D., and D. Mohrig, A unified model for subaqueous bed form dynamics, *Water Resources Res.*, *41*, W12421, doi:10.1029/2005WR004329, 2005.

3.1. Introduction

The nonlinear dependence of sediment transport on surface topography produces a bewildering array of patterns, from ripples at the centimeter scale to river networks and depositional fans at a basin scale. A natural way to characterize such patterns involves measuring static geometrical properties, spatial correlations, and scaling laws that may be exhibited between physical parameters of the system (e.g., Rubin, 1992; Dodds and Rothman, 2000). Landscapes are dynamic (i.e. variable in time), however the study of their transient behavior is hindered by the slow rate of evolution of most geological systems. Although surface evolution equations are naturally time-dependent, the dynamical predictions of erosional landscape models (see, e.g., Willgoose et al., 1991; Howard, 1994) are difficult to test. A geomorphological transport system that exhibits both transient behavior on observable time scales and statistically-robust geometrical properties allows strong tests of models, and provides a window into fundamental pattern formation mechanisms in sedimentary systems. Trains of bedforms in sand-bedded rivers are one example of such a system.

While bedform classification schemes, such as distinguishing ripples from dunes (e.g., Ashley, 1990), may be useful in describing some aspects of bedform behavior, they belie the continuum of scales of topography that make up a sand-bedded channel. Indeed, there is theoretical (Hino, 1968), laboratory (Hino, 1968; Nordin, 1971) and field evidence (Levey et al., 1980; Nikora et al., 1997) that roughness of all wavelengths exists below the scale of the largest dunes. Further, bedforms in natural systems change dimensions continuously as they migrate downstream. The internal dynamics of a train of bedforms manifests itself as variability in bedform height, length and migration rate

(celerity), and in bedform deformation, even when the topography is developing under steady and uniform macroscopic flow conditions (van den Berg, 1987; Gabel, 1993; Mohrig, 1994; Leclair, 2002). Although great progress has been made in the understanding of instability and bedform growth from a flat surface (e.g., Smith, 1970; McLean, 1990), current models cannot describe the long-time behavior of a train of finite-amplitude bedforms.

Increasingly sophisticated measurements of the flow field over rigid topography (e.g., *Nelson* et al., 1993; McLean et al., 1994; Maddux et al., 2003a,b) have demonstrated the influence of topography on turbulence production and bed stress. There is now little doubt that the most accurate model of bedform evolution will eventually come from detailed numerical solution of the Navier-Stokes equations (e.g., Shimizu et al., 2000), coupled to some force balance on sand grains and sediment continuity. Currently, however, the modeling of fluid flow over arbitrary (and rapidly deforming) topography is a formidable challenge. Moreover, a fully-coupled fluid-sediment-topography model would be sufficiently complex that it could not easily serve as an exploratory tool for understanding fundamental aspects of sand bed evolution.

At present, an incomplete understanding of how irregular bed topography controls turbulence production and how this turbulence affects local sediment transport precludes development of a bedform evolution model from first principles. Several models have been proposed that are fundamentally discrete and stochastic, with sediment transport represented by simple rules (e.g., Tufillaro, 1993; Werner, 1995; Niño et al., 2002). Self-organization of bedforms in such models is robust, and in some cases many different bedform shapes may be reproduced by variation of coefficients or transport rules (Werner,

1995). While these models have been effective in illustrating how microscopic disorder can create macroscopic order (see Tufillaro, 1993), their abstract nature prevents quantitative comparison to natural systems. Sediment transport in such models is essentially represented as stochastically-driven directed diffusion. A family of deterministic continuum models for eolian ripple formation has been proposed by physicists based on phenomenological descriptions (e.g., Terzidis et al., 1998; Prigozhin, 1999; Valance and Rioual, 1999) or conservation and symmetry principles (e.g., Csahók et al., 2000), but these approaches do not allow the interpretation of coefficients in terms of measurable physical quantities (see Csahók et al., 1999). Many more models for eolian ripples have been proposed in the literature, with similar behavior, limitations and caveats to those described above.

In bedload-dominated systems, it is well established that topography exerts a first-order control on sediment flux. In particular, Gomez et al. (1989) have linked instantaneous sediment flux, q_s, directly to the passage of bedforms, showing that the majority of variance in q_s may be explained by topography. Gomez and Phillips (1999) found that the highest frequency variations in q_s, however, cannot be related directly to the passage of bedforms, and interpreted them as representing high-dimensional chaos (deterministic uncertainty) in the transport system. Motivated by these findings, and by documented time evolution of bedforms in the North Loup River, Nebraska, USA, we develop a model including both a deterministic surface evolution equation based on parameterization of bed stress in terms of local topography and stochastic fluctuations in sediment flux. In this paper we focus on qualitative behavior not captured in the previously mentioned models for bedform evolution, and perform a preliminary analysis of

temporal and spatial scaling with comparisons to empirical data. In a future work we will report more quantitative comparisons to field data.

3.2. River Data

We present here topographic data capturing bedform evolution in time and in space that are derived from low altitude aerial photography of the braided North Loup River, Nebraska, USA (Mohrig, 1994; Mohrig and Smith, 1996), which has a bed consisting of well-sorted medium sand (Trask sorting coefficient = 1.32; median grain diameter, d_{50} = 0.31 mm). Time-lapse images taken with a camera suspended beneath a tethered helium-filled balloon were converted into topographic maps (Fig. 3.1a), where the grayscale pixel intensity was transformed into water depth using the Beer-Lambert Law (Soo, 1999) calibrated to numerous surveyed points within the channel. The spatial (downstream and cross-stream, or x- and y-direction, respectively) resolution is known to be 0.02 m from image pixel size, while we estimate vertical resolution to be ~0.01 m from analysis of sequential bedform profiles. Observations shown here were taken with an interval of one minute for a period of one hour, covering a section of the river of 30 m x 15 m. Approximately constant river stage ensured that flow was essentially steady over the observation period, so the observed variability and adjustments of bedform geometry and migration rate were caused by internal dynamics of the sediment-fluid interface. A complete statistical description of channel-bottom topography, and the method developed to measure this topography, will be the focus of a later paper. Here we present salient properties of bed evolution in the North Loup River that we believe are representative of sand-bedded rivers in general, and these observations serve to motivate the development of

a new mathematical description for the dynamics of bedforms in bedload-dominated sandy rivers.

It is convenient to examine elevation along one dimension (i.e. 1D profiles in the downstream direction) to observe changes in cross-sectional geometry, and our data show that all downstream profiles at a given snapshot in time are statistically identical (as determined by scaling methods presented below) and therefore justify a 1D analysis. Sequential profiles stacked in time (Fig. 3.1b) show that bedforms are not translation-invariant. While large-scale bed features remain recognizable over the duration of observation (40 minutes), individual bedforms are observed to split into smaller features, merge to form larger features, spontaneously form on the stoss side of larger features, and disappear in the lee slope of larger features. We see then that bedforms are inherently transient objects, such that the river bottom remains dynamic even in steady flow. Individual bedforms become unrecognizable after migrating one to two wavelengths, similar to observations of sand dunes in rivers in Eastern Europe by Nikora et al. (1997) and laboratory dunes observed by Leclair (2002).

Rather than subjectively identify and define individual bedforms from a profile, the series of elevations in a profile is treated as a random function (see Nikora et al., 1997), and its variability is characterized as roughness. A simple and common measure of roughness is the root mean square of elevation on the interface, sometimes referred to as the interface width, w (Barabási and Stanley, 1995):

$$w = \left[\frac{1}{N} \sum_{i=1}^{N} (\eta_i - \bar{\eta})^2 \right]^{1/2}, \qquad (1)$$

where N is the number of observations, η is bed elevation and the over-bar represents an average over the domain considered. For reference, the average bedform height for a profile from the North Loup River is about two times the measured value of w for that profile.

The scaling of w with observed length or "window size", l, contains information about the size distribution of roughness elements, and is often found to exhibit a power law over some range for rough interfaces:

$$w \sim l^{\alpha}, \tag{2}$$

where α is the roughness exponent, characterizing the scaling of elevation fluctuations (see Barabási and Stanley, 1995; Dodds and Rothman, 2000). For North Loup River profiles, we determine w for every box of the smallest window size, which is twice the data resolution or 0.04 m. We then take the average of all w values to obtain a characteristic roughness for that window size. This procedure is repeated for sequentially larger window sizes, up to one-half the size of the observation domain (~15 m); a similar analysis was performed *by Nikora and Hicks* (1997). An example result is shown in figure 3.2, which plots the characteristic interface width against window size for downstream profiles at a snapshot in time. There are several features worthy of note. First, there is a scale-invariant regime in which a power-law relationship holds between w and l, where the slope of the line in the scaling regime is the roughness exponent. Second, there is a gradual roll

over of the interface width with window size at the transition between the lower scaling regime and the upper saturation regime. This transition occurs at a length equal to the characteristic wavelength of the largest dunes; the associated transition length and interface width values are l_x and w_x, respectively (Fig. 3.2). Repeating this analysis of w for profiles taken at different times but at the same location yields the same values for α, l_x and w_x, suggesting the scaling of roughness elements is stationary. Taken together, these results show that despite the transience of individual topographic elements, the river-bottom maintains a statistical steady-state in terms of roughness.

The river-bed displays a continuum of scales of topography up to the wavelength of the largest features, as represented by the power-law relationship between w and l, and no clear distinction can be made between ripples and dunes. A similar conclusion is reached by computing the power spectra of bed profiles (not shown), which contains equivalent information about roughness scaling. These results are not unique to the North Loup River; similar findings have been reported in the laboratory (Hino, 1968; Nordin, 1971) and field (Levey et al., 1980; Nikora et al., 1997), and may be the rule in sand-bedded systems, rather than the exception. The two regimes present in figure 3.2, power-law roughness growth and saturation, may be indicative of different organizing physical processes. In many interface problems such as crystal growth, the scale invariant regime is generated by internal dynamics of the interface itself, while saturation occurs due to 'finite size effects', where growth is limited by the size of the container (see Barabási and Stanley, 1995). In the case of bedforms, scale invariance may be due to the local sediment transport physics, while maximum dune size is controlled by boundary conditions such as water depth or background shear stress.

Qualitatively, the existence of many scales of topography may be understood from examining the temporal evolution of topography in successive profiles (Fig. 3.1c). The largest dune features translate by the motion of smaller bedforms on their backs. These smaller features spontaneously form on a dune back, then grow in amplitude as they migrate across the dune back before disappearing in the subsequent trough (as discussed by Jain and Kennedy, 1974; Nikora et al., 1997; Gomez and Phillips, 1999). The appearance, growth and disappearance of bedforms maintains a constant distribution of channel roughness, and this process is a fundamental organizing principle that should be reproduced by a model of sand-bed evolution.

3.3. Model Development

We seek an intuitive, physically realistic, continuum model capable of reproducing both the instability of a flat sand bed subjected to a shear flow, and the long-time evolution of dynamic topography. We focus on bedforms built from a uni-modal distribution of particle sizes moving primarily as bedload because this sediment flux can be treated as responding instantaneously to changes in the flow field without accruing significant error. We hypothesize that the detailed structure of the fluid flow field is not important for determining temporal and spatial scaling, and hence we can write a "local growth model" (Barabási and Stanley, 1995; Dodds and Rothman, 2000) for the evolution of the sediment-fluid interface – this hypothesis is tested below. This said, the three main ingredients to our model are (i) a relationship between sediment flux and local bed elevation; (ii) the dependence of sediment flux on local flow strength (here characterized

by bed shear stress, τ); and (iii) the dependence of flow strength on local topography. The first model condition is simply a statement of mass conservation:

$$\frac{\partial \eta}{\partial t} = -\frac{1}{(1-p)}\frac{\partial q_s}{\partial x}, \tag{3}$$

where t is time, p is porosity and q_s is sediment flux with dimensions L^2/T. The second condition takes the form of a power-law relationship between sediment flux and boundary shear stress:

$$q_s = m\tau^n, \tag{4}$$

where n is generally 1.5 (Meyer-Peter and Müller, 1948) but may vary up to 2.5 (Fernandez-Luque and van Beek, 1976) and m can vary between 5.7 and 12 depending on the rate of sediment transport (Wiberg and Smith, 1989). Equation 4 could also be written in terms of an excess stress above that value required for initiation of grain motion; our intent here, however, is simply to write down the most generic representation of the governing equations.

Our third model condition relates the local boundary shear stress to the local bed topography. Specifically it relates shear stress to bed elevation and bed slope as

$$\tau(x) = \tau_b\left(1 + A\frac{\eta}{\langle h \rangle} + B\frac{\partial \eta}{\partial x}\right), \tag{5}$$

where ‹*h*› is the spatially-averaged depth of flow at the beginning of a run, τ_b is the background boundary shear stress associated with ‹*h*›, η is vertical distance of a point on the local sediment-fluid interface from the mean elevation, and *A* and *B* are coefficients (Fig. 3.3). This equation for stress in terms of local topography may be considered a Taylor expansion, where higher-order spatial derivatives have been neglected. Relating local bed stress to local bed elevation was first proposed by Exner (1925) who noted that conservation of fluid mass required an increase in the vertically-averaged velocity over the top of an arbitrary two-dimensional bump and derived an explicit relationship between bed stress and topography by relating bed stress to the square of vertically-averaged fluid velocity. Neglecting higher order terms (i.e., $\eta/\langle h\rangle << 1$) Exner (1925) found that:

$$\tau(x) = \tau_b\left(1 + 2\frac{\eta}{\langle h\rangle}\right). \qquad (6)$$

Smith (1970) and Engelund (1970) were the first to propose that the magnitude of local shear stress is also a function of the local bed slope. Smith (1970) argued that the relationship between local bed slope and local bed stress is a consequence of the fluid inertia. Moving water is not easily deflected and as a result, steep adverse slopes put relatively high velocity fluid closer to the bed, producing larger values of bed stress (see also Nelson et al., 1993). Equation 5 simply sums the contributions of relative bed elevation (6) and slope to arrive at a value for bed stress at every site on the bed. The predicted variation of bed stress over topography using (5) is consistent with measured bed stress over static dunes in the laboratory (Nelson et al., 1993; McLean et al., 1994).

3.3.1. One-dimensional surface evolution equation

3.3.1.a. Exner's equation

Combining equations 3, 4 and 6 gives the result:

$$\frac{\partial \eta}{\partial t} = -\langle q_s \rangle \frac{2n}{\langle h \rangle (1-p)} \left(1 + 2\frac{\eta}{\langle h \rangle}\right)^{n-1} \frac{\partial \eta}{\partial x}, \tag{7}$$

a nonlinear wave equation describing surface evolution. The explicit dependence of advection on bed elevation means that points of higher elevation move faster. Exner (1925) used (7) to explain why bedforms become skewed with downstream transport (see Smith, 1970). An angle-of-repose condition must be added to this equation to stop the lee surfaces of bedforms from oversteepening unrealistically. The nonlinear wave equation (7) is neutrally stable, i.e. perturbations neither grow nor decay in amplitude with time. While this lack of instability renders (7) inadequate as a general bedform-evolution model, (7) serves as a useful point of departure for our elaboration described next.

3.3.1.b. New surface evolution equation

Equations 3, 4 and 5 represent our complete model system in one dimension. Combining them, we arrive at a new surface evolution equation for sand-bedded channels:

$$\frac{\partial \eta}{\partial t} = -\langle q_s \rangle \frac{n}{(1-p)} \left(\frac{A}{\langle h \rangle}\frac{\partial \eta}{\partial x} + B\frac{\partial^2 \eta}{\partial x^2}\right)\left(1 + A\frac{\eta}{\langle h \rangle} + B\frac{\partial \eta}{\partial x}\right)^{n-1}. \tag{8}$$

The simple addition of a slope-dependent contribution to bed stress produces a surface evolution equation that is quite different from Exner's equation (7). Equation 8 contains

not only a nonlinear advection term, but also a nonlinear diffusion term. The diffusion term may change sign in this formulation, and negative diffusion leads to the growth of perturbations on the surface.

A formal stability analysis of (8) is beyond the scope of this paper and here we only provide a qualitative discussion of the bed instability following Smith (1970) and McLean (1990). From (3) we may write:

$$\frac{\partial \eta}{\partial t} = -\frac{1}{(1-p)} \frac{\partial q_s}{\partial \tau} \frac{\partial \tau}{\partial x}. \tag{9}$$

Since $\partial q_s/\partial \tau$ is always positive it is the shear stress gradient that determines the sign of $\partial \eta/\partial t$, and hence whether the bed undergoes erosion or deposition. Because sediment deposition occurs downstream of the stress maximum a perturbation on the stream bed may cause another bump to grow downstream of it, ultimately leading to a train of finite-amplitude bedforms. When elevation is small the stress maximum is upstream from the crest of a bump, causing the bump to continue growing. As elevation becomes large, the stress maximum shifts to the elevation maximum and deposition no longer occurs on the crest – growth ceases.

3.3.1.c. Stochastic form

High-frequency fluctuations in sediment flux are a direct consequence of turbulence-aided sediment transport (Nelson et al., 1995; Gomez and Phillips, 1999; Schmeeckle and Nelson, 2003; Sumer et al., 2003). While fluctuations in instantaneous bed stress may be modeled deterministically in a fluid-mechanical model, we treat this

variability as stochastic and explore its morphodynamic importance by addition of a noise term. The stochastic surface evolution equation then reads:

$$\frac{\partial \eta}{\partial t} = -\langle q_s \rangle \frac{n}{(1-p)} \left(\frac{A}{\langle h \rangle} \frac{\partial \eta}{\partial x} + B \frac{\partial^2 \eta}{\partial x^2} \right) \left(1 + A \frac{\eta}{\langle h \rangle} + B \frac{\partial \eta}{\partial x} \right)^{n-1} + \zeta(x,t), \qquad (10)$$

where $\zeta(x, t)$ is Gaussian-distributed low-amplitude white noise, although the time evolution of (10) turns out to be insensitive to the details of $\zeta(x, t)$. A stochastic partial differential equation like (10) can produce long-range spatial correlations on the interface even when the term describing interface growth or transport is entirely local in origin (Rubin, 1992; Barabási and Stanley, 1995).

3.3.2. Two-dimensional surface evolution equation

Our surface-evolution equation can be made two-dimensional through inclusion of a lateral diffusion term. The principle transport direction is still downstream, while lateral sediment transport has a magnitude dependent on the cross-stream (y-direction) slope (Murray and Paola, 1997; Hersen, 2004). In essence, sediment flux is calculated as one-dimensional downstream slices which are coupled to neighboring slices via the lateral diffusion of sediment. A deterministic form of the two-dimensional model then consists of (8) plus a lateral diffusion term

$$\frac{\partial \eta}{\partial t} = -\langle q_s \rangle \frac{n}{(1-p)} \left(\frac{A}{\langle h \rangle} \frac{\partial \eta}{\partial x} + B \frac{\partial^2 \eta}{\partial x^2} \right) \left(1 + A \frac{\eta}{\langle h \rangle} + B \frac{\partial \eta}{\partial x} \right)^{n-1} + D \frac{\partial^2 \eta}{\partial y^2}, \qquad (11)$$

where D is the lateral diffusivity constant (units L^2/T). Note that this treatment of lateral sediment transport is identical to equation 10 in Hersen (2004) and similar to the explicit slope-dependent transport used in Murray and Paola (1997). This approach makes the assumption that the fundamental transport mechanisms occur in the downstream direction, and that cross-stream sediment flux depends linearly on slope; it is the simplest formulation consistent with observation (e.g., Parker, 1984). A stochastic form of the two-dimensional model simply consists of (11) plus a noise term,

$$\frac{\partial \eta}{\partial t} = -\langle q_s \rangle \frac{n}{(1-p)} \left(\frac{A}{\langle h \rangle} \frac{\partial \eta}{\partial x} + B \frac{\partial^2 \eta}{\partial x^2} \right) \left(1 + A \frac{\eta}{\langle h \rangle} + B \frac{\partial \eta}{\partial x} \right)^{n-1} + D \frac{\partial^2 \eta}{\partial y^2} + \zeta(x,y,t). \quad (12)$$

Equation 12 is our new anisotropic "local growth equation" for depositional systems. We expect the applicability of (12) to be general, but it may be made specific by calibration of coefficients to a particular situation. In order to realistically simulate the morphodynamics of a train of subaqueous bedforms, several additional ingredients are required for numerical implementation and are discussed next.

3.3.3. Numerical method

We explore the dynamical behavior of our model system by solving discrete versions of eqs. (3), (4) and (5) at every location on the 2D grid, where i and j represent the x and y grid positions, respectively. Boundary conditions used are periodic in the downstream direction and zero flux in the cross-stream direction. Grid size is 100 x 50 cells. Larger domain sizes were explored, but did not have any significant effect on model results. The initial condition for model runs is a flat, horizontal surface seeded with elevation perturbations of very low amplitude produced as white noise. Values for grid

spacing Δx (equal in x and y directions), time step Δt, water depth $\langle h \rangle$, all coefficients and background shear stress, τ_b, are specified at the beginning of a model run; the exponent n = 1.5 for all simulations. At a given time step, the following sequence of operations is performed:

$$\tau_{i,j} = \tau_b \left(1 + A \frac{\eta_{i,j}}{\langle h \rangle} + B \frac{\eta_{i,j} - \eta_{i-1,j}}{\Delta x} \right), \tag{13}$$

$$\tau_{i,j} = \begin{cases} \tau_{i,j}; \geq 0 \\ 0; < 0 \end{cases}, \tag{14}$$

$$q_{a_{i,j}} = \begin{cases} E\left[\left(\frac{\eta_{i,j} - \eta_{i+1,j}}{\Delta x} \right)^2 - (\tan\theta_c)^2 \right] \left(\frac{\eta_{i,j} - \eta_{i+1,j}}{\Delta x} \right); \left(\frac{\eta_{i,j} - \eta_{i+1,j}}{\Delta x} \right) > \tan\theta_c \\ 0; \left(\frac{\eta_{i,j} - \eta_{i+1,j}}{\Delta x} \right) \leq \tan\theta_c \end{cases}, \tag{15}$$

$$q_{s_{i,j}} = m\tau_{i,j}^{\ n} + q_{a_{i,j}} + \zeta_{i,j}, \tag{16}$$

$$\Delta\eta_{i,j} = -\frac{\Delta t}{(1-p)\Delta x}\left(q_{s_{i,j}} - q_{s_{i-1,j}} \right) + \frac{\Delta t D}{(\Delta x)^2}\left(\eta_{i+1,j} + \eta_{i-1,j} + \eta_{i,j+1} + \eta_{i,j-1} - 4\eta_{i,j} \right). \tag{17}$$

Equation 13 computes bed stress using an upwind scheme for slope, and (14) makes all negative bed stresses zero, crudely mimicking the shadow zone of low transport occurring immediately downstream from a bedform lee face. In order to prevent oversteepening of lee surfaces we employ a version of the grain-avalanching proxy as presented by Hersen (2004). If the downwind-calculated slope exceeds the critical angle, θ_c, then an additional 'avalanche flux' is computed using (15). If the chosen value for coefficient E is sufficiently large, any slope that builds to an angle > θ_c relaxes instantaneously at the next time step. Equation 16 determines the sediment flux at each grid point by summing the

contributions from local bed stress, avalanching and noise; the noise term is zero for deterministic model runs. Finally, (17) finds elevation change using a 1D, upwind version of the sediment continuity equation. The second term on the right hand side of (17) is a diffusion term, solved by calculating the discrete 2D laplacian of the elevation field, and scaled using a diffusivity D which represents the importance of lateral coupling of sediment transport. Although the explicit diffusion term in (12) is for the y-direction only, in our numerical implementation (17) we add an explicit 2D diffusive term which serves the additional purpose of numerical dissipation (Press et al., 1988), helping to smooth the elevation field to enhance numerical stability.

The choice of coefficients for bed stress and sediment transport relations is presently unconstrained. In practice, A and B could be estimated empirically from laboratory observations of bed stress over topography, while cross-stream sediment transport could be treated in a more rigorous manner using an explicit method such as Parker (1984). Values for m may be selected from the literature. Varying coefficients affects the growth rate and amplitude of bed features, but does not greatly affect temporal or spatial scaling. Here we are interested in whether the general equations 13-17 can produce a variety of dynamical behavior observed in laboratory and field settings, so coefficients were selected such that the contributions of elevation and slope to the total bed stress are approximately equal, and cross-stream sediment transport is a small fraction of the downstream flux – see table 3.1. We will perform future experiments to estimate these coefficients. Grid spacing and time step values were selected from considerations of numerical stability and computation time.

3.4. Results

3.4.1. Deterministic model ($\zeta = 0$)

Numerically solving (13)-(17) with appropriately chosen coefficients (table 3.1) reproduces growth and saturation of bedforms from a perturbed flat surface, and evolving bedforms display nonuniform geometries characteristic of natural topography (Fig. 3.4). Additionally, celerity is roughly inversely related to bedform height, and merging of bedforms occurs due to varying migration speeds (as in experiments by Coleman and Melville, 1994) in a manner similar to models of eolian ripple development (Caps and Vandewalle, 2001; Prigozhin, 1999; Schwämmle and Herrmann, 2004). In contrast to these previous eolian models where the coarsening of bedforms continues until there is only one bedform in the model domain, the steady-state solution of our model consists of a train of bedforms. Steady state for model output is verified by computing α, w_x and l_x at several different times to ensure there is no systematic drift.

Cross-stream diffusion provides sufficient coupling to generate sinuous-crested bedforms whose width occupies the entire model domain (Fig. 3.4a). Crestline terminations, or defects, are observed to migrate through the system faster than the bedforms, as postulated by Werner and Kocurek (1997), and seen in previous numerical simulations (Caps and Vandewalle, 2001; Yizhaq et al., 2004). In contrast to Werner and Kocurek (1999; see also Werner, 1999) who treat bedform crestlines and defects as independent dynamical variables, crestlines and defects in our model arise naturally from the local coupling of sediment transport to topography, and so are a consequence rather than a cause of the dynamics. In the deterministic scenario, $\zeta = 0$ for $t > 0$, nonuniform transient evolution occurs because of the spatial noise inherited from initial conditions. At

long time, the bedforms evolve toward uniform, straight-crested features. In other words, the final state of the deterministic model is a static state (in a lagrangian frame), with only one scale of topography.

The growth of bed roughness with time can be quantified by calculating the interface width of downstream profiles over the entire model domain for each time step using (1). To facilitate comparison to previous data, interface width and model time are scaled by their respective equilibrium values, or the values corresponding to saturation of roughness growth. Several authors (e.g., Baas, 1994; Niño et al., 2002) have found experimentally that bedform growth is fit well by an exponential function of the form

$$\frac{w}{w_{eq}} = 1 - e^{-\gamma \frac{t}{t_{eq}}}, \tag{18}$$

where $\gamma = 6$ provides a good fit to most data (see also Nikora and Hicks, 1997) and the subscript *eq* denotes equilibrium values. Equation 18 with $\gamma = 6$ provides an excellent fit to the growth of bed roughness for the deterministic model (Fig. 3.5a), implying the essential dynamics of bedform development are captured in the model. In another set of experiments reported by Nikora and Hicks (1997), a power law relationship was observed:

$$\frac{w}{w_{eq}} = \begin{cases} \left(\frac{t}{t_{eq}}\right)^{\beta}; t < t_{eq} \\ 1; t \geq t_{eq} \end{cases}, \tag{19}$$

where β, the growth exponent (as in Barabási and Stanley, 1995), was found to be 0.28 under the laboratory conditions examined. This power law relation does not fit the deterministic model data, a topic we return to below.

The general model behavior is not very sensitive to changes in values of the coefficients. The bedform instability is present if B is positive, and sinuous-crested bedforms develop as long as there is a weak lateral coupling via diffusion. We verified numerically that spatial and temporal scaling are unaffected by varying coefficients – only growth rate and amplitude of bed features change.

3.4.2. Stochastic model

Addition of noise has a profound influence on bedform dynamics and spatial scaling. Low amplitude noise (run S – see table 3.1) produces growth of bed roughness from a flat surface that is well-fit by Nikora and Hicks' (1997) power-law relation (19), as seen in figure 3.5b. In other words, the presence of noise shifts the development of roughness from an exponential to a power law trajectory, and ultimately increases the saturation amplitude of bed features.

From a cursory glance it is apparent that bedforms of many scales co-exist on the fully developed model interface (Fig. 3.6) with 2D morphology that compares well to bedforms measured in the North Loup River (Fig. 3.1a). Stacked sequential profiles from the model at steady state show bedforms that are continuously varying in shape (Fig. 3.6b), with the emergence and disappearance of bedforms being an ongoing process. Perhaps the most notable aspect of the stochastic model results is their qualitative

similarity to steady-state dynamics observed in the river data. Sequential profiles generated by the model clearly show larger dune-like topography mantled with smaller ripple-like topography that spontaneously emerges in the troughs of the larger forms and rapidly moves over their stoss sides (Fig. 3.6c). The ripple-like forms grow in amplitude as they migrate across the stoss sides of the larger bedforms, only to be absorbed by the lee faces of the larger forms. This disappearance of the smaller bedforms provides the mass that causes the larger forms to migrate downstream. As observed for river dunes, modeled bedforms become unrecognizable after migrating one to two wavelengths downstream.

We compare the spatial roughness scaling of our noisy model to data from the North Loup River using eqs. (1) and (2), where w and l are normalized by their transition values w_x and l_x, respectively (Fig. 3.7). The roughness exponent for the model, computed over the scaling regime, is 0.56, in reasonable agreement with the North Loup River. More importantly, the form of the roughness scaling curve from the North Loup River is reproduced by our noisy model results (Fig. 3.7). In particular, the existence of a large dominant wavelength, and a continuum of scales below that wavelength, along with the long cross-over to saturation, are captured by the model.

3.5. Discussion

The striking difference in dynamical behavior between deterministic and noisy simulations provides insight into the importance of transport fluctuations in determining bed roughness properties. To gain an understanding of the physical processes controlling temporal growth of roughness we compare sediment transport conditions of two

experimental studies. Transport stage is defined as $T = \psi/\psi_c$, where $\psi = \tau_b /[(\rho_s - \rho_f)d_{50}g]$ is the dimensionless shear stress, ψ_c is the critical value for initiation of motion of grains, ρ_s and ρ_f are the sediment and fluid density, respectively, and g is acceleration due to gravity . The exponential growth of bed roughness corresponds to low transport stage, while power law growth occurs at high transport stage. Niño et al. (2002) conducted all experiments in the range $2 < T < 3.3$, and their bedform growth curves (see their figure 10) are close to the exponential relation (18). Flume runs reported by Nikora and Hicks (1997) span the range $9 < T < 30$ and display the power-law growth described by (19). Larger T certainly corresponds to larger fluctuations in sediment flux from direct influences of turbulence on bedload transport, and from suspended sediment transport where fluctuations in fluid stress have a greater influence.

The match of deterministic and stochastic model runs to the empirical exponential and power law growth relations, respectively, implies that in some sense the equations are capturing the features of sediment transport relevant to bedform evolution. Exponential growth of roughness in time is generally predicted for linear instabilities, while power law growth is a generic process of noisy interfaces (Barabási and Stanley, 1995). The effect of noise in our model is to induce more rapid bedform growth early on, such that large roughness amplitude is achieved rapidly and hence the nonlinearity governs growth. Coleman et al. (2005) fit power-law growth relations to data over a range $3.4 < T < 32.9$. In reality, there is likely a gradual transition between exponential and power-law growth such that the respective relations are two end members in a

spectrum. Indeed, numerical experiments with very low amplitude noise (not shown here) exhibit roughness growth intermediate between exponential and power law.

At long time, deterministic simulations evolve toward a steady state of uniform, periodic, straight-crested bedforms, i.e. a static steady state. Once the sediment flux field is exactly in phase with topography, evolution stops and the cross-stream diffusion ensures that all lateral variability disappears. This final state is not representative of trains of dunes in natural rivers. The long-time evolution of stochastic model runs consists of a bed that is continuously varying, but in statistical steady state. The mechanistic explanation for this phenomenon is that noise creates small perturbations on the stream-bed that allow the growth of instabilities from the governing equations. The growth of new bedforms is balanced by the disappearance of bedforms in the troughs of larger features. The bed remains continuously dynamic because the sediment flux can never be exactly in phase with topography, and hence nonuniform divergences in sediment flux force continuous adjustments of bedforms.

3.6. Conclusions

The model results obtained here are for a uniform sediment size on a freely deformable surface (i.e. no nonerodible areas exist on the bed). Pattern formation in this model is robust, as evidenced by the lack of sensitivity to model coefficients. Robustness of pattern formation implies that the details of fluid flow may not be important for a first-order description of the bed dynamics.

There is much to explore in the dynamics of our model system (13)-(17), and the analyses presented here are meant only to demonstrate the promise of this approach. A

great advantage of the model is its flexibility, which will allow examination of unsteady flow and complex boundary conditions in order to address issues relevant to river management. The fluid enters into the problem only through a small, interpretable set of coefficients that may be related to measured quantities. Equations 13-17 represent a unified model for subaqueous bedform dynamics because they provide a description of bedform initiation, development and steady-state behavior. Further, bedforms of different scales arise from the same fundamental transport processes. Variability in the geometry and kinematics of bedforms is a consequence of the deterministic relationship between sediment flux and topography, and noise.

Modeled bedforms are self-organized in the sense that large-scale features arise from a completely local description of bed evolution, i.e. bedforms are produced from interactions between adjacent grid points in the model. Measurements of fluid flow around static bedforms show that topography can generate long-range disturbances in the flow field, in the form of turbulence production and coherent flow structures (Nelson et al., 1993; McLean et al., 1994; Best et al., 1997; Maddux et al., 2004a,b). While the flow structure undoubtedly influences sediment transport, nonlocal effects introduced by turbulent fluid flow may be of second-order importance in determining the large-scale structure of the stream-bed. At the very least, this modeling approach shows that a completely local, geometric description of topographic evolution can generate realistic bedform dynamics, and even quantitatively model bedform growth (Fig. 3.5) and spatial scaling (Fig. 3.7). The presence of uncorrelated noise is sufficient to induce a dynamic steady state comparable to natural rivers. These results suggest that the presence of turbulence is important in terms of a perturbation source, but the structure of turbulence

may be less important in terms of transport (Sumer et al., 2003) and bedform dynamics. A systematic numerical exploration of the structure (distribution) of noise and its influence on model behavior is necessary to address this issue, but is beyond the scope of this paper. We have observed no effect on scaling when the stochastic term is changed from gaussian to uniformly-distributed white noise.

An improved understanding of bedform evolution is required to predict the stage-discharge relationship in sand-bedded rivers (e.g., Allen, 1973; Levey at al., 1980), and also to interpret bedform geometry from preserved cross-beds in the stratigraphic record (Chapter 4). Dunes and ripples determine the flow resistance in sandy channels because they are the principle roughness elements on the bed. The manner in which bedforms adjust in space and in time determines, to a large extent, the cross-sectional geometry of a channel, because bottom roughness adjusts much more rapidly than channel width. The model presented here can be used to explore the response of a channel bottom to changes in sediment transport conditions. In future work we will calibrate the model to field and laboratory data.

Acknowledgements

This project was motivated by discussions with the "Novel methods for modeling the surface evolution of geomorphic interfaces" Working Group, held in May, 2004 at MIT and sponsored by the National Center for Earth-surface Dynamics. We acknowledge supportive and constructive reviews by Chris Paola, Vladimir Nikora, Stephen Coleman and Jon Pelletier. In addition, Brad Murray, Brandon McElroy and Wes Watters provided very helpful and stimulating discussions. McElroy also made invaluable contributions to

data analysis of the North Loup River. This work was supported by the STC Program of the National Science Foundation via the National Center for Earth-surface Dynamics under Agreement Number EAR-0120914.

References

Allen, J.R.L., Phase differences between bed configuration and flow in natural environments, and their geological relevance, *Sedimentology*, *20*, 323-329, 1973.

Ashley, G., Classification of large-scale subaqueous bedforms: A new look at an old problem, *J. Sed. Petr.*, *60*, 160-172, 1990.

Baas, J.H., A flume study on the development and equilibrium morphology of current ripples in very fine sand, *Sedimentology*, *41*, 185-209, 1994.

Barabási, A.-L., and H.E. Stanley, Fractal concepts in surface growth, *Cambridge Univ. Press*, Cambridge, UK, 366pp, 1995.

Best, J., S. Bennett, J. Bridge and M. Leeder, Turbulence modulation and particle velocities over flat sand beds at low transport rates, *J. Hydraul.. Eng., 123*, 1118-1129, 1997.

Caps, H., and N. Vandewalle, Ripple and kink dynamics, *Phys. Rev. E*, *64*, 041302, 2001.

Coleman, S.E., and B.W. Melville, Bed-form development, *J. Hydraul. Eng.*, *120*, 544-560, 1994.

Coleman, S.E., and B.W. Melville, Initiation of bed forms on a flat sand bed, *J. Hydraul. Eng.*, *122*, 301-310, 1996.

Coleman, S.E., M.H. Zhang, and T.M. Clunie, Sediment-wave development in subcritical water flow, *J. Hydraul. Eng.*, *131*, 106-111, 2005.

Csahók, Z., C. Misbah, F. Rioual, and A. Valance, A class of nonlinear front evolution equations derived from geometry and conservation, *Physica D*, *128*, 87-100, 1999.

Csahók, Z., C. Misbah, F. Rioual, and A. Valance, Dynamics of aeolian sand ripples, *Euro. Phys. J. E*, *3*, 71-86, 2000.

Dodds, P.S., and D.H. Rothman, Scaling, Universality and Geomorphology, *Ann. Rev. Earth Planet. Sci.*, *28*, 571-610, 2000.

Engelund, F., Instability of erodible beds, *J. Fluid. Mech., 42*, 225-244, 1970.

Exner, F.M., Uber die Wechselwirkung zwischen Wasser und Geschiebe in Flüssen, *Sitzungsbericht Akad. Wiss. Wien, Abt. IIa 134*, 166-204, 1925 (in German).

Fernandez-Luque, R., and R. van Beek, Erosion and transport of bed-load sediment, *J. Hydraul Res.*, *14*, 127-144, 1976.

Gabel, S.L., Geometry and kinematics of dunes during steady and unsteady flows in the Calamus River, Nebraska, USA, *Sedimentology, 40*, 237-269, 1993.

Gomez, B., R.L. Naff and D.W. Hubbell, Temporal variations in beload transport rates associated with the migration of bedforms, *Earth Surf. Proc. Land.*, *14*, 135-156, 1989.

Gomez, B., and J.D. Phillips, Deterministic uncertainty in bed load transport, *J. Hydraul. Eng., 125*, 305-308, 1999.

Hersen, P., On the crescentic shape of barchan dunes, *Euro. Phys. J. B*, *37*, 507-514, 2004.

Hino, M., Equilibrium-range spectra of sand waves formed by flowing water, *J. Fluid. Mech.*, *34*, 565-573, 1968.

Howard, A.D., A detachment-limited model of drainage basin evolution, *Water Resour. Res.*, *30*, 2261-2285, 1994.

Jain, S.C., and J.F. Kennedy, The spectral evolution of sedimentary bed forms, *J. Fluid Mech.*, *63*, 301-314, 1974.

Leclair, S.F., Preservation of cross-strata due to the migration of subaqueous dunes: An experimental investigation, *Sedimentology, 49*, 1157-1180, 2002.

Levey, R.A., B. Kjerfve, and R.T. Getzen, Comparison of bed form variance spectra within a meander bend during flood and average discharge, *J. Sed. Petr.*, *50*, 149-155, 1980.

Maddux, T. B., J. M. Nelson, and S. R. McLean, Turbulent flow over three-dimensional dunes: 1. Free surface and flow response, *J. Geophys. Res.*, *108*, 6009, doi:10.1029/2003JF000017, 2003.

Maddux, T. B., S. R. McLean, and J. M. Nelson, Turbulent flow over three-dimensional dunes: 2. Fluid and bed stresses, *J. Geophys. Res.*, *108*, 6010, doi:10.1029/2003JF000018, 2003.

McLean, S.R., The stability of ripples and dunes, *Earth-Sci. Rev.*, *29*, 141-144, 1990.

McLean, S.R., J.M. Nelson and S.R. Wolfe, Turbulence structure over two-dimensional bed forms: Implications for sediment transport, *J. Geophys. Res., 99*, 12729-12747, 1994.

Meyer-Peter, E., and R. Müller, Formulas for bed-load transport, *Int. Assoc. Hydraul. Res., 2nd Meeting*, Stockholm, pp.39-64, 1948.

Mohrig, D., Spatial evolution of dunes in a sandy river, Ph. D. dissertation, 119 pp., Univ. of Wash., Seattle, 1994.

Mohrig, D and J.D. Smith, Predicting migration rates of subaqueous dunes, *Water Resour. Res., 32*, 3207-3217, 1996.

Murray, A.B., and C. Paola, Properties of a cellular braided-stream model, *Earth Surf. Proc. Land., 22*, 1001-1025, 1997.

Nelson, J.M., S.R. McLean, and S.R. Wolfe, Mean flow and turbulence fields over two-dimensional bed forms, *Water Resour. Res., 29*, 3935–3953, 1993.

Nelson, J.M, R.L. Shreve, S.R. McLean and T.G. Drake, Role of near-bed turbulence structure in bed load transport and bed form mechanics, *Water Resour. Res., 31*, 2071-2086, 1995.

Nikora, V.I., and D.M. Hicks, Scaling relationships for sand wave development in unidirectional flows, *J. Hydraul. Eng., 123*, 1152-1156, 1997.

Nikora, V.I., A.N. Sukhodolov, and P.M. Rowinski, Statistical sand wave dynamics in one-directional water flows, *J. Fluid Mech., 351*, 17-39, 1997.

Niño, Y., A. Atala, M. Barahona and D. Aracena, Discrete particle model for analyzing bedform development, *J. Hydraul. Eng., 128*, 381-389, 2002.

Nordin, C.F., Statistical properties of dune profiles, *U.S. Geol. Survey, Prof. Paper* 562-F, 1971.

Parker, G., Lateral bed load transport on side slopes, *J. Hydraul. Eng.*, *110*, 197-199, 1984.

Pelletier, J.D., Self-organization and scaling relationships of evolving river networks, *J. Geophys. Res.*, *104*, 7359-7375, 1999.

Press, W.H., S.A. Teukolsky, W.T. Vetterling, and B.P. Flannery, Numerical Recipes in C, Cambidge U. Press, Cambridge, 1988.

Prigozhin, L., Nonlinear dynamics of Aeolian sand ripples, *Phys. Rev. E*, *60*, 729-733, 1999.

Rubin, D.M, Use of forecasting signatures to help distinguish periodicity, randomness, and chaos in ripples and other spatial patterns, *Chaos*, *2*, 525-535, 1992.

Schmeeckle, M.W., and J.M. Nelson, Direct simulation of bedload transport using a local, dynamic boundary condition, *Sedimentology, 50*, 279-301, 2003.

Schwämmle, V., and H. Herrmann, Modelling transverse dunes, *Earth Surf. Proc. Land.*, *29*, 769-784, 2004.

Shimizu, Y., M.W. Schmeeckle, and J.M. Nelson, Three-dimensional calculation of flow over two-dimensional dunes, *Japan Soc. Civil Eng. Ann. J. Hydraul. Eng*, *43*, 623-628, 2000.

Smith, J.D., Stability of a sand bed subjected to a shear flow of low Froude number, *J. Geophys. Res.*, *75*, 5928-5940, 1970.

Soo, S.L., Ed., Instrumentation for Fluid-Particle Flow. *William Andrew Publishing*, 412 pp., 1999.

Sumer, B.M., L.H.C. Chua, N.-S. Cheng, and J. Fredsøe, Influence of turbulence on bed load sediment transport, *J. Hydraul. Eng., 129*, 585-596, 2003.

Terzidis, O., P. Claudin and J.P. Bouchaud, A model for ripple instabilities in granular media, *Euro. Phys. J. B, 5,* 245-249, 1998.

Tufillaro, N.B., Discrete dynamical models showing pattern formation in subaqueous bedforms, *Int. J. Bifurcations Chaos, 3*, 779-784, 1993.

Valance, A., and F. Rioual, A nonlinear model for aeolian sand ripples. *Euro. Phys. J. B, 10*, 543-548, 1999.

van den Berg, J.H., Bedform migration and bed-load transport in some rivers and tidal environments, *Sedimentology, 34*, 681-698, 1987.

Werner, B.T., Eolian dunes: Computer simulations and attractor interpretation, *Geology, 23*, 1107-1110, 1995.

Werner, B.T., Complexity in natural landform patterns, *Science, 284*, 102-104, 1999.

Werner, B.T, and G. Kocurek, Bed-form dynamics: does the tail wag the dog?, *Geology, 25*, 771-774, 1997.

Werner, B.T, and G. Kocurek, Bedform spacing from defect dynamics, *Geology, 27*, 727-730, 1999.

Wiberg, P. L., and J. D. Smith, Model for calculating bed load transport of sediment, *J. Hydraul. Eng., 115,* 101-123, 1989.

Willgoose, G., R.L. Bras, and I. Rodriguez-Iturbe, A coupled channel network growth and hillslope evolution model: 1. Theory, *Water Resour. Res., 27*, 1671-1684, 1991.

Yizhaq, H., N.J. Balmforth, and A. Provenzale, Blown by wind: nonlinear dynamics of aeolian sand ripples, *Physica D*, 207-228, 2004.

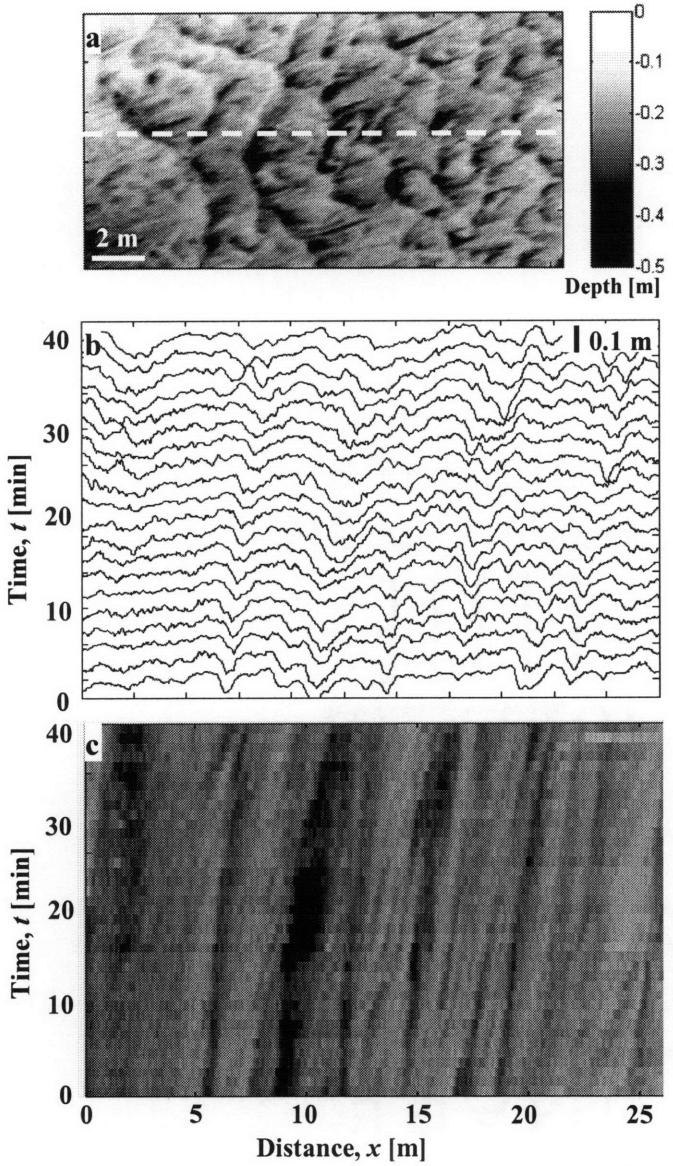

Figure 3.1. North Loup River topography extracted from images. Flow is from left to right for this and all figures. (a) Plan view snapshot in time of channel bottom, where brighness corresponds to water depth. Dashed line represents location of profiles in (b) and (c). (b) Sequential stream-bed profiles, shown every 120 s with vertical offset to allow visualization. (c) Space-time plot of sequential stream-bed profiles shown every 60 s, with elevation represented by brightness. Bedform crests and troughs are light and dark, respectively. Color scale same as (a).

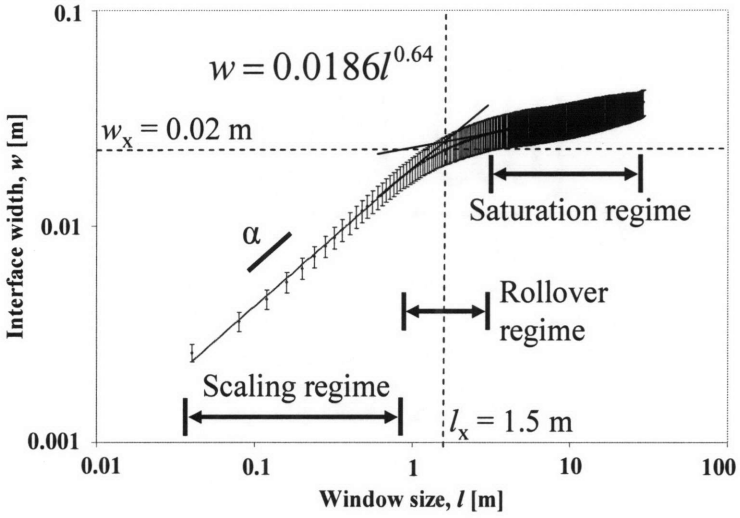

Figure 3.2. Example of North Loup River spatial scaling of roughness for 20 downstream profiles, averaged at a snapshot in time. Interface width grows as a power law in the scaling regime, with the slope equal to the roughness exponent, α; equation is a best-fit linear regression to log-log data. Growth rolls over at the transition length, l_x, with corresponding roughess value, w_x. Error bars represent one standard deviation.

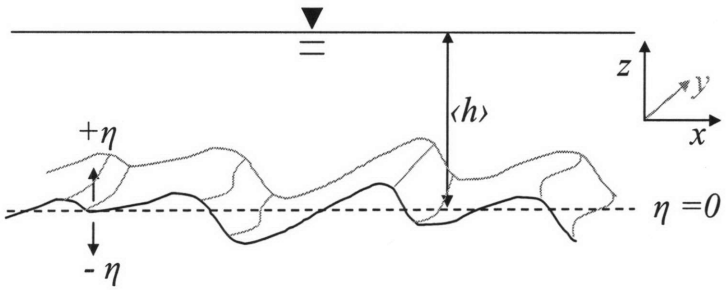

Figure 3.3. Definition sketch of the model shown in oblique perspective, with coordinate axes displayed. The mean elevation of the sediment-fluid interface (channel bottom) is shown by the dashed line, which is defined as $\eta = 0$ and used as the datum for mean water depth, $\langle h \rangle$. Elevations above and below this line are positive and negative, respectively.

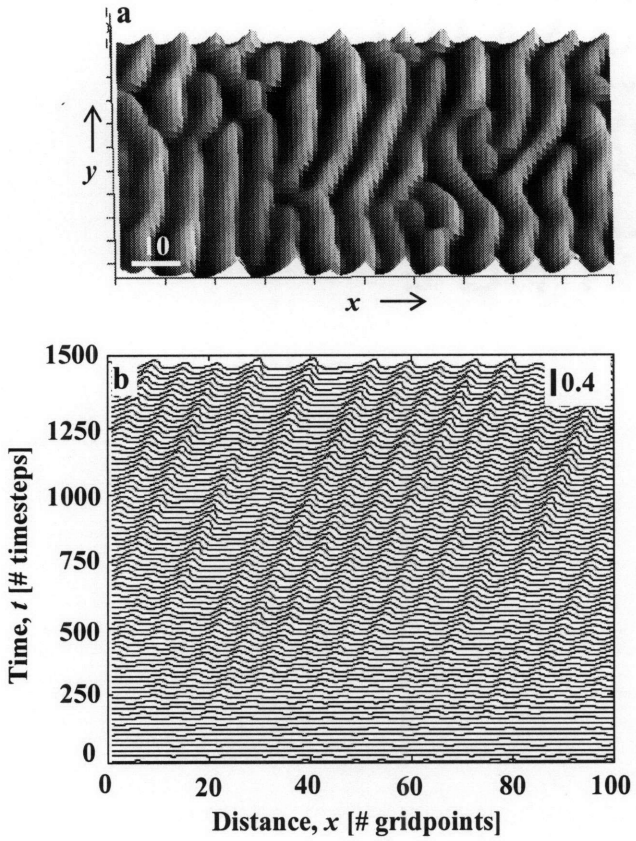

Figure 3.4. Deterministic model (run D, table 3.1) evolution. (a) Oblique view snapshot of transient evolution of bed surface, at time = $1500\Delta t$. (b) Profile down the centerline of the 2D model domain, showing growth of bedforms from a flat surface. Compare to figure 3.4 of Coleman and Melville (1996). Profiles are plotted every $20\Delta t$ from zero up to time $=1500\Delta t$.

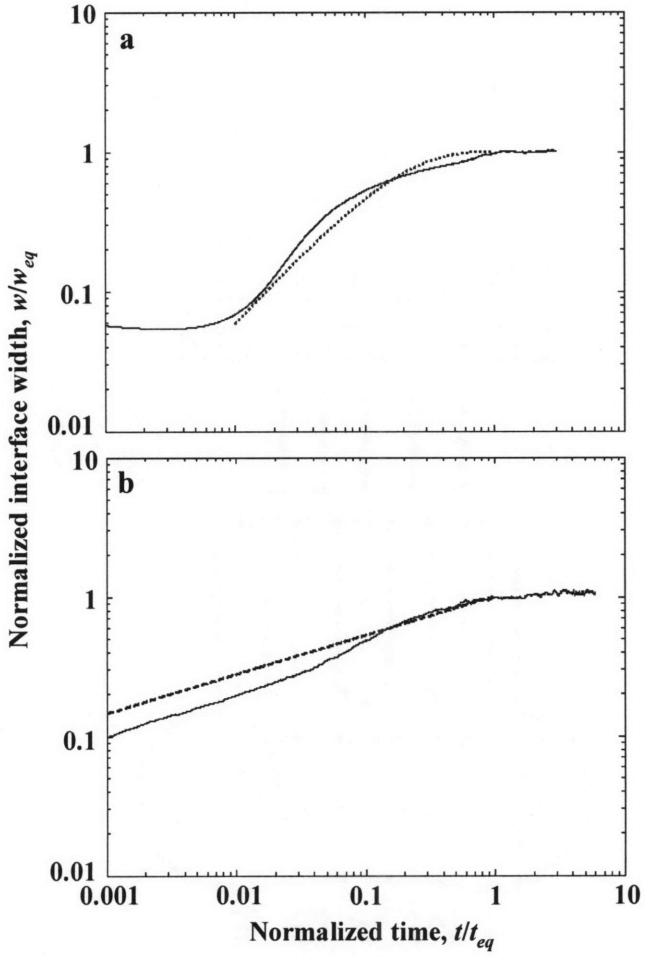

Figure 3.5. Growth of roughness in time from a flat surface, calculated from averaging all downstream profiles at each time step, for (a) deterministic, and (b) noisy simulations. Dotted line is the exponential growth relation (18) in the text with $\gamma = 6$, while dashed line is the power law growth relation (19) with $\beta = 0.28$. Interface width and time are scaled by their respective equilibrium values; see text for details. Relations (18) and (19) were derived from flume studies, and were not fit to model data.

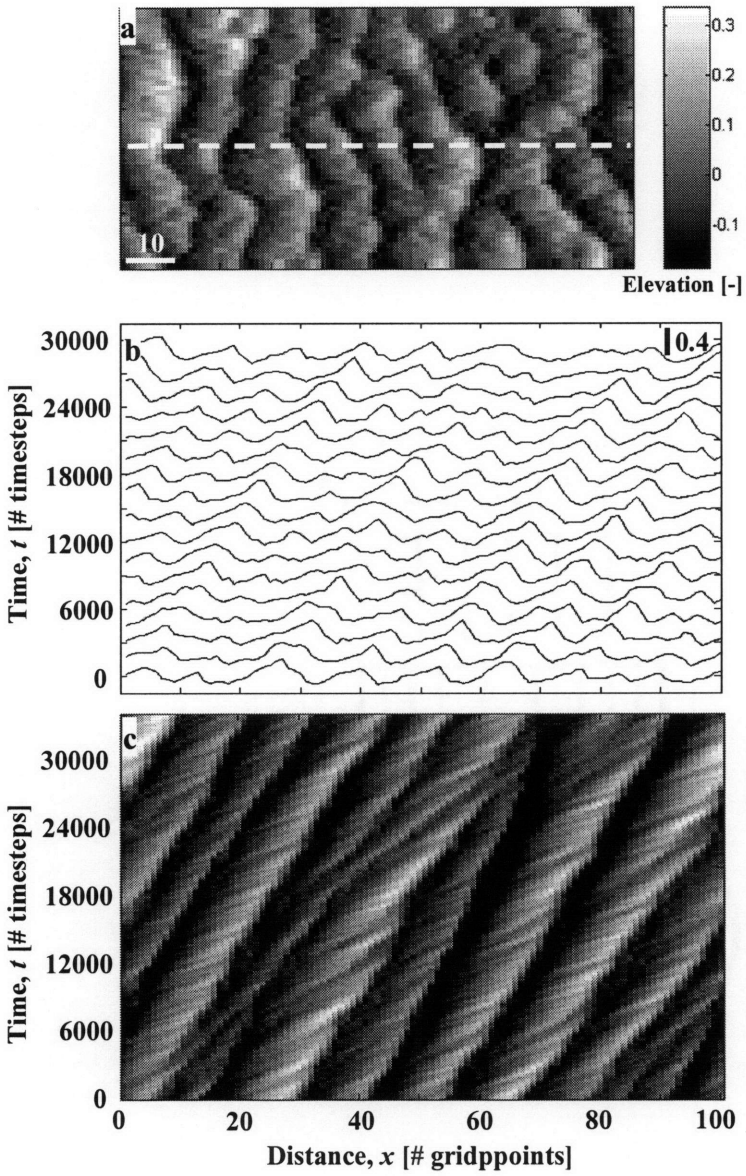

Figure 3.6. Stochastic model topography (run S, table 3.1) where roughness is in statistical steady state – compare to Fig. 3.1. (a) Plan view snapshot. (b) sequential profiles shown every $1500\Delta t$. (c) Space-time plot of sequential profiles shown every time step. Initial conditions for model run were a flat bed with low amplitude, random perturbations.

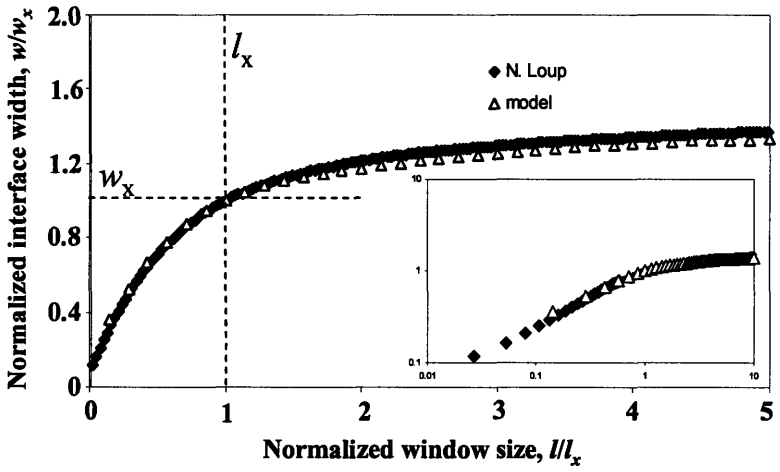

Figure 3.7. Example of spatial scaling of roughness for stochastic model (run S) and North Loup River at statistical steady state using a downstream profile at a snapshot in time; w and l are normalized by their transition values. See caption of Fig. 3.2 for explanation – note linear scale. Inset is the same data plotted on a log-log scale. No calibration was performed to match model with river data.

Table 3.1. Model parameters used for all runs – see equations 13-17.

Parameter	D	S
Δx	0.1	0.2
Δt	0.005	0.002
A	4.3	4.3
B	4.3	4.3
D	0.025	0.025
E	1	1
ζ	0	0.1(*randn*)
τ_b	0.07	0.07
$\langle h \rangle$	1	1
m	1	1
n	1.5	1.5
θ_c (°)	34	34
p	0.4	0.4

Boundary conditions are periodic in the downstream (x) direction and zero flux in the cross-stream (y) direction; the noise term ζ = 0.1(*randn*), where *randn* represents a random variable having a normal distribution with zero mean and variance of one. D and S refer to model runs where D means deterministic and S means stochastic. Units are arbitrary unless specified.

Chapter 4

Frozen dynamics of migrating bedforms[3]

D.J. Jerolmack and D. Mohrig

Department of Earth, Atmospheric and Planetary Sciences, Massachusetts Institute of Technology, Cambridge, Massachusetts 02139, USA

Abstract

Here we show how a continuum granular flow model can replicate realistic self-organizing subaqueous bedforms, and we explore how a record of this dynamic topography is transferred into the substrate where it can be fossilized. Modeled bedform behavior is quantitatively compared to laboratory and field data. Sediment scouring and deposition by migrating bedforms produces sets of partially preserved bedforms recording nonlinear behavior at the sediment-fluid interface. Model results show the importance of spatial and temporal variations in bedform size and migration rate to the generation of sets. Addition of net bed aggradation to modeled bedforms allows us to explore the preservation of topography under a wide range of depositional conditions. We present new relationships among aggradation rate, bedform migration rate, and set thickness. Variability of set thickness is shown to be a product of the competition between bed aggradation and bedform migration rates. These results show how using the entire distribution of set thickness for ancient strata can refine estimates of the formative paleoenvironmental conditions.

---

[3] From Jerolmack, D., and D. Mohrig, Frozen dynamics of migrating bedforms, *Geology*, *33*, 57-60, 2005.

4.1. Introduction

Dunes and ripples are ubiquitous on the sandy beds of rivers (Gabel, 1993; Mohrig, 1994; Carling et al., 2000), yet their behavior remains incompletely understood because of complex feedbacks among fluid flow, sediment transport, and the evolving bottom topography itself (Rubin, 1992; Nelson et al., 1995). Evidence is mounting that the sediment-fluid interface exhibits its own dynamic that may only weakly depend on the details of a particular system (Tufillaro, 1993; Werner, 1995). For example, a phenomenological continuum granular flow model designed to describe the topographic evolution of surfaces constructed from grain avalanches (known as the BCRE, after Bouchaud, Cates, Ravi Prakrash and Edwards, 1995), has been adapted to describe the morphologic evolution of eolian ripples (Terzidis et al., 1998; Valance and Rioual, 1999) and also inspired models for barchan dunes (Sauermann et al., 2001; Hersen et al., 2004). We use the one-dimensional BCRE model to describe the evolution of bed topography within trains of subaqueous dunes. This model is run under a range of depositional conditions so that we can connect the statistics of bedform kinematics to the statistics of resulting stratigraphy.

The first of two equations composing the BCRE model describes conservation of mass for a grain layer (bed-load layer) moving above the static granular bed below. This moving grain layer has a velocity, v, that is constant for simplicity, and a varying thickness, R, defined by

$$\frac{\partial R}{\partial t} = -\frac{\partial (vR)}{\partial x} - \frac{\partial z}{\partial t}, \qquad (1)$$

where x is along-stream distance, z is elevation of the static bed above a datum, and t is time. The exchange of mass between moving and static grains is governed by the nonlinear relationship

$$\frac{\partial z}{\partial t} = -R\Lambda \frac{\partial z}{\partial x}, \tag{2}$$

where Λ is a constant representing frequency of grain contact with the bed (Terzidis et al., 1998); sediment flux is $q_s = vR$, and bed-migration speed (celerity) is $c = R\Lambda$. The moving grain layer erodes the static bed on positive (stoss) slopes and deposits on negative (lee) slopes. Although Terzidis et al. (1998) and Valance and Rioual (1999) introduced higher-order terms to the BCRE model to aid simulation of the instability governing onset of eolian ripple formation, these terms are unnecessary for modeling the long-time evolution of subaqueous bedforms.

Numerically integrating equations 1 and 2 generates an interface made up of topographic elements having appropriate asymmetric shapes, as well as distribution of sizes and migration rates (Fig. 4.1). The BCRE model also reproduces interactions between subaqueous bedforms—particularly splitting and merging—that are characteristic of their statistically defined steady state (e.g., Allen, 1976). While the model is certainly oversimplified, these results indicate that parameterizing sediment flux in terms of local bed slope can explain some of the dynamic behavior of bedforms. Exploration of nonlinear interactions between topographic elements by using interface equations should not be limited to the study of active bedforms. Migrating bedforms impart a structure within beds of sediment and thereby preserve a fossilized record of

interface evolution (Fig. 4.2). We present here an adaptation of the BCRE model relating the dynamics of bedform interactions to the production of sedimentary structures and show how the record of nonlinear behavior at the sediment-fluid interface is embedded in sedimentary deposits.

Preserved bedform structures are some of the most common features used to reconstruct ancient flow conditions on the surface of the Earth and now possibly Mars. Dunes and ripples migrating on a bed leave distinct records in the substrate as a result of size sorting of particles on their lee faces (Anderson and Bunas, 1993; Makse, 2000; Blom et al., 2003) and because scouring, focused in the troughs of the bedforms, produces erosional surfaces that are preserved in the sedimentary deposits (Leclair 2002; Blom et al., 2003) (Fig. 4.2). The deposit preserved between successive erosional surfaces is referred to as a set (Fig. 4.3). Each set is made up of sediment added to the downstream face of a bedform that was not reeroded during passage of following troughs, so the rates of both bedform migration and aggradation should influence set thickness. Failure by subsequent troughs to scour down to the level required to remove all record of preceding bedforms is the combined result of (1) a rise through time in elevation of all troughs as the surface across which the dunes are moving aggrades (Allen, 1970, 1973; Ashley et al., 1982; Rubin, 1987) and (2) random variability in elevations of consecutive dune troughs (Paola and Borgman, 1991; Bridge, 1997). Rubin (1987) presented a geometric model showing how structures are produced by uniform bedforms under conditions of bed aggradation or net sediment deposition. Kolmogorov (1951) pioneered the study of stratigraphy as a stochastic process, and later Paola and Borgman (1991) developed an exact relationship between set thickness and the probability-density function

describing the distribution of bedform height in the limit of no net sediment accumulation (aggradation rate, $r = 0$). Our ability to reconstruct environmental conditions from the sedimentary patterns preserved in rocks is limited by our ability to model the dynamics of the topography that generates those patterns (Paola, 2000). We show here how the BCRE model can be used to make this connection, opening up the vast library of frozen interface behavior preserved in sedimentary rocks and deposits to contribute to studies of the sediment-fluid interface.

4.2. Model Results

Starting from a random initial topography, the BCRE model evolves to a statistical steady-state comparable to a natural river bottom (Fig. 4.1). The evolution of topography using this model, however, depends in a nontrivial manner on initial conditions, as bedforms cannot grow to a height larger than the initially prescribed elevation range. In other words, we need to begin a simulation with high-amplitude random topography rather than a flat surface with a small perturbation. Although the BCRE model does not contain the relevant physics to describe initial growth of bedforms, it does produce topography having geometric and kinematic behavior that compares well to subaqueous ripples and dunes. By calibrating mean celerity and sediment flux to measured field values (Mohrig, 1994), the model generates topography that deforms at reasonable rates so that distributions of bedform height and length are produced that are similar to the natural system (caption of Fig. 4.1). With this confirmation that the model can capture some of the elementary spatial and temporal adjustments within a field of natural subaqueous topography, we map the erosional surfaces that would be found in the

substrate owing to passage of a succession of modeled bedforms (Fig. 4.3). This approach is unique in that we combine variability of bedform size (e.g. Paola and Borgman, 1991), net bed aggradation (e.g. Allen, 1970) and bedform deformation in time, allowing us to explore the combined importance of these factors on generation of stratigraphy. In the limit of no net bed aggradation, expected mean set thickness, s_m, is calculated from the mean value of the exponential tail of a gamma function, β, fit to the bedform height probability-density function (Paola and Borgman, 1991),

$$s_m = 0.8225\beta. \quad (3)$$

The distribution of sets generated by the BCRE model agrees with predictions from this exact stochastic relation; the measured value from model output shown in Figure 4.3A is $s_m = 0.0133$ m, and the predicted value for s_m using this equation is 0.0128 m.

Aggradation rate is introduced to the model by uniformly adding elevation to the model domain after each time step. Laboratory studies indicate that bedform size, shape, and celerity do not vary with aggradation (Allen, 1973; Bridge and Best, 1997; Leclair, 2002), justifying this simple treatment. Adding net sediment deposition to the model (Fig. 4.3B) yields values for mean set thickness consistent with all available laboratory data (Bridge and Best, 1997; Storms et al., 1999; Leclair, 2002; Fig. 4.4A). Results from the BCRE model show a linear increase in mean set thickness with aggradation rate (Fig. 4.4A), whereas variability of set thickness decreases with aggradation rate (Fig. 4.4B). Model results also indicate that set thickness weakly depends on whether aggradation rate or celerity is varied (Fig. 4.4C). In other words, the relationship between set thickness

and r/c is nonunique; increasing r while holding c constant essentially drapes more sediment over topography, enhancing preservation relative to the case where c is decreased and r held constant.

To account for aggradation, Bridge and Best (1997) proposed that

$$s_m = l_m(r/c) + 0.8225\beta, \quad (4)$$

where l_m is mean bedform length. Note that in the limit of uniform topography β becomes zero, and (4) reduces to the geometric relationship proposed by Allen (1970). All parameters in (4) can be measured for each numerical experiment, and we find that values of mean set thickness predicted from this equation are larger than measured values for all of our model runs; for the case shown in Figure 4.3B, $s_m = 0.0247$ m using (4), and measured $s_m = 0.0189$ m in the BCRE model. Laboratory results (Bridge and Best, 1997; Storms et al., 1999; Leclair, 2002) do not resolve an effect of aggradation rate on mean set thickness at low values of r/c (Fig. 4.4). We propose that the contribution from aggradation is masked in these cases because the constant aggradation rate is small relative to the natural variability in bedform migration rate. Leclair and Bridge (2001) argued that in most natural systems aggradation is small, especially for dunes, and therefore may be neglected in calculations of set thickness. We have measured local values for r/c up to 0.02 for dunes in the North Loup River, Nebraska, United States (Mohrig and Jerolmack, 2004). Model results show that aggradation contributes significantly to mean set thickness at values for r/c of 0.01 and greater (Fig. 4.4A). Large values of r/c are also commonly associated with climbing ripples (Allen, 1973; Ashley et

al., 1982). Further, bedforms in high-aggradation micro-environments are more likely to be preserved, so the contribution of aggradation may be significant for the majority of subaqueously-generated cross-beds preserved in outcrops.

4.3. Summary

Up to this point we have characterized the set-thickness distribution using only its first and second moments, even though the model predicts the entire distribution. This additional information will almost certainly prove useful in future analyses of the formative topography and environmental conditions. To illustrate, we compare model-generated distributions of set thickness to measured sets from a channel-filling deposit in the Jurassic Kayenta Formation, Utah, and the Oligocene Guadalope-Matarranya system, Spain (Fig. 4.5). Model results replicate the significant change in shape of the set-thickness distribution (Fig. 4.5) and relate this effect to a difference in r/c (Fig. 4.4B). If the correlations presented here are shown to be generally true for natural systems, then it is possible to estimate the relative importance of aggradation simply from the statistics of set thickness (Fig. 4.4B) and then to estimate formative bedform height (Fig. 4.4A). These results can be tested by laboratory experiments, using aggradation rates larger than those previously reported in the literature.

By capturing some of the time- and space-varying nature of bed topography with a simple, well-known granular flow model (Bouchaud et al., 1995), we have derived relationships between stratigraphy and its formative stream-bed conditions (Fig. 4.4). It is important to note that values inferred from relationships presented here do not require any assumptions of temporal or spatial uniformity of the bedforms (e.g. Allen, 1970), nor

are they limited to low-aggradation rates (e.g. Paola and Borgman, 1991). In this study we calibrated the model to data from a natural river (Fig. 4.1), but the coefficients can be varied to explore how different values for mean sediment flux and bedform migration rate affect the generation and preservation of stratigraphy. Our results show how interface equations (Bouchaud et al., 1995) capturing some of the proper kinematics of evolving topography can be used to unravel historical processes on the Earth's surface. While the exact relationships between set thickness and bed topography obtained here are a product of bedform behavior as generated by the BCRE model, the approach is more general. The generation of stratigraphy is a geometric problem, so a model that reproduces the relevant aspects of bed kinematics can be used to explore the production of sets. Improvements in models of bedform dynamics will improve our ability to invert formative topography from set thicknesses preserved in the field. Further, if sets can be related in a straightforward way to the topography that generated them, then the catalog of "frozen dynamics" contained in the rocks is an extensive data set that may be exploited in further developing models of the evolving sediment-fluid interface. For this reason the ancient sedimentary record should be considered an important additional data source for those interested in modern interface problems.

Acknowledgements

Support for our research was provided by the Science and Technology Center Program of the National Science Foundation, under Agreement Number EAR-0120914. This project benefited from stimulating discussions with Chris Paola, Wes Watters, and Brandon McElroy. Watters and McElroy also provided help with data analysis and modeling.

References

Allen, J.R.L., 1970, A quantitative model of climbing ripples and their cross-laminated deposits: Sedimentology, v. 14, p. 5-26.

Allen, J.R.L., 1973, Features of cross-stratified units due to random and other changes in bedforms: Sedimentology, v. 20, p. 189–202.

Allen, J.R.L., 1976, Computational models for dune time-lag: General ideas, difficulties, and early results: Sedimentary Geology, v. 15, p. 1–53.

Anderson, R.S., and Bunas, K.L., 1993, Grain size segregation and stratigraphy in aeolian ripples modelled with a cellular automaton: Nature, v. 365, p. 740–743.

Ashley, G.M., Southard, J.B., and Boothroyd, J.C., 1982, Deposition of climbing-ripple beds: A flume simulation: Sedimentology, v. 29, p. 67–79.

Blom, A., Ribberink, J.S., and de Vriend, H.J., 2003, Vertical sorting in bedforms: Flume experiments with a natural and trimodal sediment mixture: Water Resources Research, v. 39, no. 2, 1025, doi: 10.1029/2001WR001088.

Bouchaud, J.P., Cates, M.E., Ravi Prakrash, J., and Edwards, S.F., 1995, Hysteresis and metastability in a continuum sandpile model: Physical Review Letters, v. 74, p. 1982–1985.

Bridge, J.S., 1997, Thickness of sets of cross strata and planar strata as a function of formative bed-wave geometry and migration, and aggradation rate: Geology, v. 25, p. 971–974.

Bridge, J., and Best, J., 1997, Preservation of planar laminae due to migration of low-relief bed waves over aggrading upper-stage plane beds: Comparison of experimental data with theory: Sedimentology, v. 44, p. 253–262.

Carling, P.A., Gölz, E., Orr, H.G., and Radecki-Pawlik, A., 2000, The morphodynamics of fluvial sand dunes in the river Rhine, near Mainz, Germany: I. Sedimentology and morphology: Sedimentology, v. 47, *p.* 227–252.

Gabel, S.L., 1993, Geometry and kinematics of dunes during steady and unsteady flows in the Calamus River, Nebraska, USA: Sedimentology, v. 40, p. 237–269.

Hersen, P., Anderson, K.H., Elbelrhiti, H., Andreotti, B., Claudin, P., and Douady, S., 2004, Corridors of barchan dunes: Stability and size selection: Physical Review E, v. 69, 011304, doi: 10.1103/PhysRevE.69.011304.

Kolmogorov, A.N., 1951, Solution of a problem in probability theory connected with the problem of the mechanism of stratification: New York, American Mathematical Society, 8 p.

Leclair, S.F., 2002, Preservation of cross-strata due to the migration of subaqueous dunes: An experimental investigation: Sedimentology, v. 49, p. 1157–1180.

Leclair, S.F., and Bridge, J.S., 2001, Quantitative interpretation of sedimentary structures formed by river dunes: Journal of Sedimentary Research, v. 71, p. 713–716.

Makse, H.A., 2000, Grain segregation mechanism in aeolian sand ripples: European Physical Journal E, v. 1, p. 127–135.

Mohrig, D., 1994, Spatial evolution of dunes in a sandy river (Ph.D. thesis): Seattle, University of Washington, 119 p.

Mohrig, D., and Jerolmack, D., 2004, Adjustments within trains of dunes driving bar growth in a sandy braided channel: American Association of Petroleum Geologists, Abstracts Volume, v. 13, p. A98.

Nelson, J.M., Shreve, R.L., McLean, S.R., and Drake, T.G., 1995, Role of near-bed turbulence structure in bed load transport and bedform mechanics: Water Resources Research, v. 31, p. 2071–2086.

Paola, C., 2000, Quantitative models of sedimentary basin filling: Sedimentology, v. 47, p. 121–178.

Paola, C., and Borgman, L., 1991, Reconstructing random topography from preserved stratification: Sedimentology, v. 38, p. 553–565.

Press, W.H., Teukolsky, S.A., Vetterling, W.T., and Flannery, B.P., 1988, Numerical recipes in C: Cambridge, Cambridge University Press, 994 p.

Rubin, D.M., 1987, Cross-bedding, bedforms and paleocurrents: Tulsa, Society of Economic Paleontologists and Mineralogists, Concepts in Sedimentology and Paleontology, v. 1; 187p.

Rubin, D.M., 1992, Use of forecasting signatures to help distinguish periodicity, randomness, and chaos in ripples and other spatial patterns: Chaos, v. 2, p. 525–535.

Sauermann, G., Kroy, K., and Herrmann, H.J., 2001, Continuum saltation model for sand dunes: Physical Review E, v. 64, 031305, doi: 10.1103/PhysRevE.64.031305.

Storms, J.E.A., van Dam, R.L., and Leclair, S.F., 1999, Preservation of cross-sets due to migration of current ripples over aggrading and non-aggrading beds: Comparison of experimental data with theory: Sedimentology, v. 46, p. 189–200.

Terzidis, O., Claudin, P., and Bouchaud, J.P., 1998, A model for ripple instabilities in granular media: European Physical Journal B, v. 5, p. 245–249.

Tufillaro, N.B., 1993, Discrete dynamical models showing pattern formation in subaqueous bedforms: International Journal of Bifurcations and Chaos, v. 3, p. 779–784.

Valance, A., and Rioual, F., 1999, A nonlinear model for aeolian sand ripples: European Physical Journal B, v. 10, p. 543–548.

Werner, B., 1995, Eolian dunes: Computer simulations and attractor interpretation: Geology, v. 23, p. 1107–1110.

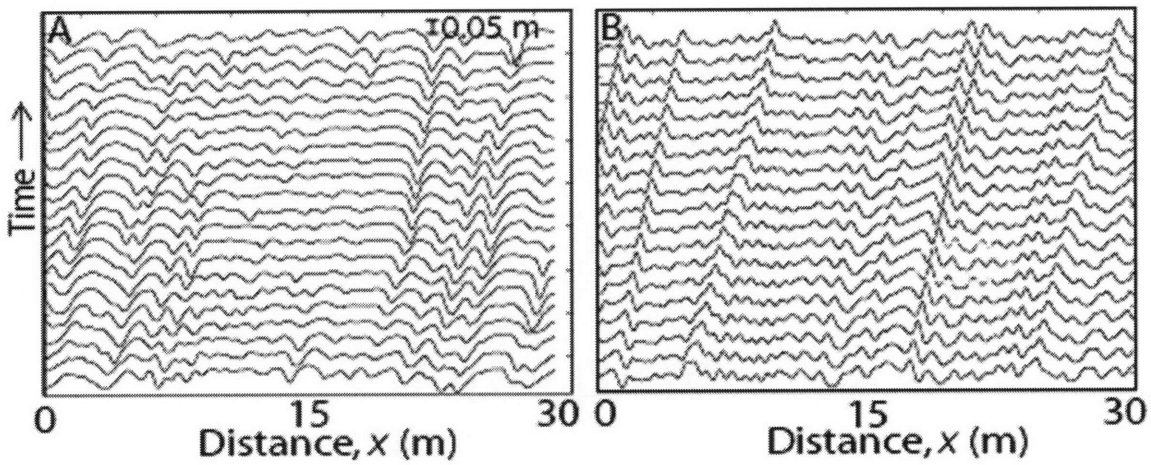

Figure 4.1. Comparison of sequential stream-bed elevation profiles. A: North Loup River, Nebraska, United States. B: BCRE model calibrated by using mean q_s and mean c for the river. Transport from left to right in each plot; 360 s separate successive profiles. Vertical scale bar shown in A. Both North Loup River data and model results exhibit statistical steady state associated with splitting and merging of individual bedforms where splitting rate approximately equals merging rate. Mean bedform height and length and their respective coefficients of variation (in parentheses) are: h_m = 0.060 m (0.48) and l_m = 1.72 m (0.45) for North Loup River; h_m = 0.030 m (0.46) and l_m = 1.31 m (0.41) for model. Model was initialized from random topography. Domain for all model runs is 500 cells long, scaled grid resolution is 0.10 m, and time step equals 1 s. BCRE equations were integrated by using two-step Lax-Wendroff scheme (Press et al., 1988). Boundary conditions for all runs were periodic.

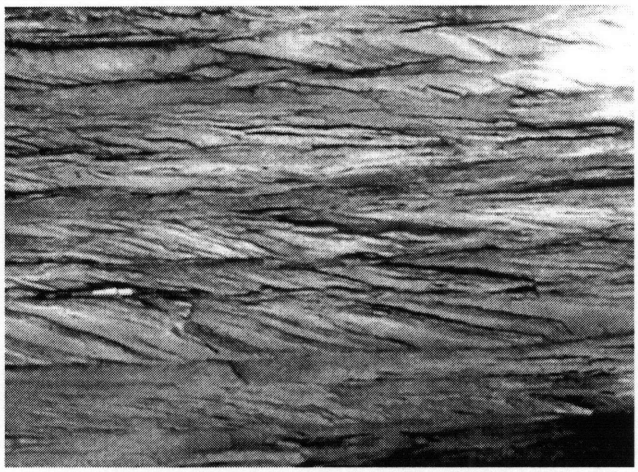

Figure 4.2. Sets of dune strata from Kayenta Formation, Utah. Transport direction from left to right. Note pencil in lower left for scale.

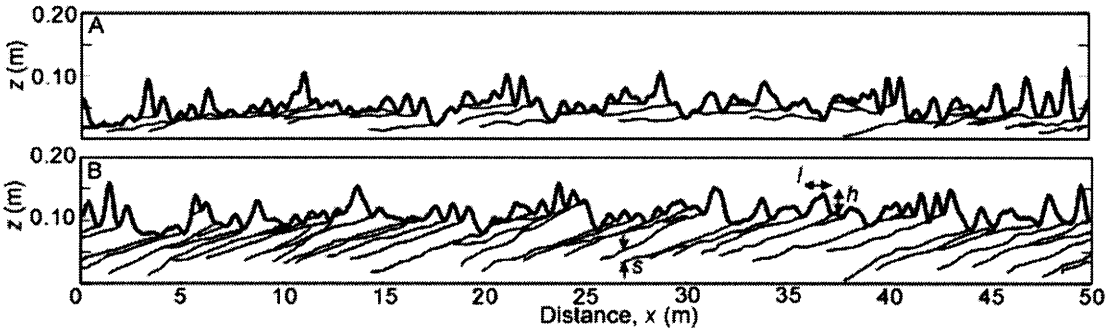

Figure 4.3. Synthetic stratigraphy produced by modeled bedforms at different values for aggradation rate, r, and bedform migration rate, c. Thick top line is stream-bed elevation profile at end of model run. Thin lines preserved in deposit are erosional surfaces created by local scouring in troughs of moving bedforms. Note exaggerated vertical axis. A: r/c = 0. B: r/c = 0.05. Note pinch-out of erosional surfaces produced by bedform merger, as described qualitatively by Allen (1973). Distance between successive erosional surfaces defines set thickness. Set thickness, bedform height, and bedform length are indicated as s, h, and l, respectively, in B. Model was run in statistical steady state for 10,000 time steps.

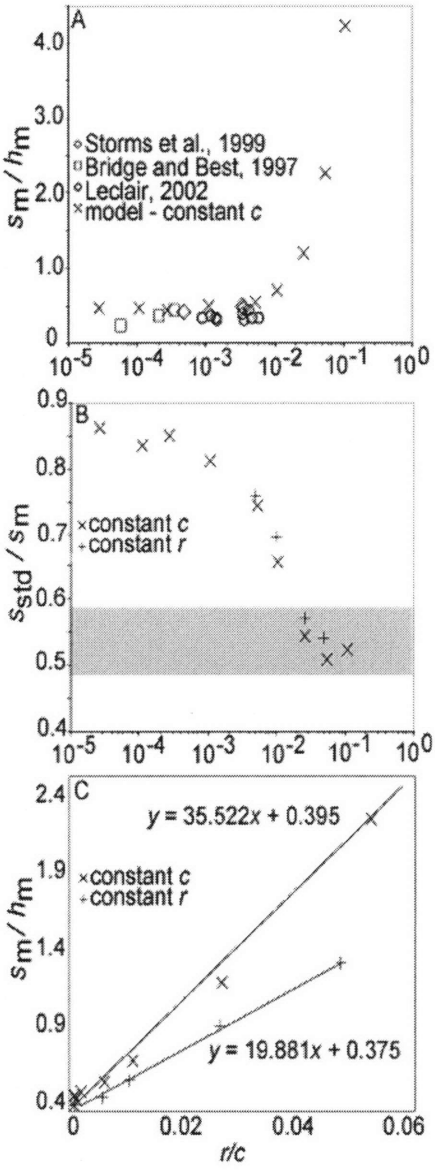

Figure 4.4. Results from BCRE model showing control of r/c on set generation, where subscripts m and std indicate mean and standard deviation, respectively, of measured quantities (see Fig. 4.3); plots A and B have semilog axis to display full range of data. A: Comparison of model results (r is varied while c is held constant) against experimental data for preservation ratio, s_m/h_m, vs. r/c (references shown in legend). B: Coefficient of variation for set thickness, s_{std}/s_m, as a function of r/c for all model runs. At large r/c values, variability in set thickness mirrors variability in generative bed topography, and values for s_{std}/s_m approach parent values of h_{std}/h_m. Gray band marks range for h_{std}/h_m from all model runs. C: Trend of preservation ratio depends on whether r or c is varied. Note that intercepts for the two trends are similar; however, s_m/h_m increases with r/c approximately two times faster when r is varied than when c is varied.

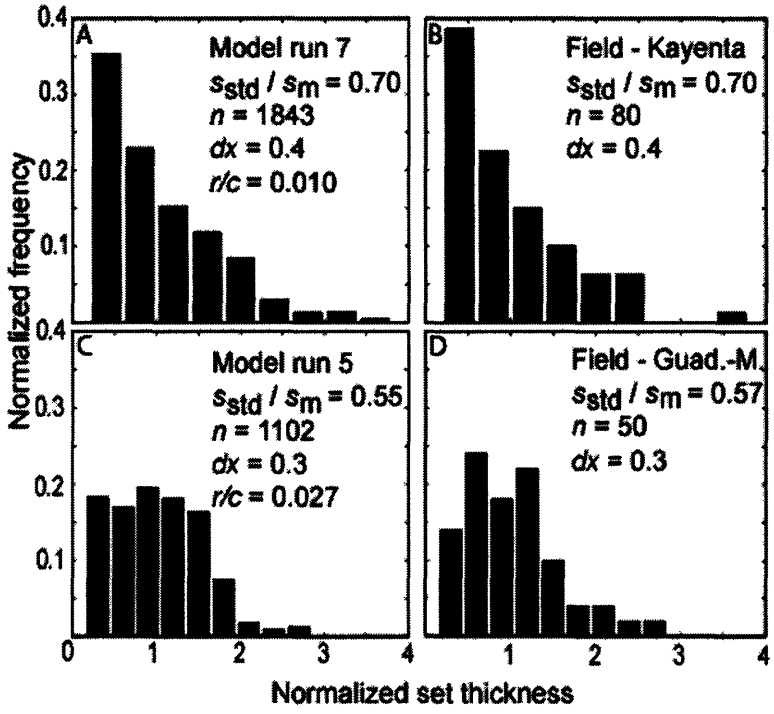

Figure 4.5. Histograms of set-thickness distributions for two field sites (B and D) compared to modeled distributions (A and C) having similar s_{std}/s_m. Set-thickness values are normalized by mean set thickness for each distribution, *dx* is bin size, and *n* is sample size. A: Model run 7. B: Kayenta Formation, Utah. C: Model run 5. D: Guadalope-Matarranya system, Spain.

Chapter 5

The conditions for avulsion-driven rivers

D.J. Jerolmack and D. Mohrig

Department of Earth, Atmospheric and Planetary Sciences, Massachusetts Institute of Technology, Cambridge, Massachusetts 02139, USA

Abstract

Here we show that anabranching (or anastomosed) rivers and deltas with distributary channel networks are morphologies that arise in net-depositional environments when avulsion is the dominant mechanism of lateral channel motion. A compilation of field and laboratory data demonstrates that avulsion frequency scales with the time required for the bed of a river to aggrade one channel-depth above the surrounding floodplain. We derive a mobility number, M, which is the ratio of this avulsion time to a scale characterizing the time associated with lateral migration of one channel width by progressive bank erosion. Data from thirty river systems show that when $M << 1$, rivers exhibit multiple active channels separated by stable overbank surfaces, while $M >> 1$ is always associated with a single active channel. The total wetted width of active channels in anabranching rivers and distributary fans agrees reasonably well with the width predicted for a single-channel system using a constant Shields stress closure.

5.1. Introduction and Theory

Anabranching rivers (or anastomosing, see Makaske, 2001) may be defined as a system of multiple channels (branches) that are separated by relatively stable, often vegetated islands (Nanson and Knighton, 1996; Jansen and Nanson, 2004). Individual branches of an anabranching river may themselves be straight, sinuous or braided (Nanson and Knighton, 1996). Currently there is no available theory to predict under what conditions a river will form multiple branches. Nevertheless, recent work has argued that anabranching rivers can be a stable equilibrium form under certain combinations of flow strength, sediment transport and vegetation (Nanson and Knighton, 1996; Jansen and Nanson, 2004). Stable distributary channels on deltas and alluvial fans are another example of multi-branch river systems. While it is known that their occurrence is associated with environments of net deposition, the conditions that cause channels to become distributary are not well quantified.

We hypothesize that the requisite condition for rivers having multiple active branches is that the lateral motion of channels via bank erosion is small relative to their vertical displacement above the surrounding floodplain via focused sediment deposition. We define the lateral migration time scale, T_C, as the time it would take a channel to migrate the distance equal to its characteristic width, B, given a representative measure of bank erosion rate, v_C (e.g., Tal et al., 2004):

$$T_C = \frac{B}{v_C}. \qquad (1)$$

Note that $B = \sum_i^N b_i$ is the total wetted width of all active channels, where N is the number of active channels and b_i is the width of each channel (Fig. 5.1). This formulation is convenient because B may be estimated from theory while N may not be known *a priori*, as demonstrated later in this paper. A representative time scale for channel aggradation, T_A, is similarly defined as the time required for the river to aggrade one average channel-depth, $\overline{h}$, above the distal floodplain. This time scale may be approximated as:

$$T_A = \frac{\overline{h}}{v_A}, \tag{2}$$

where v_A is a representative aggradation rate. Since deposition rates on the distal floodplain are very small relative to those measured in the vicinity of a channel (Heller and Paola, 1996; Tornqvist and Bridge, 2002), v_A is simply taken to equal a near or in-channel rate of sediment accumulation. In an examination of ancient river deposits, Mohrig et al. (2000) found that avulsion (abrupt lateral displacement in location of the flow) was associated with superelevation of the river channel to a height above the surrounding floodplain equal to approximately one channel depth (Fig. 5.1). In this sense (2) is an avulsion time scale, or more properly, it is the average lifetime for a single channel. The avulsion frequency of the river system, f_A, may be directly estimated from (2) as:

$$f_A = \frac{v_A N}{\overline{h}}. \tag{3}$$

We define the mobility number, M, as the ratio of aggradation and lateral-migration time scales,

$$M = \frac{T_A}{T_C} = \frac{\bar{h}}{B}\frac{v_C}{v_A}. \tag{4}$$

For rivers having $M >> 1$ we expect a system with a single channel that sweeps across its floodplain relatively rapidly, reworking the floodplain as it moves laterally. Avulsions are expected to be relatively rare (Fig. 5.1). Multi-branch rivers are expected to occur for cases of $M << 1$ because the individual channels aggrade rapidly in place compared to any lateral shifting in response to bank erosion. This production of superelevation makes avulsions a dominant mechanism of channel adjustment (Fig. 5.1). Relatively frequent avulsions mean that several channels should be active at once (Makaske, 2001). If M is $O(10^0)$ (order one), transition between single and multiple branches is expected.

Assuming steady uniform flow and a Chezy flow resistance relationship, the channel depth may be cast as $\bar{h} = \theta d_{50} R/S$ and expected channel width takes the form (Dade, 2000):

$$B = \frac{c_f^{1/2} QS}{\sqrt{R^3 \theta^3 d_{50}^3 g}}, \tag{5}$$

where θ, d_{50}, S, g, Q, and c_f are dimensionless Shields stress, median grain diameter, water surface slope, acceleration by gravity, formative water discharge and Chezy friction factor,

respectively, and $R = 1.65$ is the relative specific gravity for quartz. The mobility number then may be re-written as:

$$M = \frac{(\theta R d_{50})^{5/2} g^{1/2}}{c_f^{1/2} S^2 Q} \frac{v_C}{v_A}. \qquad (6)$$

The advantage of (6) is that Shields stress and friction factor vary little in alluvial rivers, i.e., $\theta \approx 1$ and $c_f \approx 0.01$ for sandy systems dominated by dunes and $\theta \approx 0.04$ and $c_f \approx 0.01$ for gravel systems (Parker et al., 1998; Dade, 2000), so M may be predicted using relatively few parameters.

Parker (1976) provided a theoretical stability criterion, ε, that can be used to assess whether a river should be braided (i.e., a single channel with multiple threads of high-velocity flow), or a single-thread channel with a sinuous to straight plan form (see caption of Fig. 5.2). The single-thread channel is the dominant form at $\varepsilon << 1$, while a braided form is the common channel type for $\varepsilon \geq 1$ (Parker, 1976; Dade, 2000). We propose that the mobility number and the Parker stability criterion when taken together provide a complete picture of expected river planform pattern.

5.2. Results and Discussion

To test whether the derived mobility number is capable of discriminating between single- and multi-branch systems, we have compiled data from thirty net-depositional systems reported in the literature (table 5.1). These data include lowland rivers, deltas and alluvial fans with perennial to ephemeral discharges, located in tropical to arid environments and

transporting particles ranging from fine sand to cobbles. The reported systems also cover a wide range of scales, from the laboratory to the Amazon River. Size of the data set analyzed here is limited by the number of studies providing enough information to confidently estimate v_C and v_A.

We first compare measured avulsion frequency against computed values using (3). The agreement is remarkable for this admittedly small dataset (Fig. 5.2A), demonstrating that long-term avulsion frequency may be estimated using the simple relation (3) proposed here. This result is of great significance because modeling efforts have shown that the morphology and depositional patterns of channelized landscapes are very sensitive to avulsion frequency (e.g., Heller and Paola, 1996; Sun et al., 2002) and there are competing descriptions of conditions necessary for avulsion setup (Heller and Paola, 1996; Mohrig et al., 2000; Tornqvist and Bridge, 2002; Slingerland and Smith, 2004). Varying degrees of importance have also been assigned to the frequency of avulsion triggers such as floods, ice jams and animal disturbance (see review by Slingerland and Smith, 2004). Given that our data come from field and laboratory settings representing the broadest possible range of depositional environments it appears that: (1) knowledge of the style of avulsion trigger is not necessary for modeling the long-term evolution of channel deposits, implying that occurrence of a triggering event is not a limiting factor in avulsion frequency; and (2) the condition for avulsion is well-approximated by the time required to achieve a relative superelevation of one (Fig. 5.1). These results may be applied directly to morphodynamic models of channel and fan development (Sun et al. 2002; Swenson, 2005).

All reported river systems having $M \geq 10^{1}$ exhibit a single active channel that is either single- or multi-thread (table 5.1). Systems with $M \leq 10^{-1}$ have multiple active

channels. Those river systems having M of $O(10^0)$ fall in between, generally containing one dominant channel and a small number of secondary channels. Interestingly, the Holocene deltas of many rivers such as the Rhine, Rhone, Mississippi and Brahmaputra fall into this category. Using measured river data (table 5.1) we have constructed a phase space that relates channel pattern to M and ε. We find this method effectively segregates systems into four categories: single channels with multiple threads (simple braided channels), single channels with single threads (straight-to-sinuous channels), multiple channels with multiple threads (anabranching systems with braided channels), and multiple channels with single threads (simple anabranching systems) (Fig. 5.2B). Because of the variable data quality these values for M should be taken only as order-of-magnitude estimates. Nonetheless, analysis of these data clearly demonstrates the discriminating power of the mobility number.

It is useful to focus on a few specific river systems to address the meaning of computed mobility numbers (table 5.1). The Yellow River of China has an extremely large Holocene channel aggradation rate of v_A = 100 mm/yr (Fig. 5.3). Although this river avulsed on decadal time scales before human intervention, constructing a large delta, only one channel has been active at any one time due to the high degree of channel migration by bank erosion (Wu et al., 2005). The values M = 16 and ε = 0.07 indicate that the Yellow River Delta should be a single-channel, sinuous river system (Fig. 5.2), in agreement with observation. Hence, this example serves to demonstrate that rapid aggradation alone is not sufficient to generate a multi-branch system. An interesting counter example is the anabranching Cooper Creek, in arid central Australia (Fig. 5.3). Although vertical aggradation is very small ($v_A \leq 0.1$ mm/yr), the exceedingly low channel migration rate,

estimated as $v_C \leq 8$ mm/yr, results in a maximum value for M of 0.3, indicating multiple branches. Cooper Creek shows that very stable channel banks can induce an avulsion-driven morphology, even if channel aggradation rates and avulsion frequency are very low. Another illustrative case is the Lower Mississippi River before human disturbance (Hudson and Kesel, 2000). On the alluvial plain, large bank erosion rates led to a single, meandering channel (M = 400, ε = 0.02). On the delta, v_C decreased by an order of magnitude while v_A increased by up to one order of magnitude, producing a channel system with several meandering distributaries (M = 3, ε = 0.04). A final case is the lower Niobrara River, Nebraska (Fig. 5.3). The channel has experienced rapid bed aggradation throughout the past 50 years in response to base-level rise from reservoir construction. This aggradation has driven multiple avulsions and the conversion of some reaches to narrower anabranches separated by stable, vegetated islands (Ethridge et al. 1999). Our calculations suggest that the present morphology of the lower Niobrara should be anabranching and braided (M = 0.2, ε = 2), in agreement with observations. We propose that the mobility number may be used to predict if a change in boundary conditions, whether tectonic, climatic, eustatic or anthropogenic, will result in a conversion from single- to multi-branch morphology. This is of critical importance for river management and habitat issues, and is equally important in the reconstruction of paleo-environmental conditions via the analysis of ancient fluvial deposits.

The measured values for total wetted width of rivers in our data base are plotted against calculated values of channel width (5) in Figure 5.2C. These data show that the sum of active channels in anabranching and distributary rivers share the properties of a single channel of comparable size. It appears that the conditions determining the presence

of multiple channels are external to the processes governing the instantaneous transport of fluid and sediment through the system. Indeed, the mean channel depth, total wetted width and Shields stress may all be estimated without reference to the number of channels in a river system. The existence of multiple stable branches in the rivers examined here appears to be determined by boundary conditions conducive to net deposition of sediment, combined with some degree of channel-bank stability (usually from vegetation) such that the mobility number is $O(10^0)$ or less. This point addresses the question as to whether anabranching patterns can exist as a persistent channel-system form (Makaske, 2001; Jansen and Nanson, 2004) – anabranching need not be merely a transitional pattern, however the requirement that $M < 1$ means that anabranching may only be maintained in environments experiencing bed aggradation. A major remaining challenge is to develop predictive algorithms for channel aggradation and bank erosion rates that may be incorporated into current morphodynamic models (e.g., Sun et al., 2002; Murray and Paola, 2003; Swenson, 2005), providing a more complete description of river patterns at all scales.

Acknowledgements

This work was supported by the STC Program of the National Science Foundation via the National Center for Earth-surface Dynamics under agreement EAR-0120914, with additional support from NSF grant EAR-0345312. We gratefully acknowledge the careful work of previous authors that allowed the compilation of our database. We also thank Gerald Nanson for images of Cooper Creek and early comments.

References

Dade, W.B., 2000, Grain size, sediment transport and alluvial channel pattern: Geomorphlogy, v. 35, p. 119-126.

Ethridge, F.G., Skelly, R.L., and Bristow, C.S., 1999, Avulsion and crevassing in the sandy, braided Niobrara River: Complex response to base-level rise and aggradation. In: Smith, J., and Rogers, J. (Eds.), Fluvial Sedimentology VI. International Association of Sedimentologists, Special Publication 28. Blackwell Science, London, p. 179-191.

Heller, P.L., and Paola, C., 1996, Downstream changes in alluvial architecture: An exploration of controls on channel-stacking patterns: Journal of Sedimentary Research, v. 66, no. 2, p. 297-306.

Hudson, P.F., and Kesel, R.H., 2000, Channel migration and meander-bend curvature in the lower Mississippi River prior to major human modification: Geology, v. 28, no. 6, p. 531-534.

Jansen, J.D., and Nanson, G.C., 2004, Anabranching and maximum flow efficiency in Magela Creek, northern Australia: Water Resources Research, v. 40, W04503, doi:10.1029/2003WR002408.

Makaske, B., 2001, Anastomosing rivers: a review of their classification, origin and sedimentary products: Earth-Science Reviews, v. 53, p. 149-196.

Mohrig, D., Heller, P.L., Paola, C., and Lyons, W.J., 2000, Interpreting avulsion process from ancient alluvial sequences: Guadalope-Matarranya system (northern Spain) and Wasatch Formation (western Colorado): Geological Society of America Bulletin, v. 112, no. 12, p. 1787-1803.

Murray, A.B., and Paola, C., 2003, Modelling the effect of vegetation on channel pattern in bedload rivers: Earth Surface Processes and Landforms, v. 28, p. 131-143.

Nanson, G.C., and Knighton, A.D., 1996, Anabranching Rivers: Their cause, character and classification: Earth Surface Processes and Landforms, v. 21, p. 217-239.

Parker, G., 1976, On the cause and characteristic scales of meandering and braiding in rivers, Journal of Fluid Mechanics, v. 76, no. 3, p. 457-480.

Parker, G., Paola, C., Whipple, K.X., and Mohrig, D., 1998, Alluvial fans formed by channelized fluvial and sheet flow. I: Theory: Journal of Hydraulic Engineering, v. 124, no. 10, p. 985-995.

Slingerland, R., and Smith, N.D., 2004, River avulsions and deposits: Annual Review of Earth and Planetary Science, v. 32, p. 257-285.

Sun, T., Paola, C., and Parker, G., 2002, Fluvial fan deltas: Linking channel processes with large-scale morphodynamics, Water Resources Research, v. 38, no. 8, 1151, doi:10.1029/2001WR000284.

Swenson, J.B., 2005, Relative importance of fluvial input and wave energy in controlling the timescale for distributary-channel avulsion, Geophysical Research Letters, v. 32, L23404, doi:10.1029/2005GL024758.

Tal, M., Gran, K, Murray, A.D., Paola, C, and Hicks, D.M., 2004, Riparian vegetation as a primary control on channel characteristics in multi-thread rivers. In: Bennet, S.J., and Simon, A. (Eds.), Riparian Vegetation and Fluvial Geomorphology: Hydraulic, Hydrologic, and Geotechnical Interactions 8. American Geophysical Union, p. 43-58.

Törnqvist, T.E., and Bridge, J.S., 2002, Spatial variation of overbank aggradation rate and its influence on avulsion frequency: Sedimentology, v. 49, p. 891-905.

Wu, B., Wang, G., Ma, J., and Zhang, R., 2005, Case study: River training and its effects on fluvial processes in the Lower Yellow River, China: Journal of Hydraulic Engineering, v. 131, no. 2, p. 85-96.

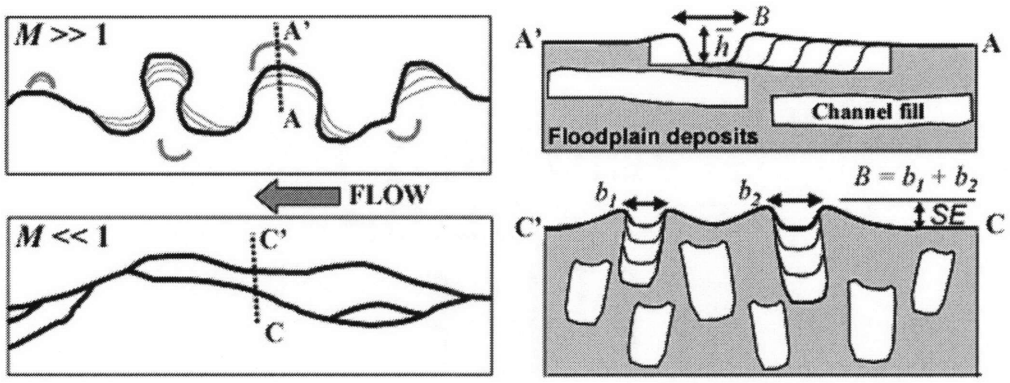

Figure 5.1. Channel types, deposits and definitions. Top shows a hypothetical single-branch meandering river in planform (left), and a representative cross section through the meander belt (right). Channel adjustment is determined principally by bank erosion. At bottom is an anabranching river with multiple stable branches. The cross section at right shows these channels are superelevated (SE), with a relative superelevation $SE/\overline{h} = 1$. This river represents an avulsion-driven morphology.

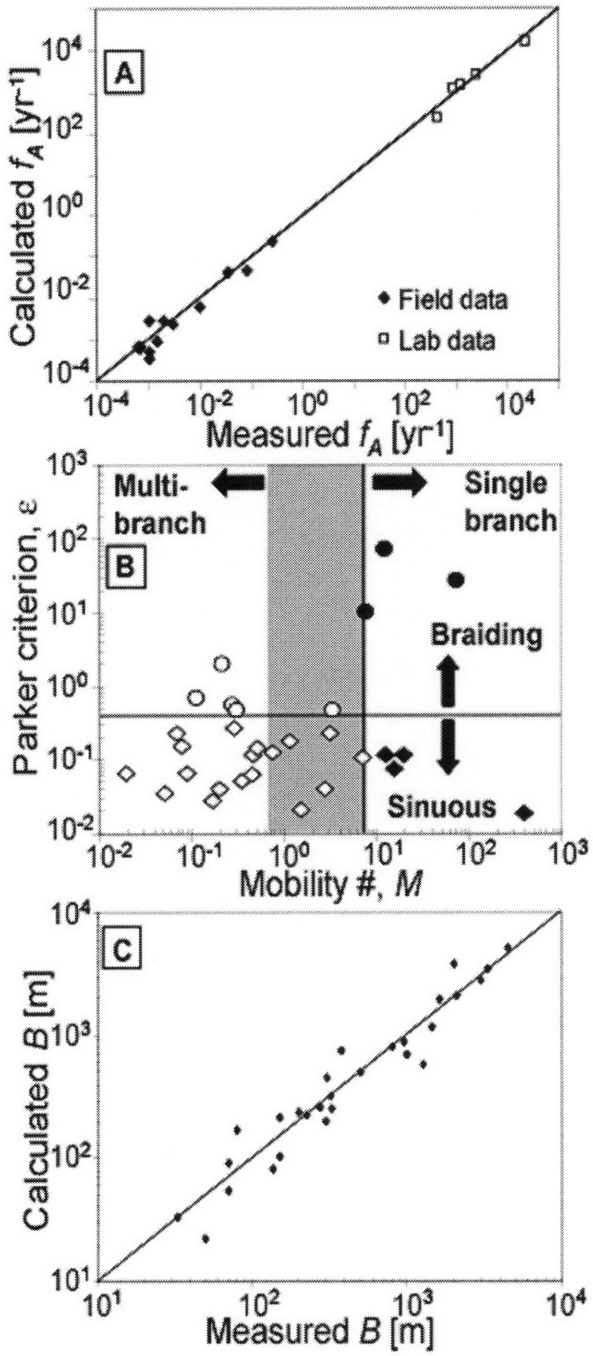

Figure 5.2. Measured and computed river characteristics (table 5.1). A: Measured vs. calculated avulsion frequency (3) for field and laboratory data. Line denotes perfect agreement. B: Phase space of mobility number (4) and Parker (1976) stability criterion $\varepsilon = S\sqrt{g\bar{h}B^4}/Q$. Lines delineate channel patterns observed from data; the gray zone indicates transitional rivers, containing one dominant channel and a small number of secondary channels. Diamonds and circles indicate single-thread and braided rivers, respectively; filled and hollow symbols are single- and multi-branch systems, respectively. C: Measured vs. calculated (5) total channel width for field data only.

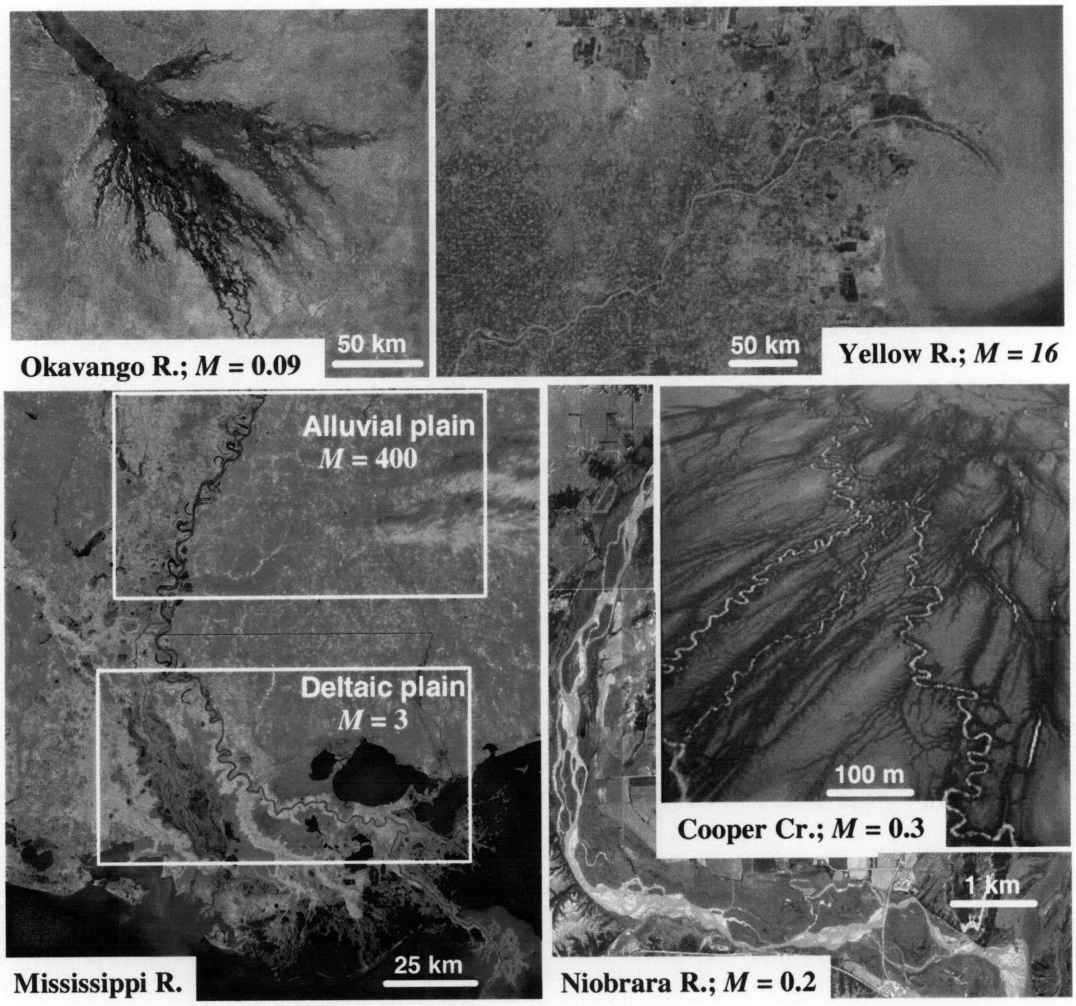

Figure 5.3. (Color) Example rivers and their mobility numbers. Images of Mississippi, Yellow, and Okavango systems from http://visibleearth.nasa.gov; Niobrara image from http://www.dnr.state.ne.us/databank/spat.html; and Cooper image courtesy of G. Nanson.

Table 5.1. Database of river characteristics. Parameters were estimated by various means and are of highly variable quality – for methods and references see Appendix. See Fig. 5.2.

System	Pattern[a]	d_{50} [mm]	θ	c_f	$\bar{h}$ [m]	B [m]	N	S	Q [m^3]	v_A [mm/yr]	v_C [mm/yr]	$1/f_A$ [yr]	M	ε
Multi-branch														
Orinoco R. Delta, Venezuela	D - M	0.3	1.5	0.01[b]	12	2000	3	6.0E-5	38000	2.1	7	1000	0.02	0.07
Upper Narew R., Poland	A - M	0.6	0.6	0.05	3	33	3	2.0E-4	35	2	1		0.05	0.03
Magdalena R., Columbia	A - M	0.35	1.0	0.01[b]	6	1630	10	9.5E-5	8800	3.8	71		0.07	0.22
Lower Sandover R., Australia	D - M	0.5	2.0	0.01[b]	3.3	225	2	5.0E-4	945	0.7	4		0.08	0.15
Okavango Delta, Botswana	D - M	0.35	1.5	0.03	4.5	50	3	1.9E-4	50	10	10	100	0.09	0.06
Magela Creek, N. Australia	A - T	0.42	0.7	0.02	1	135	14	5.0E-4	40	1.5	23		0.12	0.71
Little River, Arkansas	A - M	0.3	1.2	0.01[b]	2	75	3	3.0E-4	280	2.5	15		0.16	0.03
Upper Columbia R., B.C.	A - M	2	0.08	0.01[b]	2.6	150	4	9.6E-5	275	1.8	20	333	0.20	0.04
Lower Niobrara R., Nebraska	A - B	0.28	0.9	0.01	0.3	200	1-2	1.3E-3	48	75	10000	4	0.21	1.89
Cooper Creek, Australia	A - T	0.1	1.2	0.01	1	300	~10	2.0E-4	100	0.1	8		0.27	0.56
Gilbert R. Delta, Australia	D - M	0.5	0.4	0.01[b]	6	2100	7	6.0E-5	7488	0.7	65		0.29	0.27
Upper Parana R., Argentina	A - B	0.3	1.4	0.01	7	3000	2-3	9.6E-5	16000	5	635	1633	0.30	0.45
Lower Saskatchewan R., B.C.	A - M	0.38	1.2	0.01[b]	6.3	275	4	1.2E-4	1400	1.3	20	667	0.35	0.05
Suwanee R. Delta, Florida	D – M	0.5	0.25	0.01[b]	3	300	3	7.0E-5	570	1	35		0.44	0.06
N. Saskatchewan R., Alberta	A - T	10	0.09	0.01[b]	1.5	70	3	1.0E-3	165	1.8	40		0.48	0.11
Lower Alexandra R., Alberta	A - T	10	0.06	0.01[b]	1.6	70	3	6.0E-4	85	1.8	40		0.51	0.14
Transitional														
McArthur R. Delta, N. Australia	WD - M	0.5	0.4	0.01[b]	5	800	2	6.0E-5	2170	0.5	60		0.75	0.12
Middle Amazon (@ R. Negro)	WA - M	0.25	0.9	0.01[b]	12	4500	1-2	3.0E-5	36815	5	2250		1.20	0.18
Upper Rhone R. Delta	WD - M	0.3	0.5	0.01[b]	5.9	377	2	4.0E-5	2100	2	198	1450	1.55	0.02
Lower Mississippi Delta	WD - M	0.3	1.5	0.01[b]	25	1450	2	3.0E-5	25000	35	5700	1000	2.81	0.04
Rhine-Meuse delta	WD - M	0.5	0.7	0.01	5	1000	2	1.1E-4	3500	1.6	1000	1450	3.13	0.22
Brahmaputra R., Upper Delta	WA - T	0.5	0.8	0.01[b]	7	3300	1-2	1.0E-4	20000	20	30000	500	3.18	0.45
Middle Baghmati R., India	WA - M	0.8	0.5	0.01[b]	4.9	325	4	1.4E-4	1000	55	26000	29	7.10	0.10
Single Branch														
Emerald Lake fan, B.C.	US - B	50	0.13	0.10	0.3	20		3.5E-2	2	3650	1.8E+6		7.5	10
Rolling Stone fan, Minnesota	US - B	0.1	1.8	0.01	0.1	320		6.4E-3	8	625	3.5E+7		12	72
Beni and Mamore R., Bolivia	S - M	0.1	1.7	4.E-4	4	1270	1	7.0E-5	6000	50	200000		13	0.12
Yellow R. Delta	S - M	0.1	2.4	4.E-4	2	500	1	2.0E-4	3000	100	400000	12	16	0.07
Assiniboine R. Fan, Manitoba	S - M	0.5	2.5	0.01[b]	4.2	150	1	5.0E-4	626	1.4	1000	1000	20	0.12
XES 1999 lab fan Run1, Stage 3	US - B	0.12	3.0	0.59	0	0.45	9	6.0E-2	1E-4	17520	5.7E+7	5.E-5	72	27
Lower Mississippi alluvial plain	S - M	0.3	1.8	0.01[b]	30	950	1	3.0E-5	25000	4	50000		395	0.02

[a]Indicates [Channel branching style - channel pattern]. D = distributary, A = anabranching, S = single channel, US = unstable, ill-defined channels, WD and WA = weakly distributary and weakly anabranching, respectively, indicating the presence of a clearly dominant channel and a small number of secondary channels; M = meandering, B = braided, T = transitional.

[b]Assumed friction factor based on analysis of river data by Parker et al. (1998) and our own unpublished database.

5.3. Appendix

This appendix provides a brief description of the methods used to compute values for the avulsion time scale and channel lateral migration time scale. The bulk of rate estimates in the database come from shallow cores with radiocarbon dates. Other methods of dating used Lead and/or Cesium. For very recent rates, aerial photographs, channel surveys and erosion pins were used. All values presented are averages. Anywhere between 1 and 20 measurements from different cores or surveys may contribute to an average - generally it is 4-5. For most studies, measured bank erosion rates (and hence calculated mobility numbers, M) are maximum values (see below). This is especially true for rivers with very low lateral migration rates in which no lateral movement was detectable. All data are from modern (currently active) river systems.

Vertical aggradation rates (v_A) are derived from sandy channel deposits (often with datable material), and so represent accumulation rates on channel belts – some cores are from the bottoms of channels, while others are from bank and levee deposits at channel margins. The following methods were used to estimate v_A:

1) depth to a dated material (usually dated with radiocarbon, sometimes lead or cesium) is measured, and rate computed as depth divided by sample age;
2) some authors report in-channel deposition rate - these values are used without any quality control checks;
3) some authors report total Holocene sediment thickness, and suggest an estimate for the time associated with the onset of deposition;
4) historical surveys document the deposition of a river bed.

Lateral migration rates (v_C) were estimated from a variety of methods, generally one of the following:

1) a core taken in a river bank at a known distance from the main channel has a radiocarbon date. We assume the river has migrated less than this distance over the dated interval. In this case, bank erosion rate is a maximum. In some cases, no lateral movement was detected, so reported lateral migration rate (and hence calculated mobility number, M) may be much larger than the actual value;
2) a core taken within a channel deposit has a radiocarbon date and depth associated with it. We assume the channel has migrated less than one channel width over this time. In this case, bank erosion rate is a maximum. In some cases, no lateral movement was detected, so reported lateral migration rate (and hence calculated mobility number, M) may be much larger than the actual value;
3) authors of some papers present depth/age plots of an evolving river channel from many cores. This allows an estimate of channel migration from the diagrams;
4) authors report a bank erosion estimate (for modern river systems) - these values are used without any quality control checks;
5) repeat channel surveys were performed and reported, from which bank erosion rate could be estimated;
6) erosion pins were used;
7) aerial photography was used.

This appendix contains a table (table 5.A1) with specific comments of how each measurement was made in individual river systems, along with the relevant references.

Channel geometry was usually obtained directly from reported values in the literature. In some cases, estimates of width and depth were made from diagrams of channel surveys. In other cases, width was estimated from aerial photographs. These are documented in the database.

Channel number was reported by some authors. In some cases, channel number was estimated from aerial photographs or channel cross-section surveys.

Water discharge is usually either a "bankfull" discharge as reported by authors, or a 1-2 year flood as reported by authors. In some cases discharge was estimated as the annual flood from records available online. In a few cases, discharge was estimated from water surface slope, mean channel geometry and an assumed friction factor. These cases are documented on the database.

Grain size is always a median value and was often reported by the authors. In some cases, only qualitative descriptions of grain size were reported (e.g., medium/coarse sand). For these cases an estimate of grain size was assigned. They are marked in the database.

Friction factor was computed directly from reported shear stress and water velocity measurements using a Chezy flow resistance relationship, if data were available. This method is described in Chapter 6. If no data were available, friction factor was taken as 0.01, the mean value from an extensive data set reported in Parker et al. (1998) and expanded on by us. These data are marked in the database.

Avulsion frequency was reported by authors, or was easy to calculate from the documented record of avulsions in aerial photographs presented by authors.

References used for the database.

1. Aalto, R., Maurice-Bourgoin, L., Dunne, T., Montgomery, D.R., Nittrouer, C.A., and Guyot, J.L., 2003, Episodic sediment accumulation on the Amazonian flood plains influenced by El Nino/Southern Oscillation: Nature, 452, 493-497.
2. Abbado, D., Slingerland, R.L., and Smith, N.D., 2005, The origin of anastomosis in the upper Columbia River, British Columbia, Canada: In Blum, M.D., Marriott, S., and Leclair. S. (eds.), Fluvial Sedimentology VII, Internat. Assoc. Sedim. Special Publ. 35.
3. Allison, M.A, Khan, S.R., Goodbred, S.L., and Kuehl, S.A., 2003, Stratigraphic evolution of the late Holocene Ganges-Brahmaputra lower delta plain: Sedimentary Geology, 155, 317-342.
4. Antonelli, C., and Provansal, M., 2004, Characterisation and assessment of sand fluxes in the lower Rhine River, France: Unpublished manuscript.
5. Arnaud_Fassetta, G., 2004, The Upper Rhone Delta sedimentary record in the Arles-Piton core: Analysis of delta-plain subenvironments, avulsion frequency, aggradation rate and origin of sediment yield: Geografiska Annaler, 86A, 367-383.
6. Ashworth, P.L., Best, J.L., and Jones, M., 2004, Relationship between sediment supply and avulsion frequency in braided rivers: Geology, 32(1), 21-24.
7. Aslan, A., and Autin, W.I., 1999, Evolution of the Holocene Mississippi River floodplain, Ferriday, Louisiana: Insights on the origin of the fine-grained floodplains: J. Sedimentary Res., 69, 800-815.

8. Aslan, A., Autin, W.J., and Blum, M.D., 2005, Causes of river avulsion: Insights from the late Holocene avulsion history of the Mississippi River, U.S.A.: J. Sedimentary Res., 75, 650-664.

9. Aslan, A, White, W.A., Warne, A.G., and Guevara, E.H., 2003, Holocene evolution of the western Orinoco Delta, Venezuela: GSA Bulletin, 115(4), 479-498.

10. Bryant, M., Falk, P., and Paola, C., 1995, Experimental study of avulsion frequency and rate of deposition: Geology, 23(4), 365-368.

11. Fagan, S., and Nanson, G.C., 2004, The morphology and formation of floodplain-surface channels, Cooper Creek, Australia: Geomorphology, 60, 107-126.

12. Gibling, M.R., Nanson, G.C., and Maroulis, J.C., 1998, Anastomosing river sedimentation in the Channel Country of central Australia: Sedimentology, 45(3), 595-619

13. Goedhart, M.L., and Smith, N.D., 1998, Braided stream aggradation on an alluvial fan margin: Emerald Lake fan, British Columbia: Canadian J. Earth Science, 35, 534-545.

14. Goodbred, S.L., Kuehl, S.A., Steckler, M.S., Sarker, M.H., 2003, Control on facies distribution and stratigraphic preservation in the Ganges-Brahmaputra delta sequence: Sedimentary Geology, 155, 301-316.

15. Gradzinski, R., Baryla, J., Doktor, M., Gmur, D., Gradzinski, M., Kedzior, A., Paszkowski, M., Soja, R., Zielinski, T., and Zuek, S., 2003, Vegetation-controlled modern anastomosing system of the upper Narew River (NE Poland) and its sediments: Sedimentary Geology, 157, 253-276.

16. Guccione, M.J., Van Arsdale, R.B., and Hehr, L.H., 2000, Origin and age of the Manila high and associated Big Lake "sunklands" in the New Madrid seismic zone, northeastern Arkansas: GSA Bulletin, 112(4), 549-590.

17. Guyot, J.L., Jouanneau, J.M., and Wasson, J.G., 1999, Characterisation of river bed and suspended sediments in the Rio Madeira drainage basin (Bolivian Amazonia): J. South American Earth Sciences, 12, 401-140.

18. Hickson, T.A., Sheets, B.A., Paola, C., and Kelberer, M., 2005, Experimental test of tectonic controls on three-dimensional alluvial facies architecture: J. Sedimentary Res., 75, 710-722.

19. Hudson, P.F., and Kesel., R.H., 2000, Channel migration and meander-bed curvature in the lower Mississippi River prior to major human modification: Geology, 28(6), 531-534.

20. Jain, V., and Sinha, R., 2004, Fluvial dynamics of an anabranching river system in Himalayan foreland basin, Baghmati River, north Bihar plains, India: Geomorphology, 60, 147-170.

21. Jansen, J.D., and Nanson, G.C., 2004, Anabranching and maximum flow efficiency in Magela Creek, northern Australia: Water Resources Res., 40, W04503, doi:10.1029/2003WR002408.

22. Jerolmack, D.J., Mohrig, D., Straub, K.M., and Leung, V., Chapter 6.

23. Jones, B.G., Woodroffe, C.D., and Martin, G.R., 2003, Deltas in the Gulf of Carpentaria, Australia: Forms, processes, and products: SEPM Special Publication #76, 21-43.

24. Latrubesse, E.M., Franzinelli, E, 2002, The Holocene alluvial plain of the middle Amazon River, Brazil: Geomorphology, 44, 241-257.

25. Makaske, B., Smith, D.G., and Berendsen, H.J.A., 2002, Avulsions, channel evolution and floodplain sedimentation rates of the anastomosing upper Columbia River, British Columbia, Canada: Sedimentology, 49, 1049-1071.

26. McCarthy, T.S., Stanistreet, I.G., Cairncross, B., Ellery, W.N., Ellery, K., Oelofse, R., and Grobicki, T.S.A., 1988, Incremental aggradation of the Okavango delta-fan, Botswana: Geomorphology, 1, 267-278.

27. Mertes, L.A.K., 1994, Rates of flood-plain sedimentation on the central Amazon River: Geology, 22, 171-174.

28. Mertes, L.A.K., Dunne, T., and Martinelli, L.A., 1996, Channel-floodplain geomorphology along the Salimoes-Amazon River, Brazil: GSA Bulletin, 108(9), 1089-1107.

29. Nanson, G.C., and Knighton, A.D., 1996, Anabranching rivers: Their cause, character and classification: Earth Surface Processes and Landforms, 21, 217-239.

30. Orfeo, O., and Stevaux, J., 2002, Hydraulic and morphological characteristics of the middle and upper reaches of the Parana River (Argentina and Brazil): Geomorphology, 44, 309-322.

31. Paola, C., Parker, G., Mohrig, D.C., and Whipple, K.X., 1999, The influence of transport fluctuations on spatially averaged topography on a sandy, braided alluvial fan: SEPM Special Publications #62, 211-218.

32. Parker, G., Paola, C., Whipple, K.X., Mohrig, D., Toro-Escobar, C.M., Halverson, M., and Skoglund, T.W., 1998, Alluvial fans formed by channelized fluvial and sheet flow. II: Application: J. Hydraulic Research, 24(10), 996-1004.

33. Patterson, L.J., Muhammed, Z., Bently, S.J., Britsch, L. Del, and Dillon, D.L., 2003, ^{210}Pb and ^{137}Cs geochronology of the Lake Fausse Pointe region of the lower Atchafalaya Basin, GCAGS 53rd Annual Convention, Baton Rouge, Louisiana 668-675.

34. Perez-Arlucea, M., and Smith, N.D., 1999, Depositional patterns following the 1870s avulsion of the Saskatchewan River (Cumberland Marshes, Saskatchewan, Canada): J. Sedimentary Res., 69(1), 62-73.

35. Rannie, W.F., 1990, The Portage La Prairie 'Floodplain Fan', in Alluvial Fans: A Field Approach, edited by A.H Rachocki and M. Church, pp. 180-193, Wiley, New York.

36. Sarma, J.N., 2005, Fluvial process and morphology of the Brahmaputra River in Assam, India: Geomorphology, 70, 226-256.

37. Saynor, M.J., Erskine, W.D., and Evans, K.G., 2003, Bank erosion in the Ngarradi catchment: Results of erosion pin measurements between 1998 and 2001: Australian Government Dept. Environment Heritage, Supervising Scientist Report 176, 48 p.

38. Smith, D.G., 1976, Effect of vegetation on lateral migration of anastomosed channels of a glacial meltwater river: GSA Bulletin, 87, 857-860.

39. Smith, D.G., 1986, Anastomosing river deposits, sedimentation rates and basin subsidence, Magdalena River, northwestern Colombia, South America: Sedimentary Geology, 46, 177-196.

40. Smith, D.G., and Smith, N.D., 1980, Sedimentation in anastomosed river systems: Examples from alluvial valleys near Banff, Alberta: J. Sedimentary Petrology, 50(1), 157-164.

41. Smith, N.D., McCarthy, T.S., Ellery, W.N., Merry, C.L., and Ruther, H., 1997, Avulsion and anastomosis in the panhandle region of the Okavango Fan, Botswana: Geomorphology, 20, 49-65.

42. Stevaux, J.C., and Souza, I.A., 2004, Floodplain construction in an anastomosed river: Quaternary International, 114, 55-65.

43. Stouthammer, E., and Berendsen, H.J.A., 2001, Avulsion frequency, avulsion duration, and interavulsion period of Holocene channel belts in the Rhine-Meuse Delta, The Netherlands: J. Sedimentary Research, 71(4), 589-598.

44. Tooth, S., 1999, Downstream changes in floodplain character on the Northern Plains of arid central Australia. In: Fluvial Sedimentology VI, Int. Assoc. Sedimentologists Special Publication #28, 93-112.

45. Törnqvist, T.E., 1993, Holocene alternation of meandering and anastomosing fluvial systems in the Rhine-Meuse Delta (central Netherlands) controlled by sea-level rise and subsoil erodibility: J. Sedimentary Petrology, 63(4), 683-693,

46. Törnqvist, T.E., 1994, Middle and late Holocene avulsion history of the River Rhine (Rhine-Meuse delta, Netherlands): Geology, 22, 711-714.

47. van Gelder, A., van den Berg, J.H., Cheng, G., and Xue, C., 1994, Overbank and channelfill deposits of the modern Yellow River delta: Sedimentary Geology, 90, 293-305.

48. Warne, A.G., Meade, R.H., White, W.A., Guevara, E,H,, Gibeaut, J, Smyth, R.C., Aslan, A., and Tremblay, T., 2002, Regional controls on geomorphology, hydrology, and ecosystem integrity in the Orinoco Delta, Venezuela: Geomorphology, 44, 273-307.

49. Wilburs, A., 2004, The development and hydraulic roughness of subaqueous dunes (Unpublished Ph. D. thesis): Utrecht University, 227 p.

50. Wolfert, H.P., Schnoor, M.M., Maas, G.J., and Middelkoop, H, 2005, Embanked river reaches in the River Rhine depositional zone - I. Historical geomorphology: submitted to Geomorphology. (Unpublished thesis, Chapter 7).

51. Wright, E.E., Hine, A.C., Goodbred, S.L., and Locker, S.D., 2005, The effect of sea-level and climate change on the development of a mixed siliciclastic-carbonate, deltaic coastline: Suwanee River, Florida, U.S.A.: J. Sedimentary Res., 75, 621-635.

52. Wu, B., Wang, G., Ma, J., and Zhang, R., 2005, Case study: River training and its effects on fluvial processes in the lower Yellow River, China: J. Hydraulic Engineering, 31(2), 85-96.

Table 5.A1. Supplemental information for database of river characteristics – see table 5.1. Source numbers refer to references listed in the Appendix.

Sources	River	Method
9; 48	Orinoco River Delta, Venezuela	Bank migration is maximum, estimated from core on meander banks indicating presence of channel for 1500 yr - core was within 10 m of present channel. Aggradation rates from cores.
15	Upper Narew River, Poland	Bank migration estimated from core showing less than 2 channel width (11 m) movement in 9727 years; aggradation rate was reported by authors; grain size reported only as medium/coarse sand.
39	Magdalena River, Columbia	Lateral migration is upper bound, estimated from the time sandy channel fill occupied the location of a core. Aggradation rate reported by authors.
44	Lower Sandover-Bundy River	Bank migration is maximum, estimated from core that is ~2m from channel edge and 2400 yr old. Aggradation estimate is also crude, comes from same core. Only 1 core available
26; 40	Okavango Delta, Botswana	Lateral migration is negligible from cores - I am conservative and say channel migrated less than 1 m over its 100 year lifetime. Aggradation rate from surveys of channel.
21; 37	Magela Creek, N. Australia	Lateral erosion estimated from 6 nearby channels using erosion pins, but no direct measurements of this channel. Aggradation rate reported by authors.
16	Little River, Arkansas	Lateral migration is upper bound, estimated from the time sandy channel fill occupied the location of a core. Aggradation rate from cores.
2; 25	Upper Columbia River, B.C.	Later migration estimated from depth/age plots of Makaske et al., 2002. Aggradation rate reported by authors.
22	Lower Niobrara River, Nebraska	Lateral migration measured from cross section survey, aggradation rate known from historical data.
11; 12; 30	Cooper Creek, Australia	Discharge, grain size and channel geometry reported. Very long-lived system, at least 100,000 yr - lateral migration estimated from dated bank accretion surface in core. Aggradation reported by authors.
23	Gilbert River Delta, Australia	Bank migration estimated from cores showing channel migrated less than 1 channel width over measured times; mean aggradation rate reported by authors.
30; 42	Upper Parana River, Argentina	Bank migration estimates from cross section showing floodplain position over 3150 yr. Aggradation estimated from cores.
34	Lower Saskatchewan River, B.C.	Lateral migration constrained by core on levee that shows no migration over 50 yrs. Aggradation rate reported by authors.
51	Suwanee R. Delta, Florida	Lateral migration is upper bound, estimated from the time sandy channel fill occupied the location of a core. Aggradation rate from cores.
40	North Saskatchewan River, Alberta	Lateral migration and aggradation rates reported by authors. Discharge estimate is maximum discharge from last year, Alberta Government-Environment
38; 40	Lower Alexandra River, Alberta	Lateral migration comes from cores in banks, and erosion pin measurements. Aggradation rate reported by authors.
23	McArthur River Delta, N. Australia	Bank migration estimated from cores showing channel migrated less than 1 channel width over some time, mean aggradation rate reported by authors.
24; 27; 28	Middle Amazon	Bank migration estimates from percent of area change of channel measured over 8 yr; Aggradation rate and grain size reported by authors.
4; 5	Upper Rhone River Delta	Channel properties from authors. Lateral migration is upper bound, estimated from the time sandy channel fill occupied the location of a core. Aggradation rate reported by author.
7; 8; 19	Lower Mississippi Delta	Lateral migration from aerial photographs and historical documents ; Aggradation is from Lead and Cesium measurements of cores; Grain size assumed same as further upstream.
43; 45; 46; 49; 50	Rhine-Meuse delta	Bank migration from historical photographs and diagrams; Aggradation rate reported by authors.
3; 14; 36	Brahmaputra River, Upper Delta	Lateral migration estimates from aerial photographs and channel surverys; Aggradation rates reported by authors. Observed avulsion time is very crude, average from 2 sources.
20	Middle Baghmati River, India	Aerial photographs and channel surveys used to estimate lateral migration and aggradation rates.
13	Emerald Lake fan, B.C.	Bank migration estimates from map of lobe development, aggradation measured surveys of lobe deposition over 15 days. Discharge crudely estimated from slope, channel area and estimated friction factor
31; 32	Rolling Stone fan, Minnesota	Bank migration from photographs, and aggradation rate is from historical data. Discharge crudely estimated from slope, channel area and estimated friction factor
1; 17	Beni and Mamore Rivers, Bolivia	Bank migration rate and channel width from NASA website of space images, depth is crude estimate from 2 sources. Aggradation rate comes from cores dated with Lead.
47; 52	Yellow River Delta	Aggradation estimate reported by authors, Lateral migration reported by authors.
35	Assiniboine River Fan, Manitoba	Aggradation estimated from 10 m Holocene deposition in 7000 yr. Lateral migration estimated from aerial photographs.
18	Jurassic Tank Experiment, Stage 3	Photographs and topographic surveys were used.
7; 8; 19	Lower Mississippi alluvial plain	Lateral migration reported by authors; Aggradation is more rapid Holocene value reported by Aslan et al., 2005.

Chapter 6

The interplay of channel pattern, avulsions and sediment transport in a sandy river

D.J. Jerolmack, D. Mohrig, K.M. Straub, and V. Leung

Department of Earth, Atmospheric and Planetary Sciences, Massachusetts Institute of Technology, Cambridge, Massachusetts 02139, USA

Abstract

The lower section of the sandy braided Niobrara River, Nebraska, has experienced up to 2.5 m of aggradation over 50 years driven by base-level rise due to reservoir construction on the Missouri River. An apparent response has been frequent avulsions due to superelevation of the channel, which has led to the creation in some reaches of multiple channels separated by vegetated islands. A simple stability analysis suggests that bifurcations in this sandy river should be unstable, however aerial photographs show that individual channel bifurcations persist for many decades. Despite the alternation between single-branch and anabranching reaches in our study area, measured average bed stress, water surface slope and sediment flux were the same in almost all sections of the river. Results indicate that the river is dynamically adjusted by sediment continuity so that planform geometry has little effect on the routing of flow and sediment through the river. We suggest that bifurcations in aggrading rivers such as the Niobrara are created and maintained by continuous channel avulsion, which prevents one anabranch from completely capturing the discharge. The setup for avulsions is superelevation of the

channel above its floodplain, and the avulsion trigger is the presence of exposed sand bars at the mouths of anabranches, which act to deflect flow. We present a conceptual model and scaling analysis to explain the existence of anabranching reaches in net-depositional rivers experiencing avulsions.

6.1. Introduction

If the transport of fluid and sediment in various alluvial rivers is governed by the same physical processes, then differences in pattern should reflect the influence of boundary conditions such as water and sediment discharge, tectonics, bank vegetation and grain properties on these transport processes. Indeed, this concept is the premise for regime models of alluvial channels that attempt to predict equilibrium channel cross-section for a specified set of boundary conditions (e.g., Dade and Friend, 1998; Dade, 2000; Eaton et al., 2004). In order to close the system of equations to find a unique solution for channel width and depth, additional empirical relations (Dade, 2000) or extremal hypotheses (see Eaton et al., 2004) have been proposed. In a separate development, Parker (1976) provided a unified process description of braided and meandering rivers by showing that these different patterns arise from the same fundamental instability associated with sediment transport and bar formation. Although we do not yet have a complete theoretical description for equilibrium alluvial channel morphology, these works represent important steps toward that goal.

Current equilibrium models cannot predict whether flow will be distributed in one or multiple channels. This is partly because such models do not consider avulsions and subsequent partial or complete abandonment of channels (Chapter 5), a process that is

fundamental to the evolution of many net-depositional rivers (e.g., Slingerland and Smith, 2004). In Chapter 5 I showed that rates of channel aggradation and bank erosion processes may play a large role in determining stable channel patterns, demonstrating that dynamical information is crucial for predicting some aspects of steady-state planform morphology. Further, for many problems of interest in river management and geological investigation it is important not only to accurately predict the "steady-state" form of a river, but also to know how a river will adjust its geometry to some change in boundary conditions, and the rates associated with these adjustments. Laboratory experiments (Gran and Paola; 2001; Tal et al., 2004), numerical models (Murray and Paola, 2003) and field observations (Schumm, 1985) have shown that the addition of vegetation can force a transition from a braided to anabranching or single-thread channel due to enhanced bank strength. Currently, our understanding of the feedbacks among channel pattern, sediment transport and boundary conditions is wanting.

Simulations of fluid and sediment transport at small scales may appear to provide at least a partial solution to this problem, as flow routing schemes may be applied to arbitrary channel geometries to predict transport. Modeling the evolution of river channel patterns using calculations of instantaneous fluid and sediment transport may be effective for short-range prediction of channel adjustment. Scaling these results up to geologically relevant timescales, however, is not trivial because the governing equations are nonlinear and errors associated with inevitable parameterizations attenuate as we consider longer durations and larger spatial domains (e.g., Murray, 2003; Werner, 2003). Discontinuous processes such as channel avulsions, or historical contingencies such as stratigraphic controls and climate, cannot be treated easily in a detailed model. In the cases where

dynamic boundary conditions exert a strong control on channel morphology, such as anabranching rivers and deltas (Chapter 5), sophisticated models of instantaneous fluxes are not appropriate for predicting large-scale channel pattern.

The preceding paragraphs lead to several questions. What are the appropriate scales to consider in the transport of fluid and sediment in a (potentially rapidly) evolving river system? How do we incorporate dynamic boundary conditions into models of channel evolution? What are the most important feedbacks between sediment transport and channel pattern? How tightly coupled is the fluid flow to the topography, and the sediment transport to the fluid flow, in sandy alluvial systems? How do bifurcations and multiple channel branches arise in net depositional rivers? To address these questions we undertook an empirical study of the sandy, braided lower Niobrara River in northeastern Nebraska. The Niobrara empties into the Missouri River, and since the construction of dams on the Missouri in the mid 1950's, base-level forced deposition has de-stabilized the river and forced frequent channel avulsions (Bristow et al., 1999; Ethridge et al., 1999), apparently inducing the conversion of some reaches to relatively narrow anabranches separated by vegetated islands (see Background). We collected detailed measurements of channel geometry, fluid flow, sediment flux and bed topography in braided and anabranching reaches of the river. More specifically, we reoccupied the site of the 1995 avulsion reported by Ethridge et al. (1999) in 2004 and 2005 (Fig. 6.1), and undertook surveys and discharge measurements to assess the evolution of the two anabranches at the bifurcation site 10 years after the avulsion. These instantaneous measurements are combined with historical aerial photography and data on long-term aggradation rate in order to relate transport mechanics to larger-scale channel pattern.

In this paper we explore the co-existence of braided and anabranching river reaches of the lower Niobrara from a mechanistic point of view, using conservation of mass as a guiding principle. The stability of channel bifurcations is assessed using the nodal point formulation of Bolla Pittaluga et al. (2003). We compare the relative time scales of vertical aggradation and lateral channel mobility (Chapter 5) to better understand the conditions causing avulsions in the present Niobrara. It is our hope that this research will contribute to a better understanding of river planform geometry in general, the formation and maintenance of channel bifurcations in particular, and also to the conditions leading to channel avulsion.

6.2. Background

Extensive information on the geology and recent history of the lower Niobrara River is available in Ethridge et al. (1999), Bristow et al. (1999) and Skelly et al. (2003), which are the sources for the brief summary provided here. The Niobrara River has its headwaters in eastern Wyoming and flows mostly eastward through, skirting the northern margin of the Nebraska Sand Hills before turning north for its final 10 km to drain into the Missouri River in northeast Nebraska (Fig. 6.1) – this is our study area. The river does not have any dams along its entire length, save for a "run of the river" dam 70 km upstream of our study site that has no storage capacity. Bed material in the study area consists of medium sand (median diameter, d_{50} = 0.275 mm) whose grain size does not vary significantly in space throughout the lower Niobrara, and the bottom is almost entirely populated with depth-limited dunes, with sparse gravel ($d \approx 10$ mm) present in the troughs of bedforms located in channel thalwegs. Groundwater is the primary source of flow in the Niobrara and flow

variability is fairly low, with a mean annual discharge of 48 m^3/s. Lowest average monthly flows (31 m^3/s) occur in August when irrigation is most intense, and the highest monthly flows (72 m^3/s) are in April following snow melt. In the study section (Fig. 6.1) the Niobrara flows through a 1 km wide valley cut into Cretaceous shale and limestone having a total relief of 15 m. The active channel itself is about 300 m wide and the average water depth is 0.3 m, with the remaining valley floor composed of floodplain, abandoned channels or low terraces restricted to the east side of the valley.

The closure of the Gavins Point Dam on the Missouri River in 1957 has gradually raised base level at the mouth of the Niobrara River (Fig. 6.2), resulting in aggradation and large-scale channel pattern change in the lower Niobrara (Resource Consultants and Engineers, 1993). This rise in base level is not directly due to stage increase (the Missouri at the Niobrara mouth is upstream of the reservoir), but rather to deposition on the bed of the Missouri River induced by the presence of the Lewis and Clark Reservoir downstream. Before damming of the Missouri, the study area appeared to be entirely braided with a significantly wider channel belt and well-defined channel margins (Figs. 6.2 and 6.3). From 1957 to 1996 the Niobrara River approximately kept pace with the rise of gage elevation on the Missouri, aggrading at an average rate of 4 cm/yr at the Highway 12 bridge, located 2.25 km upstream of the mouth (Fig. 6.2). Much of the valley bottom has been converted to flooded wetland due to the rise in groundwater levels from impoundments on the Missouri, and intense vegetation growth has followed. Before the dam, the channel bottom was almost two meters below the surrounding floodplain (Bristow et al., 1999). The Niobrara began to experience crevassing and avulsions when the channel bottom aggraded to an elevation higher than that of the adjacent floodplains,

i.e. became superelevated (Bryant et al., 1995; Mohrig et al., 2000). Several documented avulsions have occurred between 1988 and the present in which the river has generally moved to occupy older, abandoned channels at lower elevation. These avulsions have created anabranching reaches in the Niobrara River where several channels remain active, separated by vegetated islands (Fig. 6.3). One such example is at the Highway 12 bridge, where in 1995 a crevasse splay developed that connected the Niobrara River to the Mormon Canal (which is actually a natural channel). Ethridge et al. (1999) reported that by 1996 the Mormon Canal had captured a majority of the discharge. Floodplain aggradation has been slower than that of the active channels, and is primarily driven by crevasse splay development rather than distributed overbank deposition.

In August 2004, we visited the site of the Highway 12 avulsion (Bristow et al., 1999; Ethridge et al., 1999) on reconnaissance, to assess the evolution of this bifurcation 9 years after its genesis. Comparison of our preliminary data to Ethridge et al. (1999) showed the channels to be quite dynamic over short time scales, and we endeavored to study the form and process of the lower Niobrara in more detail. We returned in August, 2005 for a focused study of the lower 6 km of the river, where aggradation has been highest and historical aerial photographs indicate that the river has undergone a significant change in planform geometry. Our study area contains two major anabranching reaches, both of which consist of two branches separated by relatively long-lived islands.

6.3. Methods

Aerial photographs

Digital orthophotoquads for our study region are available from the Nebraska Department of Natural Resources (http://www.dnr.state.ne.us/databank/spat.html) for the years 1993, 1999 and 2003. We took additional aerial photographs during the week of our study (August 5-13, 2005) for comparison to previous years, however these images are oblique and therefore may be used only qualitatively. Our discussion of river morphology prior to 1993 is based on historical photographs and interpretative sketches presented by Ethridge et al. (1999), Bristow et al. (1999) and Skelly et al. (2003), the earliest of which is from 1938.

Hydraulic measurements

All hydraulic measurements were conducted during low flow conditions. Although this sampling is biased, we believe that sediment transport and bed topography observed under these conditions may be reasonably representative of the lower Niobrara. The wide and shallow nature of the river means that large increases in discharge induce relatively small increases in water depth. This is illustrated by data from a gage at Highway 12, which show that water discharges of 28 m^3/s, 57 m^3/s and 85 m^3/s correspond to water depths of approximately 0.35 m, 0.43 m and 0.53 m – in other words, a tripling of discharge increases water depth by only 50%. While we do not have sufficient data to reconstruct the entire stage-discharge relationship at Highway 12, available data from Verdel (15 km upstream) show that stage increases slowly with discharge (Fig. 6.2). Further, the range of water surface slopes during low flow ($1.1 \times 10^{-3} - 1.3 \times 10^{-3}$) agrees well with the overall channel-bottom slope of the lower Niobrara (1.1×10^{-3}), and it is

unlikely that water surface slope deviates substantially from the channel-bottom slope at higher discharges.

The hydraulic geometry of single-branch and anabranching reaches was assessed by measuring water depth, h, along transects oriented perpendicular to channel banks. The sampling interval was 3-4 m in the cross-stream direction. Depths almost everywhere were less than 1.5 m, and therefore our data were collected by walking the channels. Depth was measured using a meter stick, while position was marked using a Trimble ProXH differential GPS receiver with 30-cm spatial resolution. As transects were never perfectly straight lines, a linear regression was fit to location data, and the locations were projected back onto this line in order to allow more accurate estimation of cross-sectional area, A, and wetted perimeter, P. The value of A was obtained by numerically integrating the area under the transect profile, while P was computed as the sum of distances between points in which water depth was greater than zero (i.e., exposed bar tops were not counted). Channel width, B, was also computed using only wetted river, and hydraulic radius was calculated as $h_r = A/P$. The active channel width, W, is simply the total width of all channels between vegetated banks – this value is the total width of the channel that would be inundated during flood (Fig. 6.4). Due to the wide and shallow nature of the river, $P \approx B$ and $h_r \approx \overline{h}$, where the overbar denotes a cross-sectional average.

For some transects the fluid velocity, u, was measured at each location at a distance of $0.4h$ above the bed, using a Sontek portable Acoustic Doppler Velocimeter (ADV) mounted to a top-set wading rod. Measurements were always taken at the crests of bedforms. These data allowed us to compute fluid discharge, Q, at each cross-section using the following formula:

$$Q = \sum_i^N u_i h_i \left[\frac{w_{i-1:i} + w_{i:i+1}}{2} \right], \quad (1)$$

where N is the total number of individual measurements i in a transect, and w is the distance between two subsequent measurement locations. The margins of channels, large bars and islands in our study reaches were delineated by walking their borders and logging GPS locations every 1 s. To compute water surface slope, S, water surface elevations were measured with a Leica laser theodolite; the bottom of the survey rod was equipped with a disk that was placed gently on the water surface. Elevation was recorded at least every 20 m down the channel centerline, and in some cases every 3-4 m, for distances of 300-400 m, and a best-fit linear regression to the elevation data was used to compute slope of the reach.

Sediment transport measurements

For a small number of transects we also measured sediment flux, q_s, in a manner analogous to water velocity. Sediment was trapped using three scaled-down Helley-Smith samplers, each with an opening of 2.54 cm × 2.54 cm, allowing estimation of near-bed load and suspended load. These samplers were stacked vertically so that the bottom trap captured sediment traveling between the bed and 2.54 cm, the next between 2.54 and 5.08 and the final between 5.08 and 7.62 cm above the bed (Fig. 6.5); a comparable system was described in Mohrig and Smith (1996). Mesh size of sampling bags was 0.125 mm, so grains having a significantly smaller dimension were incompletely captured. As collection of these data was far more labor intensive than other measurements, only three transects

were sampled, with a distance of 5-10 m between points. The sampler was placed flush on a dune crest (Mohrig and Smith, 1996) and held in place for 30 s. At the same time, fluid velocity, depth to the dune crest, and depth to the dune trough were also measured. Local water depth was taken as the average of dune trough and crest depths – local water velocity was measured at $0.4h$ from the dune crest and is not corrected for this small discrepancy. Sediment samples were later dried and weighed, and sediment mass flux for each bin estimated as sample weight divided by sample width and sampling duration. For all samples, about 90% of the total mass was captured in the bottom sampler (Fig. 6.6). Reported values for sediment flux in this paper refer to this near-bed load (which also contains some suspended sediment load due to the size of sediment traps), which was converted to a volume flux per unit width, q_s, using a grain density of $\rho_s = 2650$ kg/m^3 (Fig. 6.6). Sediment discharge, Q_s, was computed in a manner similar to fluid discharge:

$$Q_s = \sum_i^N q_{si} \left[\frac{w_{i-1:i} + w_{i:i+1}}{2} \right] \quad (2)$$

The nominal grain diameter for each sample was estimated using a Camsizer (Retsch Technology), which digitally images and measures most grains in a given sample and therefore has negligible errors.

6.4. Results

Aerial photographs (Fig. 6.3) and topographic surveys (Resource Consultants and Engineers, 1993) document the channel narrowing of the lower Niobrara (Fig. 6.2C), and the conversion of the valley floor to wetland floodplain covered with dense vegetation

following base-level rise since 1957 (Ethridge et al., 1999; Skelly et al., 2003). Bristow et al. (1999) reported that in 1976 there were no crevasse splays in the vicinity of Highway 12, but by 1988 crevassing and avulsions began upstream of the bridge (see Ethridge et al., 1999), with the Mormon Canal capturing some discharge from the Niobrara. Peak annual discharge during this time was not larger than normal (Fig. 6.2E), so the onset of crevassing cannot be explained by flooding alone.

All data presented below are from the 2005 field campaign, unless otherwise specified. Cross-section geometries show the wide range in channel form exhibited by the Niobrara River (Fig. 6.7). We split the measured transects into three general sections (Fig. 6.7): (1) the most upstream transect down to (and including) the first anabranching region is considered "Verdigre site" (Fig. 6.4), as the mouth of Verdigre Creek is located approximately 1 km upstream of this area; (2) the middle study area, including the second anabranching region, is referred to as "Highway 12 site" (Fig. 6.4); and (3) the most downstream reach is called "RR site", after the old railroad bridge that also marks the downstream edge of the Niobrara Valley and the beginning of the delta. Within each site, transects are split into reaches, i.e., single-branch or anabranching. In order to compare hydraulic geometry and flow among single-branch and anabranching sections, the data are reach-averaged to obtain representative values (table 6.1).

The closest USGS gaging station is at Verdel, approximately 20 km upstream of the study area. The only discharge reading close to the time of our study (August 5-13, 2005) was on August 22, with a reading of Q = 32 m^3/s. Our measured discharge range over the week of study was 29-35 m^3/s (table 6.1), indicating good agreement with the gage and relatively steady flow over the study duration.

Verdigre site

Photographs of this area indicate that the present bifurcation and anabranching structure was established sometime between 1957, when only one channel was present, and 1974, the next available photograph. From 1974 to 1993 a third channel to the west of the present bifurcation was also active. By 1999 (the next available image), this channel had mostly filled with sediment, and is now inactive and covered with vegetation (Fig. 6.8). The studied anabranches at the Verdigre site have changed little in width and length since 1974, although photos indicate that in 2003 the mouth of the left anabranch was almost completely choked with sediment due to the presence of a large, exposed sand bar. No such obstruction was seen August 2005, however an attached bar on the right side of the river upstream of the bifurcation was substantially larger in 2005 compared to 2003 (Fig. 6.8). These plan view data indicate that flow switching and its associated channel filling and scouring have occurred several times at this site since the 1970s.

At the Verdigre bifurcation in 2005, flow diverged into two channels of uneven width, with the right anabranch twice as wide as the left (table 6.1; Fig. 6.4a, Fig. 6.7). The hydraulic radii of the two anabranches were comparable (0.33 m and 0.37 m for left and right channels, respectively), and nearly identical to that of the upstream single-belt channel (0.35 m). Water surface slopes were also nearly identical in the upstream reach and both anabranches. Sediment flux was measured across a transect upstream of the bifurcation (transect V3 in Fig. 6.4a), and sediment discharge computed as $Q_s = 3.4\times10^{-3}$ m^3/s (9 kg/s).

Highway 12 site

As discussed above, the Niobrara River at Highway 12 has been extremely dynamic since the mid 1990s (Fig. 6.9). In 1988, a crevasse splay developed that connected the mostly-abandoned Mormon Canal to the Niobrara River approximately 1 km upstream of the Highway 12 bridge (Bristow et al., 1999; Ethridge et al., 1999), diverting some flow into the Mormon. More crevasse splays developed in the early 1990s, and in 1995 a breach in the left levee of the Niobrara 250 m upstream of the bridge caused the river to avulse into the Mormon Canal, creating the present bifurcation and island at this study area. By spring of 1996 the Mormon had captured a majority of the flow (Bristow et al., 1999). The next available photographs in 1999 and 2003 show the Mormon Canal retaining most of the discharge, and by 2003 the old Niobrara channel had narrowed from 100 m to 20 m due to intense vegetation growth and consequent bank stabilization.

Discharge measurements (cross sections M4 and O5 of Fig. 6.4b) in August 2004 show that the Mormon canal contained 91% of the flow, had an active thalweg exceeding 2 m in depth and a total width of 70 m (Fig. 6.10). The old Niobrara, meanwhile, was less than 0.5 m deep everywhere, and contained only 9% of the discharge – it appeared that the avulsion to the Mormon Canal was almost complete. In August 2005 we returned to these same cross sections to find that the situation had reversed dramatically (Fig. 6.9). In one year the Mormon canal had filled an average of 0.3 m with sand at the site of the bridge, but with no decrease in width. This anabranch also had a large sand bar at its mouth, and contained only 16% of the total discharge. The river had reverted back to the old Niobrara channel, which widened by 20 m and deepened an average of 0.4 m (Fig. 6.10) over the

course of one year. Several area residents claimed that such channel switching is commonplace, often following large storms.

These changes may have been influenced by the presence of the Highway 12 bridge, whose abutments restrict the width of the present Mormon Canal (Fig. 6.9). Surveyed cross sections reveal, however, that the bridge is a site of channel scour – both in the Mormon Canal and the old Niobrara channel (Fig. 6.7). It is thus unlikely that the bridge creates any substantial backwater that would induce deposition and lead to avulsion. The filling and scouring of channels by flow switching occurs in the unrestricted Verdigre bifurcation as well, as revealed by aerial photographs (Fig. 6.8). Without more data we cannot determine what role, if any, the Highway 12 bridge plays in the morphology and dynamics of the bifurcation at this site.

The configuration observed in our 2005 campaign appeared to be evolving rapidly, as bank collapse in the old Niobrara delivered large chunks of sod to the channel bottom. Between the downstream end of the Verdigre island and the bifurcation at the Highway 12 site, the channel was wide (almost 300 m, Fig. 6.7) and shallow (table 6.1). While the Mormon Canal was shallower than the upstream channel, the old Niobrara had eroded such that its mean depth was 0.6 m deeper than the upstream reach. Remarkably, water surface slope in the all three reaches was the same (Fig. 6.11), and nearly identical to the values at Verdigre site. Flow resistance was also similar among these reaches. Sediment flux and discharge were measured for each anabranch just downstream of the bifurcation tip (Fig. 6.4b). Unfortunately, flow in the thalweg of the old Niobrara channel was too fast and deep to allow sediment sampling, so values had to be extrapolated over 23 m (total width at the sample site was 81 m) from the deepest measurements made at the last two

sampled sites, likely resulting in an underestimate of Q_s. Computed sediment discharge from measured flux data was 1.1×10^{-3} m^3/s for the Mormon and 1.8×10^{-3} m^3/s for the old Niobrara, for a total of $Q_s = 2.9\times10^{-3}$ m^3/s. This volume flux is close to but smaller than the value of 3.4×10^{-3} m^3/s estimated at the Verdigre site; it is not possible to determine whether this difference is a result of measurement error or a true decrease in sediment discharge between the two sites.

RR site

The final kilometer of the Niobrara River includes the Niobrara delta, which has prograded more than 500 m into the Missouri River. Upstream of the railroad bridge the channel is still confined by the valley, and is similar in hydraulic geometry to upstream single-belt channels (Fig. 6.7). Downstream of the railroad bridge the river begins to widen on the delta top, and many large, exposed bars result from flow divergence on approach to the Missouri. Nevertheless, water surface slope and depth over this entire reach were comparable to the Verdigre site (table 6.1).

Variability in fluid and sediment transport

In the above sections we discussed bulk hydraulic properties such as mean streamwise velocity, water surface slope, and total fluid (eq. 1) and sediment (eq. 2) discharges. Measured values of instantaneous water velocity and sediment flux varied widely at each collection point along the channel (Fig 6.12), due in part to the large spatial variations in bottom topography of this braided river. To further explore this variability, we performed additional measurements of sediment flux, water velocity and depth over 30

dunes in the thalweg of the old Niobrara channel upstream of the Highway 12 bridge. Combining all measured values, we find that instantaneous sediment flux is only weakly correlated with local velocity and water depth, while water velocity is not correlated to water depth (Fig. 6.13). In other words the sediment transport was not tightly coupled to the local fluid transport, and the fluid flow was not strongly dependent on local topography. The combined distribution of bed stress (see section 6.5) from several river reaches is well fit by a gamma function that is skewed towards values larger than the mean, in agreement with Paola et al. (1999). The distribution of sediment flux is even more skewed, with the best fit function being the exponential (Fig. 6.14).

6.5. Interpretation and discussion

Calculated parameters

From these fundamental measures of fluid and sediment transport, we computed many derivative parameters in order to relate transport mechanics to cross-sectional geometry and river planform pattern. While the variability in measured quantities across a transect contains valuable information, we reduced many of these data to mean quantities for each transect in order to proceed with a simple, one dimensional (1D) analysis of sediment and fluid routing down the river. Despite the dangers and limitations of this simplified approach, we show that much insight can be gained without immediately proceeding to more sophisticated algorithms. Our results also show the importance of collecting a large number of samples to generate a meaningful average. Assuming steady and horizontally uniform flow we compute mean boundary shear stress, $\bar{\tau}$, as

$$\bar{\tau} = \rho g h_r S\,, \tag{3}$$

where $\rho = 1000$ kg/m^3 is the density of water and g is acceleration due to gravity. We can also compute the Chezy friction factor, c_f, as a measure of flow resistance due to channel roughness:

$$c_f = \frac{g h_r S}{\bar{u}^2}\,, \tag{4}$$

where $\bar{u} = Q/A$. If we take the computed value of c_f as constant for a given river reach, we can also estimate the local stress, τ_o, at each point where velocity was measured across a transect (Paola et al., 1999):

$$\tau_o = \rho c_f u^2\,. \tag{5}$$

With sufficient measurements, the average of local stresses should be approximately equal to the reach-averaged stress computed from the depth-slope product (3).

In order to compute sediment flux from calculated bed stress, we must correct for momentum extraction of the flow due to form drag, τ_d, of dunes on the river bottom:

$$\bar{\tau} = \tau_d + \tau_{sf}\,, \tag{6}$$

where remaining skin friction, τ_{sf}, is the stress available to transport sediment. There are many available formulae of varying complexity for computing τ_{sf} – here we choose a fairly simple formulation recently derived by Lynds (2005). The analysis starts with the well-known expression for form drag developed by Nelson and Smith (1989). Lynds (2005) then assumes that the river bottom is covered in depth-limited dunes (Fredsøe, 1982) having a height, $H = 0.3\overline{h}$, and a steepness, $H/\lambda = 0.063$, where λ is dune wavelength. These values are in fact very close to measured bedform geometries in the Niobrara River. With a few further (much less drastic) assumptions, Lynds (2005) arrives at the relation

$$\frac{\overline{\tau}}{\tau_{sf}} = 1 + 0.04\left[\ln\left(\frac{2.14H}{d_{50}}\right) - 1\right]^2. \tag{7}$$

The dimensionless skin friction, $\theta_{sf} = \tau_{sf}/(\rho_s - \rho)gd_{50}$, may be used to directly estimate bedload flux through the Meyer-Peter and Müller (1948) relation

$$\Phi = 8.5(\theta_{sf} - 0.047)^{3/2}, \tag{8}$$

where $\Phi = \overline{q}_s/\sqrt{Rgd^3}$ is dimensionless bedload flux and $R = (\rho_s/\rho - 1)$ is relative submerged density of grains. Sediment discharge at a cross section may then be calculated:

$$Q_s = \int_0^B \overline{q}_s = \overline{q}_s B. \tag{9}$$

Measured and calculated sediment flux

The wide variability in instantaneous measured parameters shows the importance of collecting sufficient data, in order to populate probability distributions and obtain representative average values (Fig. 6.14). We have seen that local sediment flux is not well predicted from local bed stress (Fig. 6.13). This lack of correlation may be a consequence of two factors: (i) the relationship between bed stress and sediment flux does not hold at these scales in the Niobrara River, or (ii) variability in the friction factor, which we have assumed to be constant. At present, we cannot independently constrain the friction factor, and therefore we cannot conclusively determine the reason for the observed poor correlation. The bedload transport equation (8) is only strictly valid for conditions approximating steady and uniform flow, in which case spatially-averaged values for bed stress and sediment flux may be appropriate. To assess the validity of using mean bed stress as a proxy for sediment flux, we compare measured values of mean sediment flux to those computed using eq. 8. There are four values that may be used for comparison; one each from the Verdigre, Mormon and old Niobrara transects (table 6.1), and an additional average value from the thalweg dunes in the old Niobrara channel. When these averaged values of measured q_s are plotted against values computed using reach-averaged skin friction (eq. 8) we find remarkable agreement (Fig. 6.15a), despite the fact that variability in sediment flux within a transect is very large. Comparison of estimated versus measured sediment discharge shows even better agreement (Fig. 6.15b), giving confidence that we may use these equations to assess sediment and fluid routing throughout our study area.

At present, the reason for this agreement between spatially-averaged sediment flux and calculated sediment flux is uncertain. Paola et al. (1999) found that spatially-averaged sediment flux measured from active channels on a braided fan was two to three times larger than the predicted value, and attributed this difference to fluctuations in fluid velocity and water depth which contribute an additional "stress". Our measurements in the Niobrara include both active channels and inactive, shallow bars. It is possible that by averaging sediment flux from the entire channel, and not just from deeper channel threads, we have offset the stress contribution from "deviatoric" local velocities and channel depths. A more detailed future sampling campaign may resolve this issue, which is crucial for predicting channel evolution over long times.

Conservation of mass

The continuum 1D form of mass continuity with negligible suspended sediment transport is:

$$\frac{\partial \eta}{\partial t} = -\frac{1}{(1-p)}\frac{\partial q_s}{\partial x}, \tag{10a}$$

while its discrete form may be written as:

$$\frac{\eta_2 - \eta_1}{t_2 - t_1} = -\frac{1}{(1-p)}\frac{q_{sout} - q_{\sin}}{L}, \tag{10b}$$

where η is elevation, t is time, $p = 0.35$ is assumed sediment porosity, and x is the direction of transport. In the discrete form, elevation is measured at two points in time (hence the subscripts), while divergence of sediment flux is considered over a given length of river, L. Equation 10a may be rearranged in the following manner (Smith, 1970),

$$\frac{\partial \eta}{\partial t} = -\frac{1}{(1-p)} \frac{\partial q_s}{\partial \tau} \frac{\partial \tau}{\partial x}. \tag{11}$$

This equation shows that $\partial \eta / \partial t$ depends on the relationship between sediment flux and bed stress, and on gradients in bed stress. Since $\partial q_s / \partial \tau$ is always positive (eq. 8), it is shear stress gradients that determine the sign of $\partial \eta / \partial t$, and hence whether the bed undergoes erosion or deposition.

Using eqn. 10b we can quantify the average depositional flux (divergence) in the lower Niobrara River. Surveyed channel profiles from the Army Corps of Engineers (Resource Consultants and Engineers, 1993) show that the stretch of river from 8.3 km to 11.7 km upstream of the mouth aggraded more or less uniformly by a thickness of 0.9 m over 27 years, giving a net depositional flux of 2×10^{-6} m^2/s. According to our measurements, this depositional flux is approximately 10% of the bedload flux passing through the Niobrara River, a substantial amount.

Bed material samples from the Niobrara show a uniform grain size distribution with negligible spatial variability, indicating that the bed does not adjust through grain size. If we assume that channel evolution tends toward a condition where bed erosion or deposition is minimized, this implies from eq. 11 that the river will also evolve to

minimize spatial variations in bed stress (Dade and Friend, 1998). Indeed, values for dimensionless stress in the lower Niobrara were similar among single-branch and anabranching reaches in Verdigre and RR sites (table 6.1), with a mean value $\theta = 0.88$ and a range of 0.82-0.95. The highly dynamic Highway 12 site had values of θ significantly higher (in old Niobrara) and lower (Mormon Canal and single-branch channel) than this range (table 6.1). However, combining the Mormon and old Niobrara channels gives $\theta = 0.97$, suggesting that the unit anabranching region behaves similarly to other reaches.

Instantaneous measurements show that the transport of sediment is not tightly coupled to the fluid at a local scale (Figs 6.12, 6.13), however spatial integration over a cross section reveals a simple balance between bed stress and sediment transport for all sections of the river. Overall, these results show that even though the lower Niobrara is out of grade and exhibits highly varying planform geometry, the river is dynamically adjusted by sediment continuity such that water and sediment are routed through all reaches in a similar manner. From this perspective, the very different planform geometries present in the Niobrara represent statistically similar realizations of channel configuration (e.g., Lewin and Brewer, 2001). While this result may seem obvious, it defies our expectation that channel planform pattern may be predicted from instantaneous values of sediment discharge, water discharge and channel slope.

Bifurcations

We have observed several relatively stable channel bifurcations and vegetated islands in the lower Niobrara. Aerial photographs and field surveys have shown that these river junctions are far from static, however, with channel switching a common occurrence.

A case in point is the Highway 12 bifurcation: observations from 1996, 1999, 2003 and 2004 indicated that the Niobrara was steadily abandoning the old channel and avulsing to the Mormon Canal. The reversal in discharge distribution that occurred between 2004 and 2005 was surprising in this light. Local knowledge suggests, however, that such switching is commonplace, and the rapidity of channel switching means this process may have taken place several times over the past decade without being resolved by aerial photographs. While we cannot rule out the influence of the Highway 12 bridge on bifurcation evolution at that site, the apparent similarity in channel switching at the Verdigre bifurcation indicates that the bridge is not responsible for the general dynamical behavior.

We assess the stability of bifurcations and their anabranching channels using a simplified nodal point formulation (Bolla Pittaluga et al., 2003) based on a 1D conservation of mass. We divide each bifurcation site into three sections: an upstream single-branch reach (*a*), the left bifurcation mouth (*b*), and the right bifurcation mouth (*c*) (Fig. 6.16). The model assumes that width of channels adjusts substantially slower than channel depth (due to vegetation) such that banks can be treated as static. Sediment flux for each section is estimated using the respective values for estimated mean skin friction and eq. 8 – i.e., calculated values for sediment flux are used, rather than measured values which are not available for all sites. Field observations have shown that flow may begin to diverge upstream of a channel bifurcation (Richardson and Thorne, 2001), and experiments by Bolla Pittaluga et al. (2003) indicate this occurs over a distance of approximately three channel widths. To estimate erosion or deposition at the mouth of each anabranch, conservation of mass (10b) is applied between section a and each anabranch over a length $L = 3B_a$ (Fig. 16):

$$\frac{\partial \eta_b}{\partial t} = -\frac{1}{(1-p)} \frac{q_{sb} - q_{sa}}{3B_a}, \tag{12a}$$

and

$$\frac{\partial \eta_c}{\partial t} = -\frac{1}{(1-p)} \frac{q_{sc} - q_{sa}}{3B_a}, \tag{12b}$$

In applying the nodal point formulation to gravel rivers, Bolla Pittaluga et al. (2003) included a transverse sediment flux term to account for the gravity-driven transport down transverse bed slopes at low Shields stress. In the Niobrara River, however, Shields stress is far above critical and our measurements show that, in a mean sense, sediment discharge closely follows water discharge. In applying this model, we use flow conditions present at the time of observation – these flow conditions ($Q_w \approx 34$ m^3/s) were not very different from the 2004 annual mean ($Q_w \approx 43$ m^3/s), so computed mean erosion and deposition rates should be of the appropriate magnitude.

The nodal point model indicates that the Verdigre Creek bifurcation was relatively stable. This result is in a sense obvious, because the computed bed stresses (and therefore sediment fluxes) for sections *a*, *b* and *c* were nearly the same (table 1), and therefore the divergence in sediment flux should be close to zero. Calculations for Highway 12 using equation 12 indicate that the Mormon Canal should have been filling at a rate of 0.07 cm/day and the old Niobrara channel eroding at 0.8 cm/day. Measured values from surveys in 2004 and 2005 give a deposition rate of 0.08 cm/day and an erosion rate of 0.1 cm/day

for the Mormon and old Niobrara channels, respectively. It is not surprising that the calculated and measured values for erosion in the old Niobrara are different, given the unsteady nature of sediment transport in this very dynamic reach. Moreover, the old Niobrara widened by 100%, while the nodal point formulation forces all adjustment into channel depth – this is the most likely explanation for the over-prediction of bottom erosion. It is worthy of note that measured and calculated values for deposition rate in the Mormom Canal, whose width did not vary, are nearly identical. More important is the inescapable conclusion that the old Niobrara channel is eroding at an unsustainable rate, while the Mormon Canal is filling. In the absence of some external control, the Niobrara seems likely to eventually capture all flow.

If water surface elevations and slopes are roughly equal in all channels, as observed in the Niobrara, then according to the nodal point formulation there are only two stable solutions for the geometry of a channel bifurcation with high Shields stress under steady flow; either that both anabranches have equal depth and hence equal stress, or that one channel eventually captures the entire discharge. The reasoning is as follows: if one channel becomes significantly deeper than the other, then it also has greater stress and therefore it scours, further deepening and capturing more flow until the other channel is abandoned. We know, however, that bifurcations on the Niobrara are stable on decadal time scales – where have we gone wrong?

We propose that bifurcations on the lower Niobrara are both created and maintained by channel avulsions, a process not considered in models of bifurcation stability. Slingerland and Smith (2004) described the avulsion process in terms of the setup, i.e., the conditions causing a channel to become unstable, and a trigger, which is an

event that perturbs the unstable channel and forces an avulsion. The setup on the Niobrara River is superelevation of the river channel (Heller and Paola, 1996; Mohrig et al., 2000) above its floodplain. In Chapter 5 I showed that rivers become susceptible to avulsion when the channel aggrades to an elevation of one channel depth above the floodplain (Mohrig et al., 2000), i.e., a relative superelevation of 1. The characteristic time scale for avulsion setup, T_A, is the time required for the channel to achieve a relative superelevation of 1 (Chapter 5) and may be approximated as:

$$T_A = \frac{\bar{h}}{v_A}, \tag{13}$$

where v_A is an average channel aggradation rate. This avulsion time scale is approximately 4 yr for the lower Niobrara, in agreement with the recent avulsion history of the Highway 12 bridge site reported by Bristow et al. (1999). We hypothesize that the trigger of channel switching is the diversion of flow due to exposed sand bars. Experiments have shown that sand bars migrating into the bifurcation region can induce dramatic discharge oscillations (Bolla Pitaluga et al., 2003; Bertoldi et al., 2005) by deflecting flow from one anabranch to the other. On the Niobrara we have observed large, exposed bars apparently blocking the mouth of one anabranch in a bifurcation (Figs 6.8, 6.9). We suspect that these bars form during high stage events and deflect flow toward the open anabranch, possibly causing flow switching from superelevated channels.

The nodal point formulation cannot predict the evolution of bifurcations in which long-term aggradation and avulsions are important. Using the Niobrara as an example, we propose a conceptual model for the creation and maintenance of bifurcations in channels

that are experiencing net deposition and avulsion (Fig. 6.17). A single-branch channel will become unstable and eventually avulse when it achieves a relative superelevation of approximately 1, creating a bifurcation. When an avulsion first occurs, incision follows because the new channel is under-fit for the incoming flow (Mohrig et al., 2000; Slingerland and Smith, 2004), as observed in the old Niobrara channel in 2005. Avulsed rivers often re-occupy previously abandoned channels (Heller and Paola, 1996; Mohrig et al., 2000). After this initial incision phase, the new channel begins aggrading while flow in the old channel diminishes. In the case of the Niobrara, the abandoned channel first fills with sediment while maintaining its width (e.g., Mormon Canal, Fig. 6.10). Slowly, this channel decreases in width at a rate that is determined by the growth of vegetation (Tal et al., 2004). Eventually, the dominant channel becomes superelevated relative to the floodplain and is susceptible to abandonment. When an avulsion trigger such as a bar or flood perturbs the superelevated dominant channel, flow is diverted into the old channel which erodes anew and begins to capture more flow. If the avulsion setup time (eq. 13) is small compared to the time associated with the growth of vegetation and channel abandonment, then flow switching will be common and a bifurcation will be maintained. Not all overbank events result in avulsion. On the Niobrara, crevasse splays commonly occur and appear to be the principle means of floodplain aggradation (Bristow et al., 1999), however only a few of these events lead to a channel avulsion.

Although the model presented above is not quantitative, we may use simple scaling to anticipate the conditions under which bifurcations will be maintained and a multi-branch pattern will occur in rivers (Chapter 5). The characteristic time scale associated with channel migration may be written as (e.g., Tal et al., 2004)

$$T_C = \frac{B}{v_C}, \tag{14}$$

which is the time required to erode one channel width by bank erosion, where v_C is a representative bank erosion rate. If a channel migrates laterally much faster than it aggrades, multiple channels will not be maintained because reworking of the floodplain by the channel will absorb previously abandoned channels. Multiple branches and bifurcations are expected when the time scale of avulsions is substantially smaller than that of significant bank erosion, such that abandoned channels remain intact and connected to the dominant channel while avulsions are relatively frequent. This can be cast in terms of the mobility number, *M*, which is the ratio of avulsion and lateral migration time scales (Chapter 5):

$$M = \frac{T_A}{T_C} = \frac{h}{B}\frac{v_C}{v_A}. \tag{15}$$

Field data from 30 river systems show that multiple branches and bifurcations are present for $M < 1$, while single branch rivers are always associated with $M > 10$ (Chapter 5). For the present lower Niobrara (using v_C = 10 m/yr, the measured value in the old Niobrara from 2004 to 2005), $M = 0.2$.

One last comment on the stability of Niobrara bifurcations deserves mention here. The condition for conservation of mass for sediment discharge at a bifurcation is

$$Q_{sa} = Q_{sb} + Q_{sc}, \tag{16a}$$

which may also be written:

$$\overline{q}_{sa} B_a = \overline{q}_{sb} B_b + \overline{q}_{sc} B_c. \tag{16b}$$

Condition 16b illustrates that a channel section may adjust its depth and roughness (which both contribute to τ_{sf}, and hence q_s) or its width to accommodate a given sediment discharge. In the case of Verdigre Creek, calculated values for the left- and right-hand sides of 16b were equal ($Q_s = 3.3\times10^{-3}$ m^3/s) indicating a stable situation. For the Highway 12 site $Q_{sa} = 3.7\times10^{-3}$ m^3/s, while $Q_{sb} + Q_{sc} = 2.9\times10^{-3}$ m^3/s. This result suggests the bifurcation site should have been aggradational at the time of study, and that the old Niobrara channel was under-fit in terms of capacity to transport the imposed sediment discharge. The abrupt filling of the Mormon Canal, which may have been caused by flow diversion due to a bar, likely forced flow into the old Niobrara channel. The implication is that the old Niobrara will widen and deepen until it can accommodate the upstream sediment load.

6.6. Conclusions

Dams on the Missouri River have increased base level and elevated the groundwater table in the lower Niobrara River valley, forcing rapid in-channel aggradation and allowing the growth of wetland vegetation in the floodplain. Currently, 10% of the sediment load supplied to the lower Niobrara River is deposited on the bed. Rapid and unpredictable

adjustments in channel geometry and planform have occurred in the last 50 years that have resulted in the destruction of farmland and relocation of the town of Niobrara. Currently no theory exists to predict what the new equilibrium state of the river will be. Using the Niobrara as a natural laboratory, we have combined detailed measurements of flow and sediment transport with physical reasoning to assess what is general about form and process of sandy rivers.

At the smallest temporal and spatial scales, flow and sediment transport are not strongly correlated in the Niobrara River. The extreme variability of instantaneous transport rates across a channel transect, and the decoupling of topography, fluid flow and sediment flux, suggests the nature of transport in this braided river is inherently stochastic. Nevertheless, spatial averaging shows a balance between the driving force (bed stress) and channel response (sediment flux) at larger scales. Data show that mean stress and sediment flux are the same in river reaches having very different planform geometries, indicating that many different channel patterns represent statistically-equivalent realizations in terms of mean transport. The dynamics of channel pattern, then, are decoupled from the smaller-scale dynamics of sediment transport.

Aggradation-driven avulsion has caused the formation of channel bifurcations that are stable on decadal time scales. The temporal consistency of bifurcation patterns in map view, however, belies their dynamic nature, as the depths of anabranches can change substantially over the lifetime of a bifurcation – since the 1970s, two bifurcations in the lower Niobrara have exhibited channel scour and filling associated with avulsions. We suggest a conceptual model for the formation and maintenance of bifurcations in rivers experiencing net deposition and avulsion. In this model, the superelevation of channels is

the setup for avulsion, and the trigger for the Niobrara is flow diversion by exposed sand bars, inducing channel switching which prevents one anabranch from completely capturing the discharge. Thus, persistence of bifurcation patterns in sandy systems, whether in anabranching rivers or distributary deltas, does not necessarily imply steadiness of flow (Makaske, 2001).

At the planform scale, base-level induced aggradation in the lower Niobrara River following closure of the Gavins Point Dam appears to have created conditions conducive to the formation of anabranches, which has been quantified using simple scaling arguments (Chapter 5). Vegetation growth likely contributed to the gradual decrease in channel width observed since the closing of Missouri River dams (Ethridge et al., 1999), and may have acted to suppress lateral channel mobility due to enhanced bank strength (Murray and Paola, 2003; Tal et al., 2004). It is possible that continued avulsions and vegetation growth will force a transition from a primarily braided to an anabranching pattern along the entire aggrading reach.

The coexistence of different channel patterns having essentially the same transport conditions should give reason for pause in applying detailed sediment transport models to large-scale channel evolution. Vegetation, flow unsteadiness, avulsions and historical contingency all play a role in generating the planform geometry of the Niobrara River, and would be difficult to represent in a first-principles approach. At present, it appears that the requisite conditions for modeling planform pattern and dynamics in a sandy river are: (a) the simplest possible representation of the small-scale sediment transport processes that contribute to dynamics at a larger scale; and (b) a framework that allows complex and time-varying boundary conditions. Recent work by Murray and Paola (2003) has

demonstrated the promise of using alternative approaches for modeling the evolution of planform patterns. By abstracting the details of fluid and sediment transport to a set of physics-based rules, they were able to model the large-scale dynamical behavior of braided rivers (Murray and Paola, 1994; 1997). The simplicity of the model allowed incorporation of vegetation growth, which acted to decrease bank erosion through sediment stabilization (Murray and Paola, 2003). Some of their main results, that vegetation can induce channel narrowing and force a transition from a braided to a single-thread river, have been verified experimentally (Gran and Paola, 2001; Tal et al., 2004) and in the field (Schumm, 1985; Tal et al., 2004). While vegetation alone may select for a narrow single-thread channel, forced aggradation leads to avulsion and the generation of anabranches in their model – the very same conditions that we propose are causing the formation of anabranches in the Niobrara, and that others have described for anabranching rivers in general (Nanson and Knighton, 1996; Makaske, 2001). The Murray and Paola (2003) model shows that the same physical processes – when subject to different boundary conditions – can produce qualitatively diverse river patterns. This approach, when coupled with field data from rivers such as the Niobrara, seems especially promising for exploring how changes in boundary conditions and sediment character can cross process thresholds and force transitions in planform.

Acknowledgements

This work was supported by the STC Program of the National Science Foundation via the National Center for Earth-surface Dynamics under agreement EAR-0120914. We thank Paul Heller, Neil Humphrey, Joel Johnson, Heather Jones and Margaret Wilson for

company and support in our field campaign, and Neil in particular for the wild ride in the sky.

References

Bertoldi, W., and Tubino, M, 2005, Bed and bank evolution of bifurcating channels: Water Resources Research, v. 41, W07001, doi:10.1029/2004WR003333.

Bolla Pittaluga, M., Repetto, R., and Tubino, M., 2003, Channel bifurcation in braided rivers: Equilibrium configurations and stability: Water Resources Research, v. 39, 1046, doi:10.1029/2001WR001112.

Bristow, C.S., Skelly, R.L., and Ethridge, F.G., 1999, Crevasse splays from the rapidly aggrading, sand-bed, braided Niobrara River, Nebraska: effect of base-level rise: Sedimentology, v. 46, p. 1029-1047.

Bryant, M., Falk, P., and Paola, C., 1995, Experimental study of avulsion frequency and rate of deposition: Geology, v. 23, no. 4, p. 365-368.

Dade, W.B., 2000, Grain size, sediment transport and alluvial channel pattern: Geomorphology, v. 35, p. 119-126.

Dade, W.B., and Friend, P.F., 1998, Grain-Size, Sediment-Transport Regime, and Channel Slope in Alluvial Rivers: Journal of Geology, v. 106, p. 661-675.

Eaton, B.C., Church, M., and Rosenau, M., 2004, Rational regime model of alluvial channel morphology and response: Earth Surface Processes and Landforms, v. 29, p. 511-529.

Ethridge, F.G., Skelly, R.L., and Bristow, C.S., 1999, Avulsion and crevassing in the sandy, braided Niobrara River: Complex response to base-level rise and aggradation.

In: Smith, J., and Rogers, J. (Eds.), Fluvial Sedimentology VI. International Association of Sedimentologists, Special Publication 28. Blackwell Science, London, p. 179-191.

Fredsøe, J., 1982, Shape and dimensions of stationary dunes in rivers: Journal of the Hydraulics Division – ASCE, v. 108, no. 8, p. 932-947.

Gran, K., and Paola, C., 2001, Riparian vegetation controls on braided stream dynamics: Water Resources Research, v. 37, no. 12, p. 3275-3283.

Heller, P.L., and Paola, C., 1996, Downstream changes in alluvial architecture: An exploration of controls on channel-stacking patterns: Journal of Sedimentary Research, v. 66, no. 2, p. 297-306.

Lewin, J., and Brewer, P.A., 2001, Predicting channel patterns: Geomorphology, v. 40, p. 329-339.

Lynds, R.M., 2005, Fine-grained sediment in modern and ancient sandy braided rivers (Ph.D. thesis): University of Wyoming, 163 p.

Makaske, B., 2001, Anastomosing rivers: a review of their classification, origin and sedimentary products: Earth-Science Reviews, v. 53, p. 149-196.

Meyer-Peter, E., and Müller, R, 1948, Formulas for bed-load transport. In: Proceedings of the 2nd Meeting of the International Association for Hydraulic Structures Research, Madrid, p. 39-64.

Mohrig, D., and Smith, J.D., 1996, Predicting the migration rates of subaqueous dunes: Water Resources Research, v. 32, no. 10, p. 3207-3217.

Mohrig, D., Heller, P.L., Paola, C., and Lyons, W.J., 2000, Interpreting avulsion process from ancient alluvial sequences: Guadalope-Matarranya system (northern Spain) and

Wasatch Formation (western Colorado): Geological Society of America Bulletin, v. 112, no. 12, p. 1787-1803.

Murray, A.B., 2003, Contrasting the goals, strategies, and predictions associated with simplified numerical models and detailed simulations. In: Wilcock, P.R., and Iverson, R.M., Prediction in Geomorphology: Geophysical Monograph 135. American Geophysical Union, p. 151-168.

Murray, A.B., and Paola, C., 1994, A cellular-model of braided rivers: Nature, v. 371, p. 54-57.

Murray, A.B., and Paola, C., 1997, Properties of a cellular braided-stream model: Earth Surface Processes and Landforms, v. 22, no. 11, p. 1001-1025.

Murray, A.B., and Paola, C., 2003, Modelling the effect of vegetation on channel pattern in bedload rivers: Earth Surface Processes and Landforms, v. 28, p. 131-143.

Nanson, G.C., and Knighton, A.D., 1996, Anabranching Rivers: Their cause, character and classification: Earth Surface Processes and Landforms, v. 21, p. 217-239.

Nelson, J.M., and Smith, J.D., 1989, Mechanics of flow over ripples and dunes: Journal of Geophysical Research, v. 94, no. C6, p. 8146-8162.

Paola, C., Parker, G., Mohrig, D.C., and Whipple, K.X., 1999, The influence of transport fluctuations on spatially averaged topography on a sandy, braided fluvial fan. In: Numerical experiments in stratigraphy: Recent advances in stratigraphic and sedimentologic computer simulations, SEPM Special Publications No. 62, p. 211-218.

Parker, G., 1976, On the cause and characteristic scales of meandering and braiding in rivers, Journal of Fluid Mechanics, v. 76, no. 3, p. 457-480.

Resource Consultants and Engineers, Inc, 1993, Niobrara River sedimentation impacts study, Phase II: Unpublished report prepared for the U.S. Army Corps of Engineers, Omaha District, Omaha, NE, 260 pp.

Richardson, W.R., and Thorne, C.R., 2001, Multiple thread flow and channel bifurcation in a braided river: Brahmaputra-Jamuna River, Bangladesh: Geomorphology, v. 38, p. 185-196.

Schumm, S.A., 1985, Patterns of alluvial rivers: Annual Review of Earth and Planetary Sciences, v. 13, p. 5-27, 1985.

Skelly, R.L., Bristow, C.S., and Ethridge, F.G., 2003, Architecture of channel-belt deposits in an aggrading shallow sandbed braided river: the lower Niobrara River, northeast Nebraska: Sedimentary Geology, v. 158, p. 249-270.

Slingerland, R., and Smith, N.D., 2004, River avulsions and deposits: Annual Review of Earth and Planetary Science, v. 32, p. 257-285.

Smith, J.D., 1970, Stability of a sand bed subjected to a shear flow of low Froude number: Journal of Geophysical Research, v. 75, p. 5928-5940.

Tal, M., Gran, K, Murray, A.D., Paola, C, and Hicks, D.M., 2004, Riparian vegetation as a primary control on channel characteristics in multi-thread rivers. In: Bennet, S.J., and Simon, A. (Eds.), Riparian Vegetation and Fluvial Geomorphology: Hydraulic, Hydrologic, and Geotechnical Interactions 8. American Geophysical Union, p. 43-58.

Werner, B.T., 2003, Modeling landforms as self-organized, hierarchical dynamical systems. In: Wilcock, P.R., and Iverson, R.M., Prediction in Geomorphology: Geophysical Monograph 135. American Geophysical Union, p. 133-150

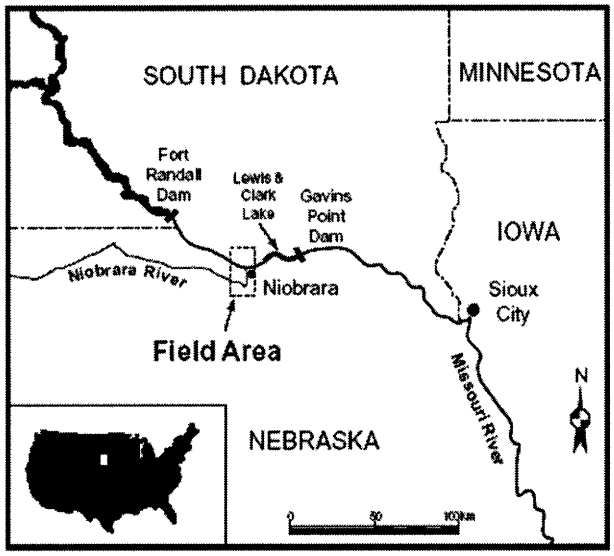

Figure 6.1. Location map of Niobrara River, with study area denoted by dashed box. From Bristow et al. (1999).

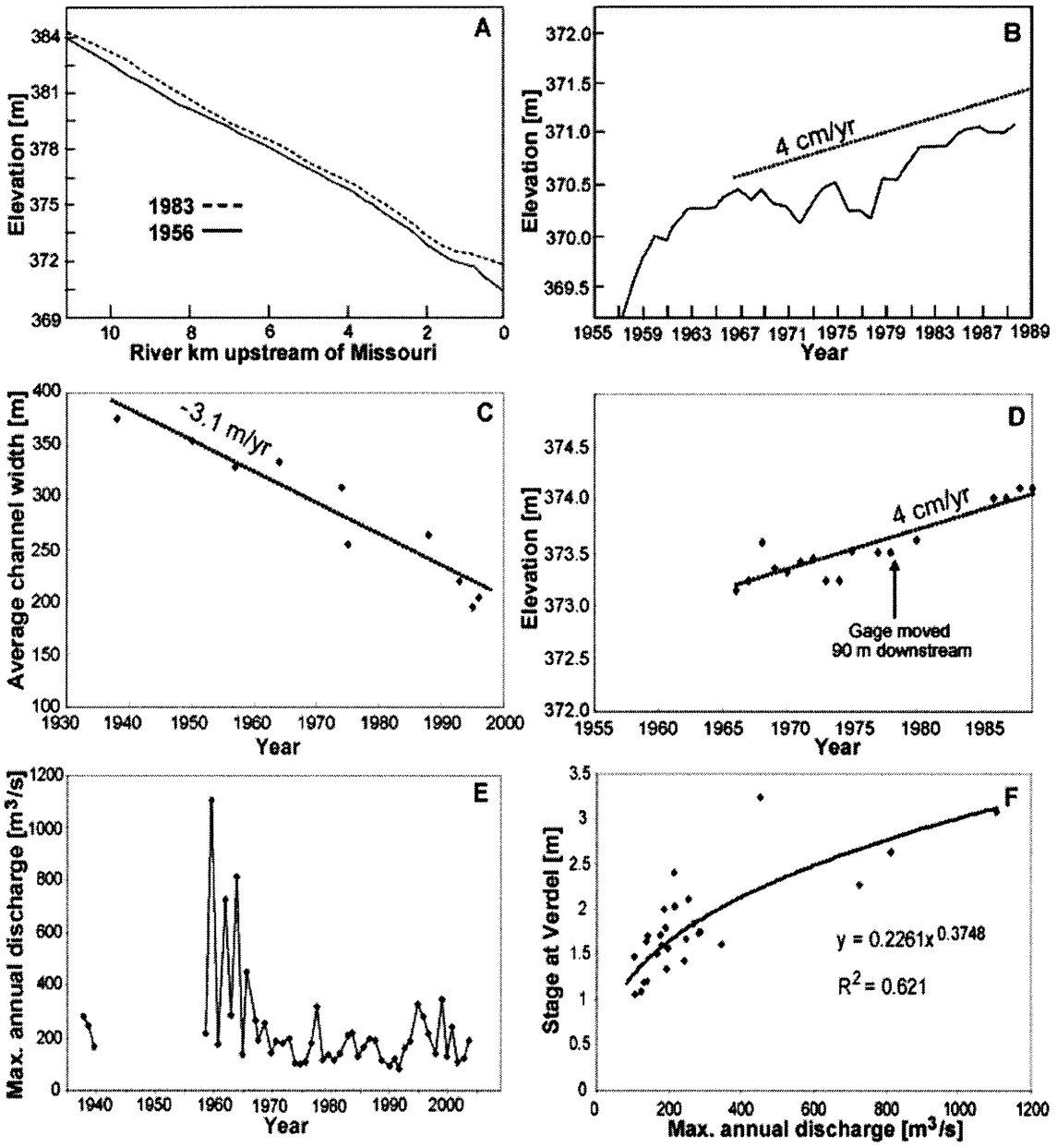

Figure 6.2. Historical data from the lower Niobrara River (adapted from Resource Consultants and Engineers, 1993). A: Long profile aggradation. B: Gage height on the Missouri River at mouth of Niobrara since closing of the Gavins Point Dam, for a discharge of 567 m^3/s. Dotted line shows the aggradation trend of the bed of Niobrara at Highway 12. C: Change in mean channel width of the lower 6 km of the Niobrara, with best fit trend shown by dotted line. Adapted from Ethridge et al. (1999). D: Gage elevation on Niobrara at Highway 12, with the best-fit mean aggradation rate shown by the dotted

line. E: Peak annual daily discharge on the Niobrara River at Verdel, approximately 15 km upstream of the study reach. F: Stage-discharge relation for peak annual discharge events on the Niobrara at Verdel. Line is a best-fit power law.

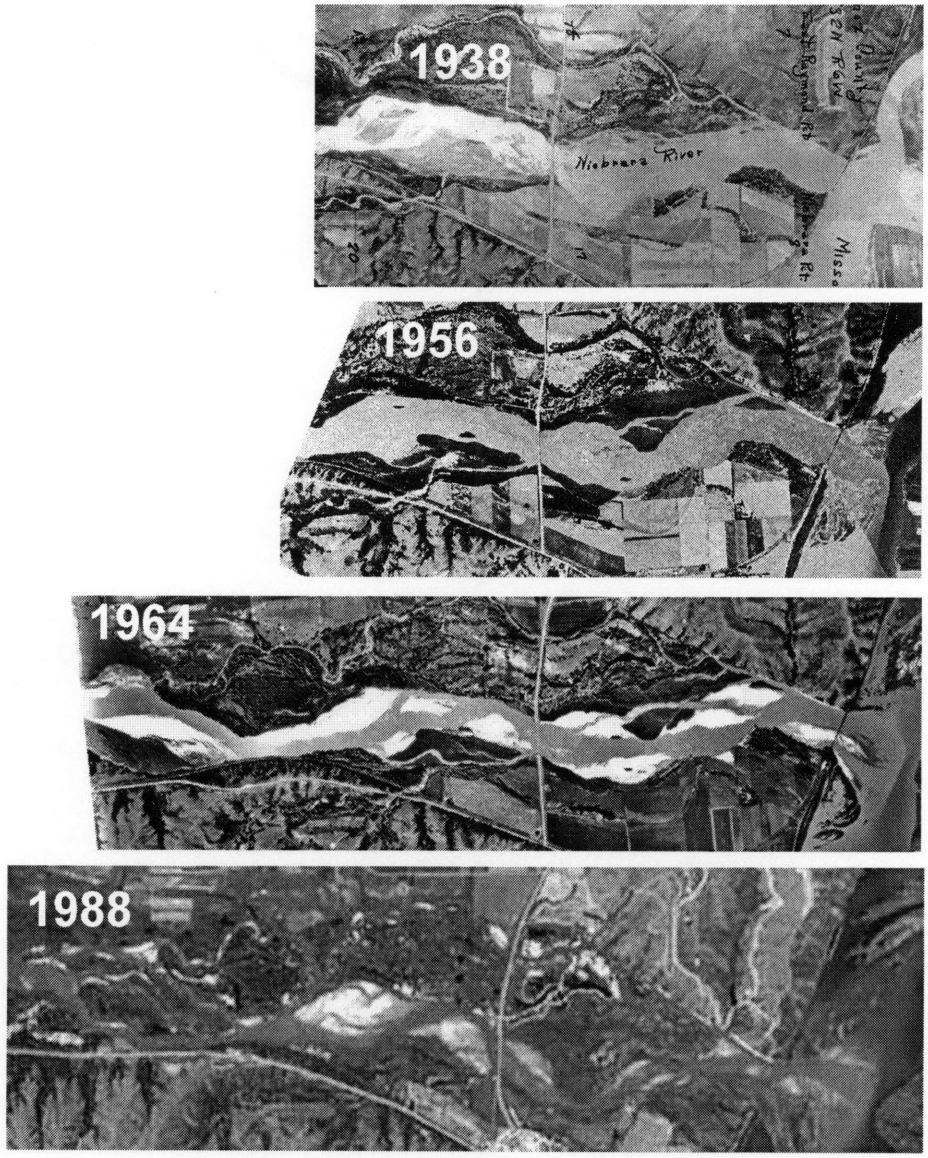

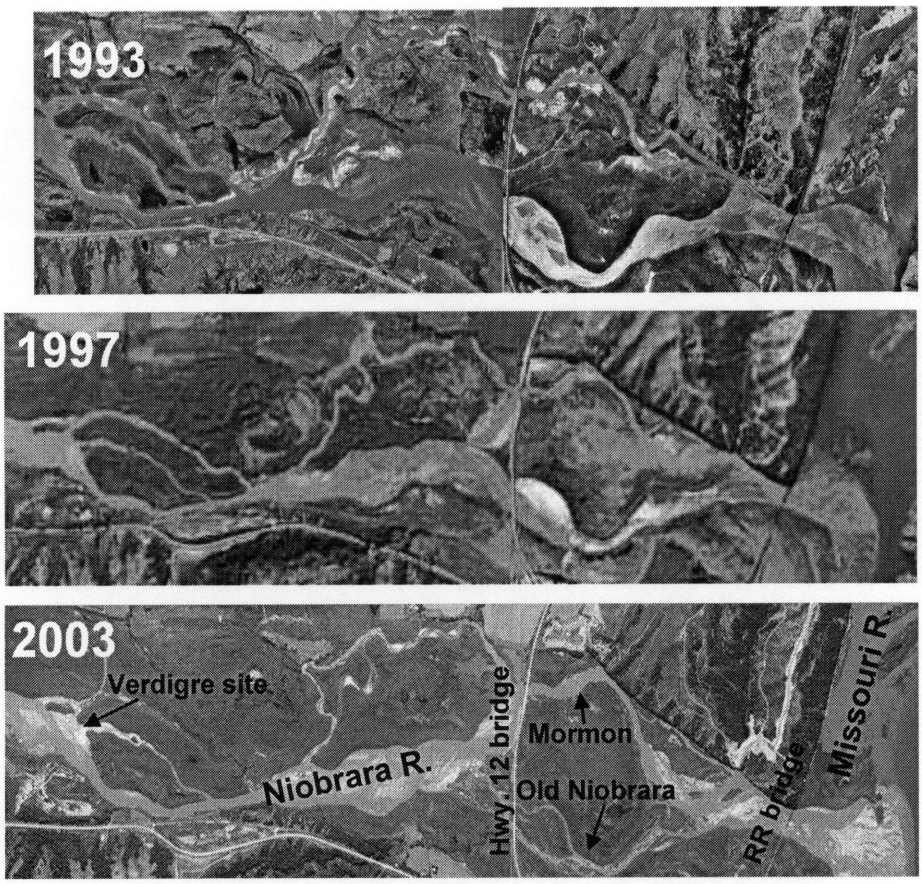

Figure 6.3. Aerial photographs of the study area – flow is from left to right for this and all figures, unless stated otherwise. Gavins Point Dam was closed in 1957. Note loss of farm land in lower right section of images beginning after 1956, and difference in river morphology. 2003 image shows locations of features described in the text.

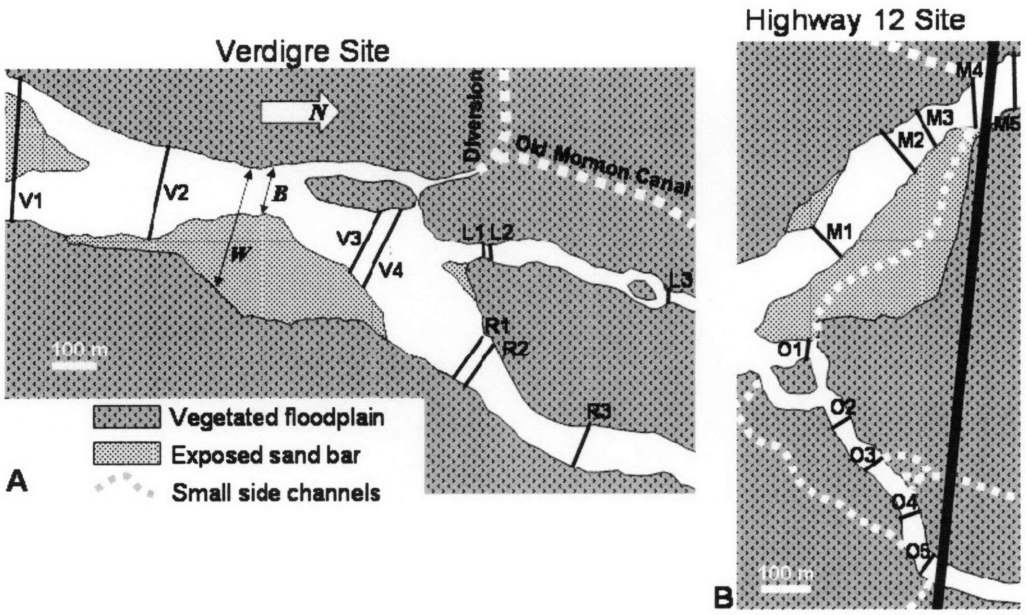

Figure 6.4. Mapped bifurcation sites. The borders of channels and sand bars were delineated using GPS, while dotted lines show approximate locations of small side channels determined from oblique aerial photographs taken during the study. Dark, solid lines show transects where hydraulic geometry measurements were taken. Labeled transects correspond to cross sections shown in Fig. 6.7, and were averaged by reach (Fig. 6.7) to make table 6.1. A: Verdigre Site – channel wetted width (*B*) and active channel width (*W*) are defined. V, L and R denote Single-branch transects, left channel transects and right channel transects, respectively. B: Highway 12 site, where heavy solid line is the Highway 12 bridge. Fig. 6.10 shows transects M4 and O5, where M denotes Mormon Canal and O is Old Niobrara channel.

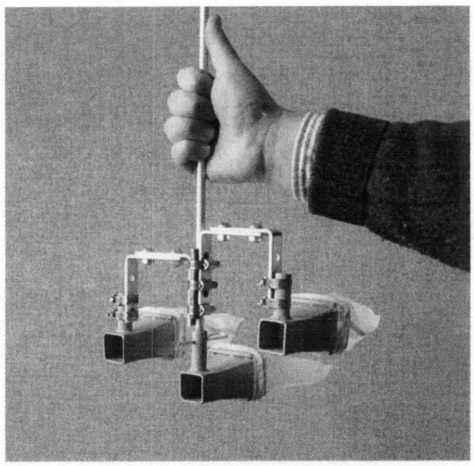

Figure 6.5. Sediment sampler consisting of three staggered, scaled-down Helley-Smith samplers. Setup is described in text.

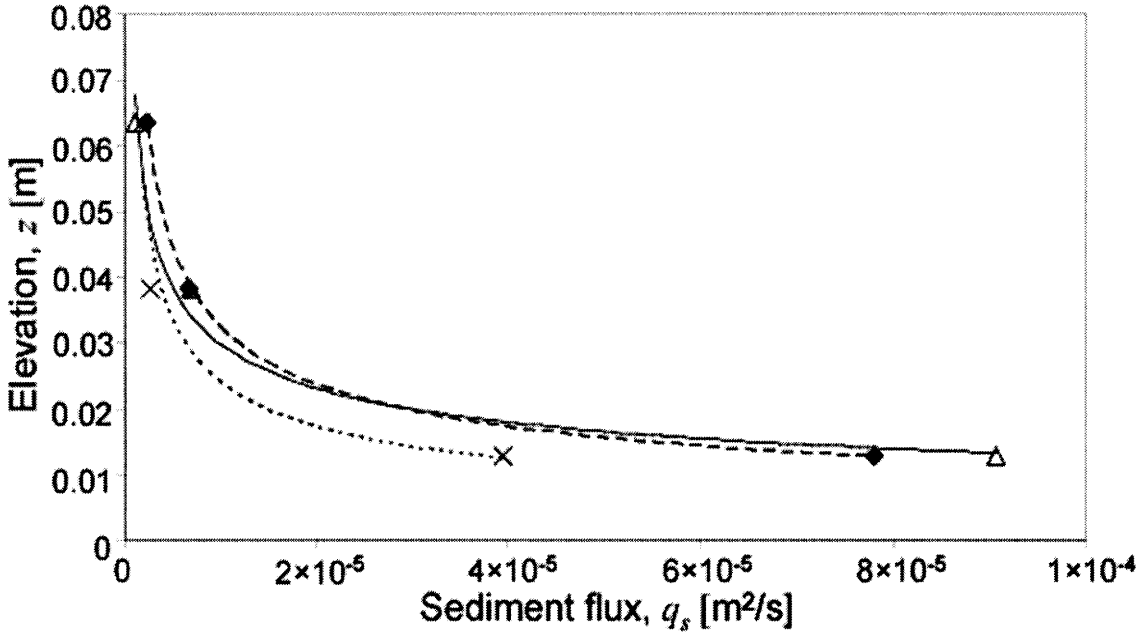

Figure 6.6. Typical profiles of volumetric sediment flux captured over the crests of three dunes at Verdigre Site, where lines show power-law functions fit to the data.

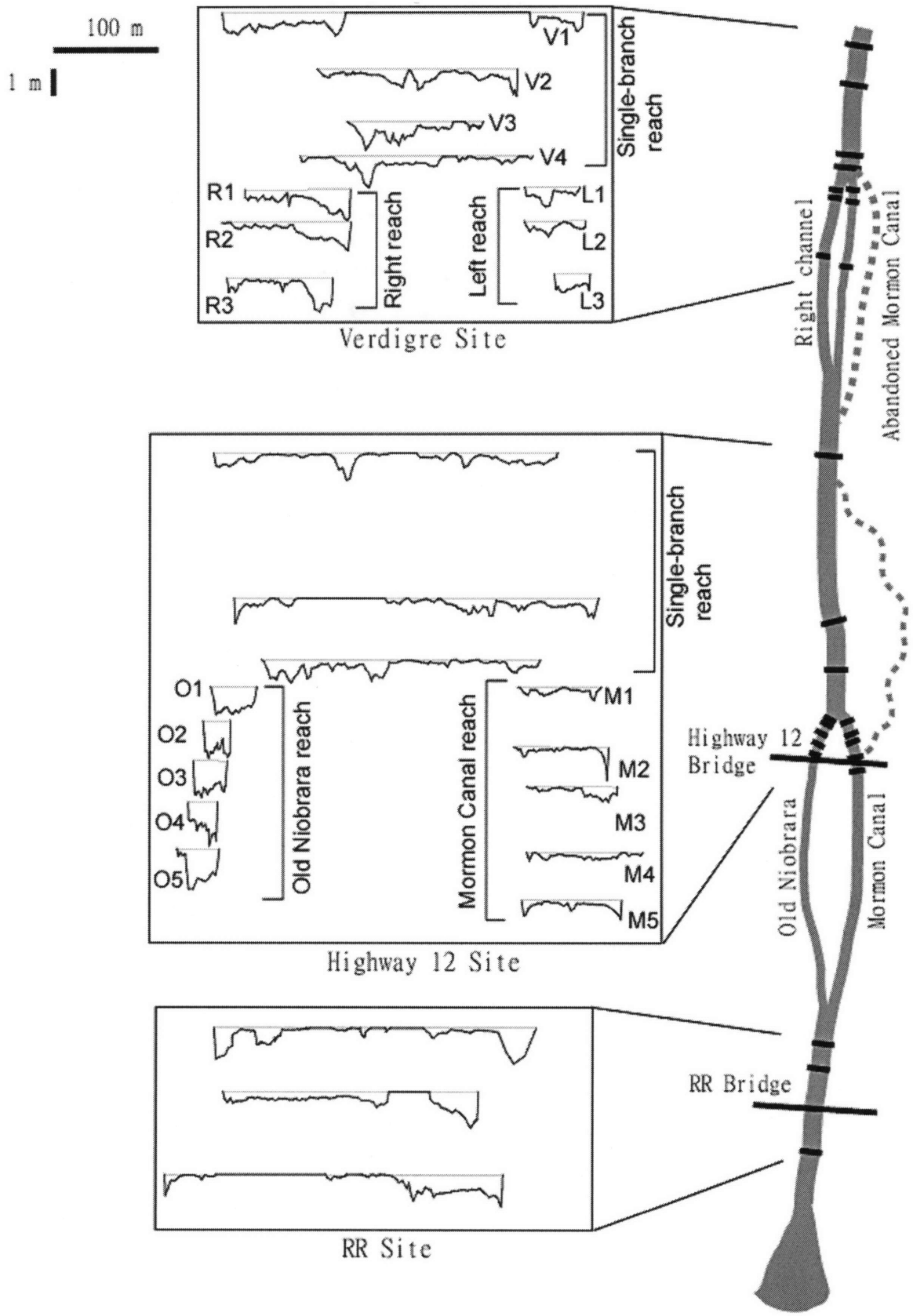
100 m
1 m
V1
V2
V3
V4
Single-branch reach
R1
R2
R3
Right reach
Left reach
L1
L2
L3
Verdigre Site
Right channel
Abandoned Mormon Canal
Single-branch reach
O1
O2
O3
O4
O5
Old Niobrara reach
Mormon Canal reach
M1
M2
M3
M4
M5
Highway 12 Bridge
Old Niobrara
Mormon Canal
Highway 12 Site
RR Bridge
RR Site

Figure 6.7. Channel cross section geometry at all sampled transects – location map is shown at right, and flow is from top to bottom. The three study sites are defined by boxed areas. Labeled transects correspond to Fig. 6.4.

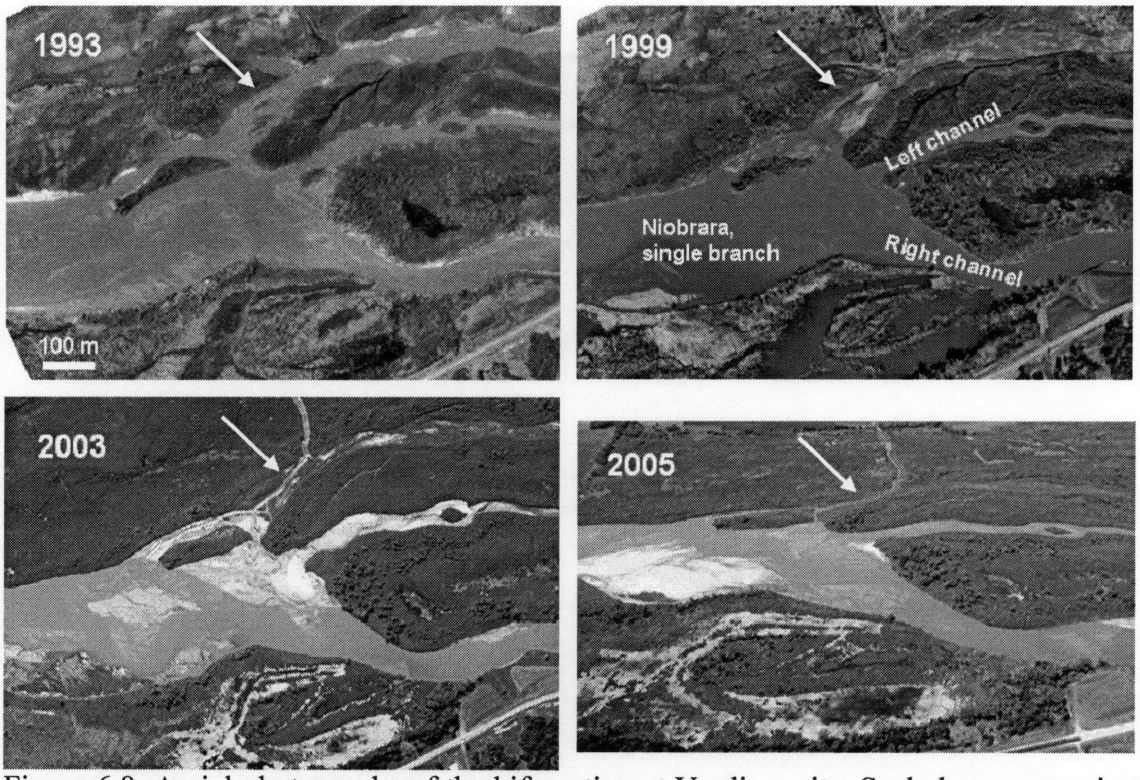

Figure 6.8. Aerial photographs of the bifurcation at Verdigre site. Scale bar appears in top left image. 2005 photograph is oblique. Arrow marks channel that has filled in over the period of these photographs.

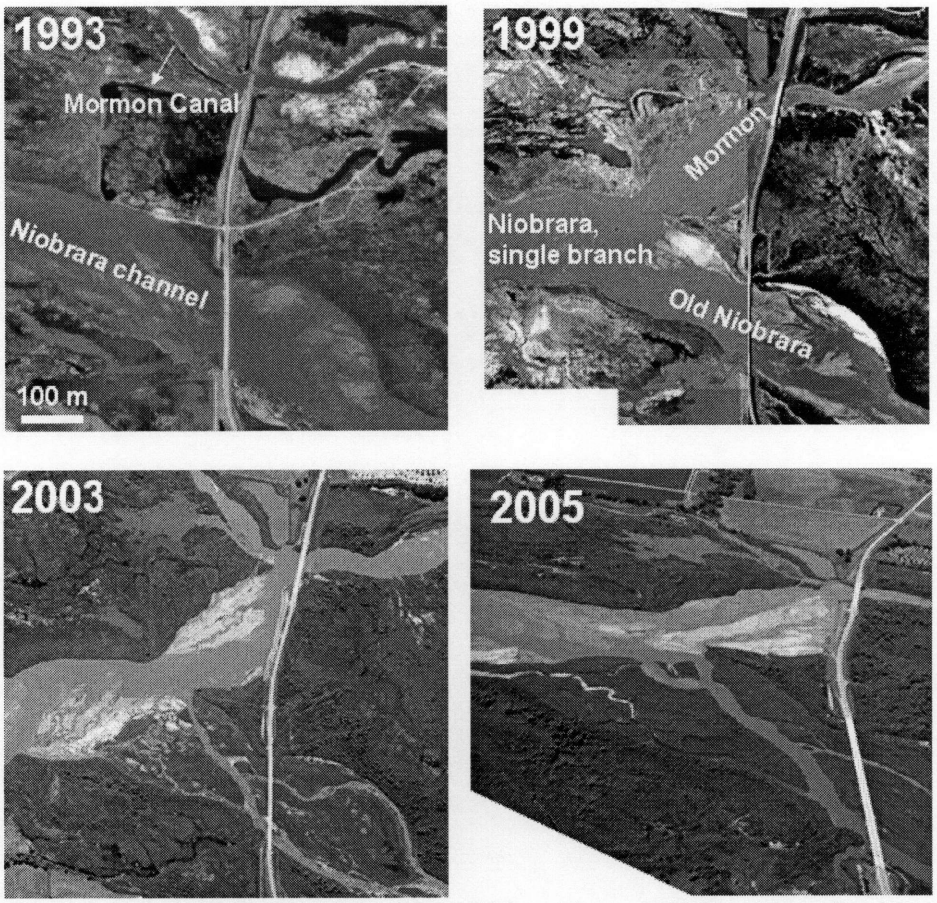

Figure 6.9. Aerial photographs of the bifurcation at Highway 12 site. Note configuration of the channel in 1993. In 1995-1996 the avulsion of the Niobrara into the Mormon Canal occurred, creating the present bifurcation. Channel reaches described in the text are labeled in 1999 image.

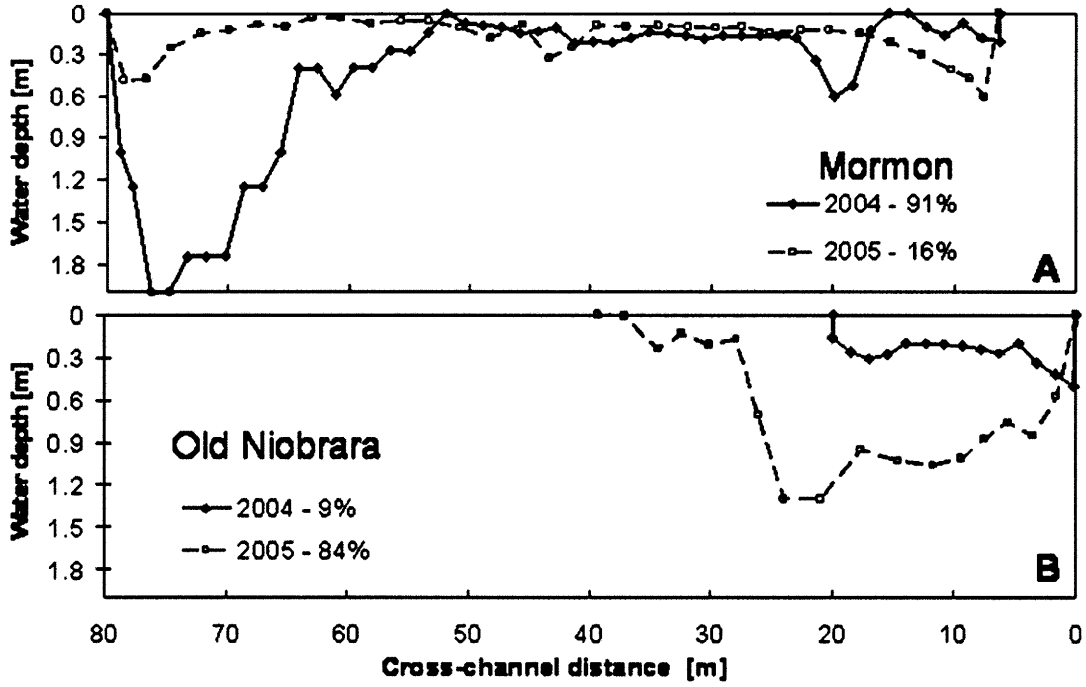

Figure 6.10. Cross sections of the (A) Mormon Canal and (B) Old Niobrara at the Highway 12 bridge (locations M4 and O5 in Fig. 4a) measured in August 2004 and August 2005. Figure legends indicate the percentage of fluid discharge in the channel during each survey. Note the filling of the Mormon Canal without changes in width and the dramatic decrease in discharge. The Old Niobrara channel deepened and widened substantially, accompanied by a very large increase in discharge. Total fluid discharge during the time of both surveys was approximately equal to 30 m^3/s.

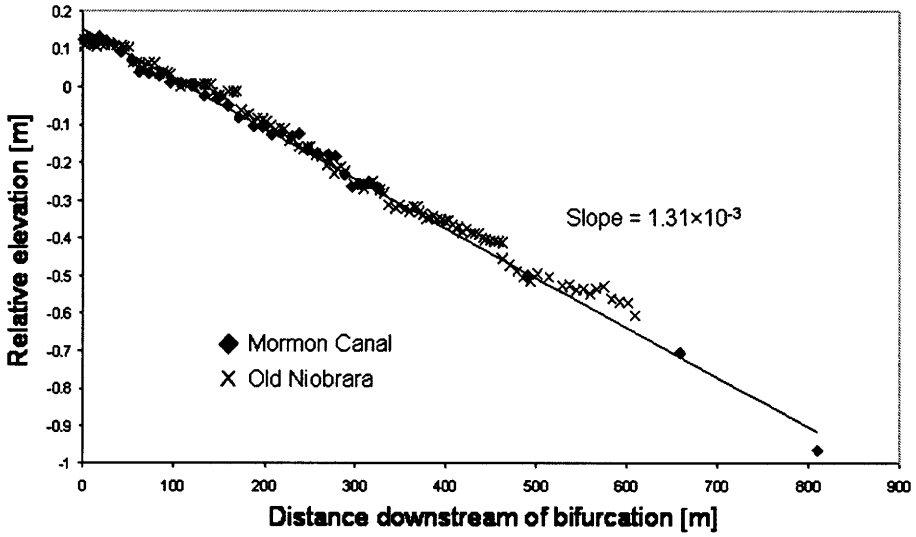

Figure 6.11. Water surface elevations measured at Highway 12 site for both the Mormon Canal and Old Niobrara channel. Solid line is best-fit water surface slope to all data. Note there is no real difference in water surface elevation between the two branches.

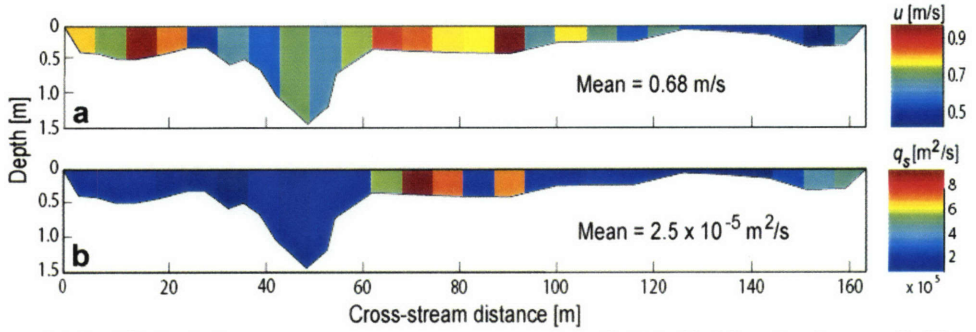

Figure 6.12. (Color) Instantaneous measurements of (A) fluid velocity and (B) sediment flux in a representative transect at Verdigre site (scale bars on right). Velocity and sediment flux are neither strongly correlated with each other nor with the topography of the stream channel.

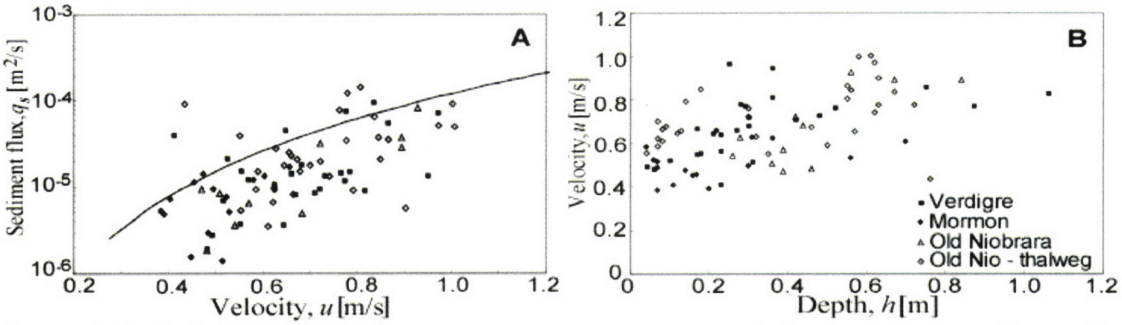

Figure 6.13. Relations among instantaneous measurements. A: Instantaneous sediment flux is not well correlated to local fluid velocity. Line is the expected bedload flux from eq. 8, assuming the friction factor at each point in a river reach is equal to the reach-averaged value computed from eq. 4. B: Fluid velocity shows almost no dependence on local water depth. Legend applies to both figures.

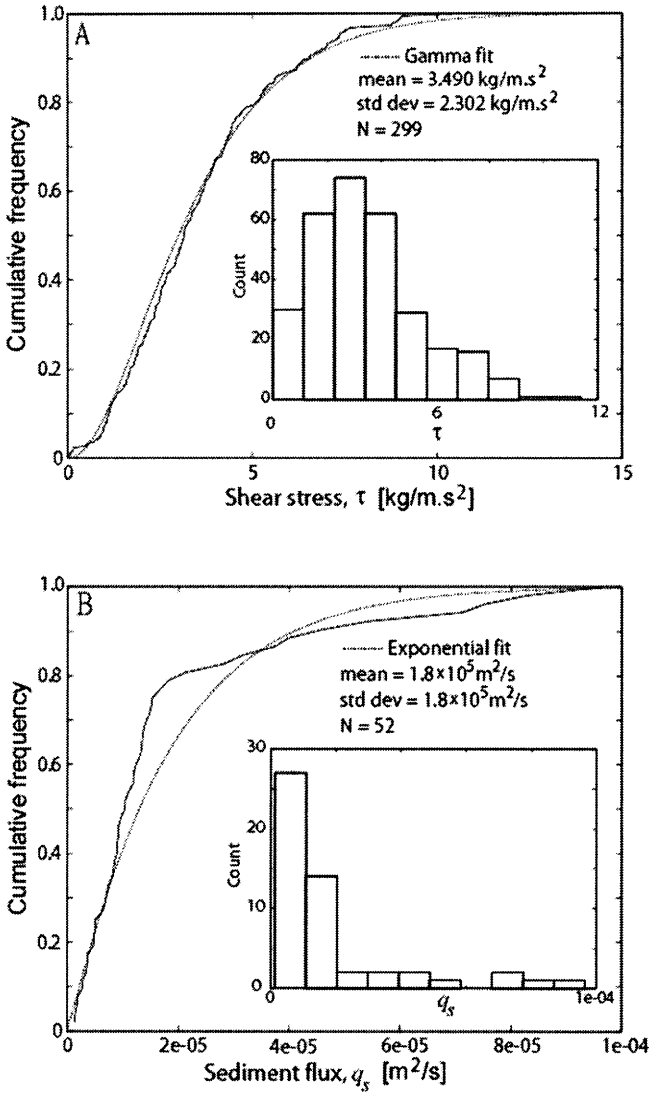

Figure 6.14. Probability distributions and fitted functions for local stress and sediment flux measurements. A: Cumulative frequency of local shear stress values, which were computed from instantaneous fluid velocity using eq. 5 and assuming constant friction factor for a reach. Data are combined from 6 transects at two sites. Inset is histogram of the data. The shear stress distribution is well fit by a gamma function, in agreement with Paola et al. (1999). B: Distribution of instantaneous sediment flux, with description as in (A). These data are combined from three transects at two sites. The best fit function is an exponential, however agreement is poor.

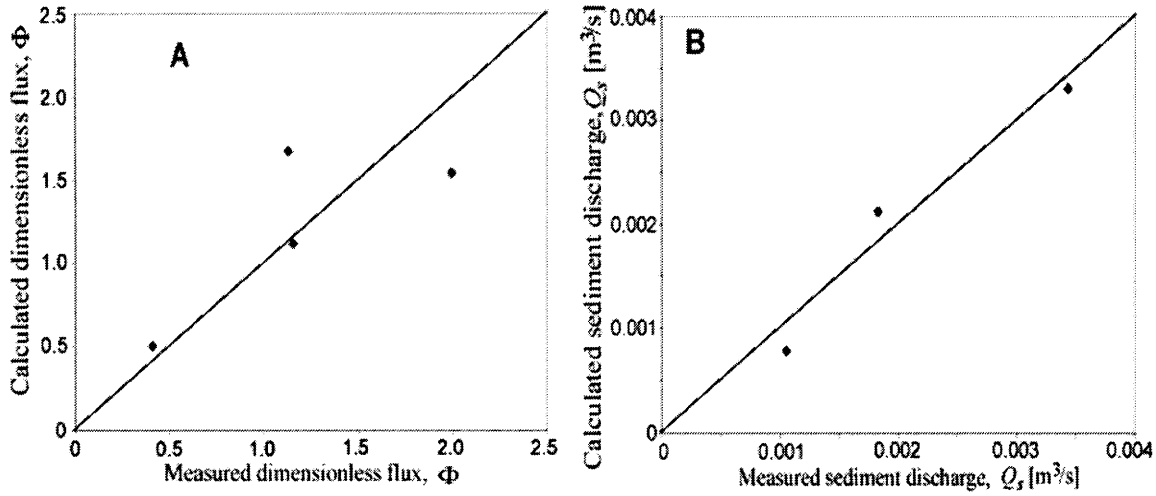

Figure 6.15. Comparison of measured and calculated values for (A) reach-averaged sediment flux, and (B) reach-averaged sediment discharge. Note that (B) contains one less datum than (A), because there is no sediment discharge value corresponding to the mean sediment flux measured over thalweg dunes. Sediment flux was computed using equations 3, 7 and 8. Sediment discharge was calculated using eq. 9. Solid lines are lines of perfect agreement.

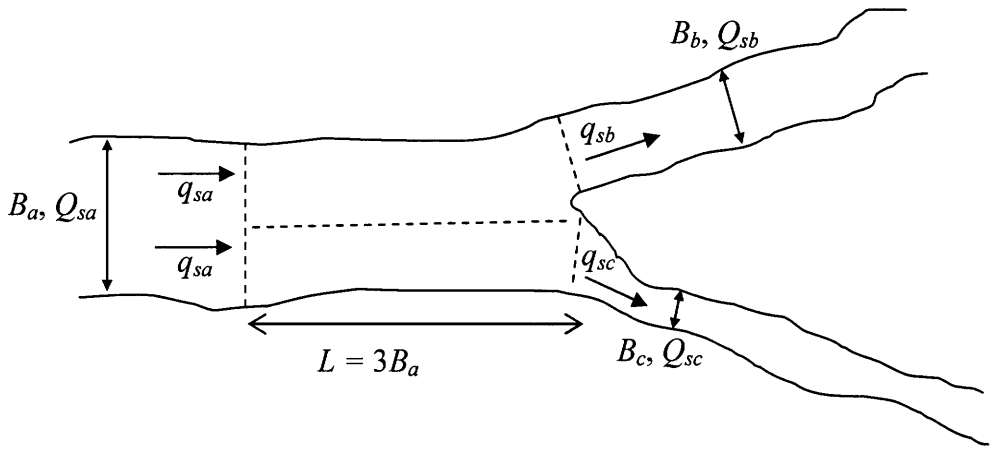

Figure 6.16. Definition sketch of a bifurcation for the nodal point formulation (after Bolla Pitaluga et al., 2003). Erosion/deposition is considered over the control length L where the flow diverges into the anabranches (denoted by dashed lines), and is calculated for each branch using eq. 10b. Sediment flux into each branch is q_{sa}, while sediment flux out of branch b and c is q_{sb} and q_{sc}, respectively.

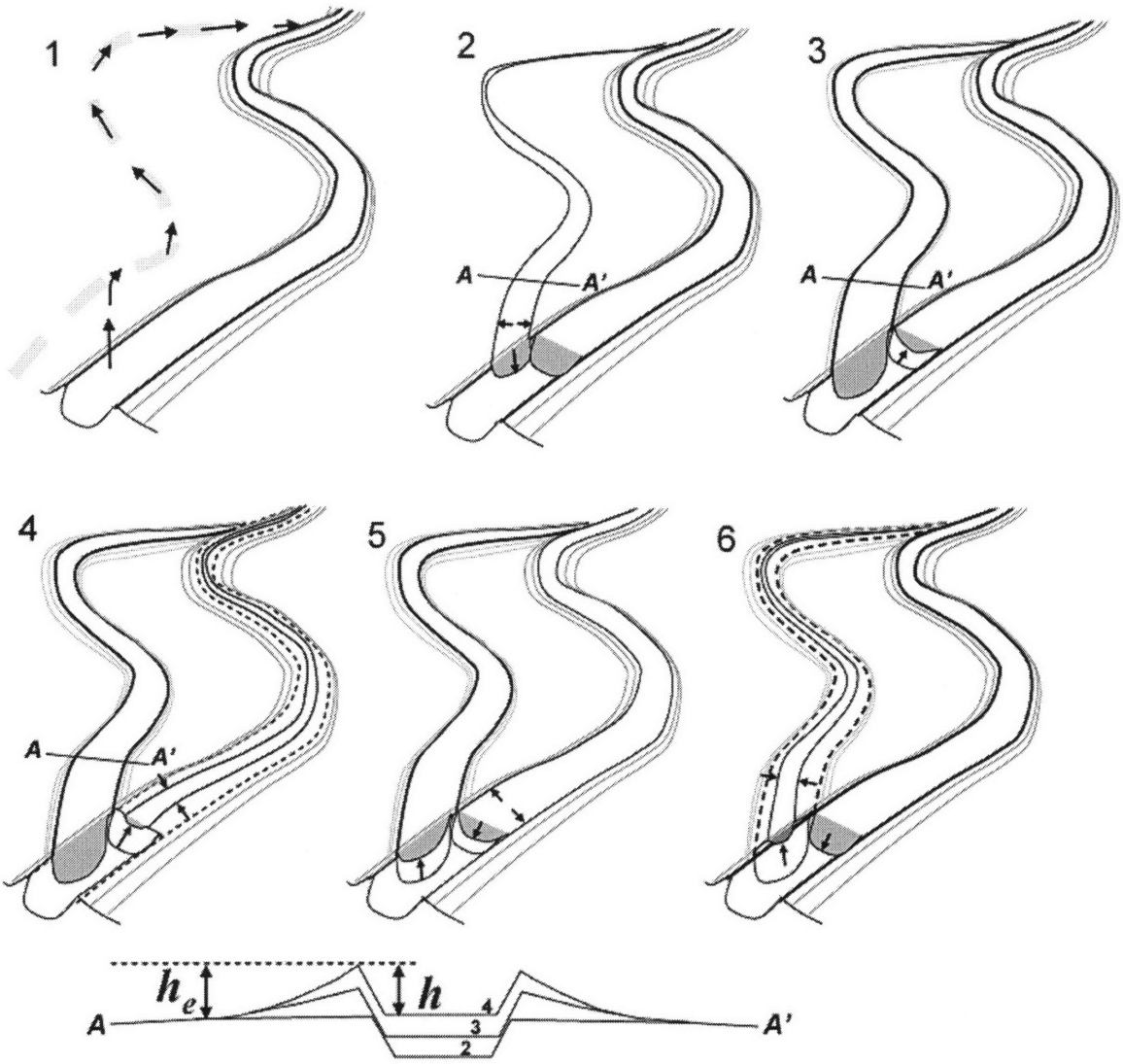

Figure 6.17. Conceptual model for the formation and maintenance of bifurcations in net depositional rivers driven by avulsion – flow is from bottom to top. (1) A superelevated channel that has deposited to an elevation of one channel depth above the floodplain (see bottom sketch) is unstable and begins to avulse into a previously abandoned channel, denoted by the dashed line. (2) The previously abandoned channel begins to deepen and widen by incision because it is lower in elevation and underfit in terms of flow capacity. (3) The incised (left) channel captures more of the flow and begins to aggrade, while the old (right) channel begins to fill with sediment without change in width. (4) The left channel has captured most of the flow and aggraded such that it approaches a relative superelevation of one (i.e., $h/h_e = 1$), while the right channel continues to fill with sediment and narrow due to vegetation growth. (5) Superelevation of the left channel eventually drives flow into the right channel, which incises into its previous deposit and widens while the left channel begins to fill. (6) The right channel captures most of the flow, while the left channel continues to fill and begins narrowing due to vegetation growth.

Table 6.1. Measured and computed hydraulic and transport parameters. Variables defined in text.

		Q_w (m^3/s)	A (m^2/s)	P (m)	h_r (m)	$\overline{u}$ (m/s)	S	c_f	θ	θ_{sf}	Φ meas.	Φ calc.	Q_s meas (m^3/s)	Q_s calc (m^3/s)
V	Single-branch	33.9	54.1	161.0	0.35	0.63	1.27E-03	0.010	0.89	0.31	1.15	1.12	0.0034	0.0033
V	Left	11.0	15.8	50.4	0.33	0.70	1.15E-03	0.008	0.85	0.29		1.04		0.0010
V	Right	22.6	38.6	103.7	0.37	0.59	1.15E-03	0.012	0.95	0.32		1.22		0.0023
V	L + R	33.7	54.4	154.1	0.35	0.62	1.15E-03	0.010	0.89	0.31		1.13		0.0033
H	Single branch	33.0	64.7	268.4	0.24	0.51	1.24E-03	0.011	0.66	0.24		0.74		0.0037
H	Mormon	4.7	13.6	84.2	0.16	0.35	1.40E-03	0.020	0.50	0.20	0.41	0.50	0.0011	0.0008
H	Old Niobrara	24.5	28.5	34.3	0.84	0.87	1.09E-03	0.012	2.01	0.59	1.13	1.68	0.0018	0.0021
H	M + O	29.2	42.1	118.5	0.36	0.69	1.30E-03	0.009	0.97	0.33		1.30		0.0028
RR	Single-branch	35.0	66.2	208.9	0.32	0.53	1.15E-03	0.013	0.82	0.29		1.00		0.0038

V, H and RR refer to Verdigre, Highway 12 and RR Sites, respectively. All numbers presented here are reach-averaged values, computed using d_{50} = 0.275 mm. L+R is the sum of left and right channels for comparison to the single-branch reach; M+O is similarly the sum of Mormon and Old Niobrara channels.

Chapter 7

A minimum time for the formation of Holden Northeast Fan, Mars[4]

D.J. Jerolmack, D. Mohrig, M.T. Zuber, and S. Byrne

Department of Earth, Atmospheric and Planetary Sciences, Massachusetts Institute of Technology, Cambridge, Massachusetts 02139, USA

Abstract

The recently discovered deposits of a channelized fan located northeast of Holden Crater preserve a history of vertical and lateral accretion and avulsion of many channels, indicating water flowed freely across the surface of the fan during its construction. These sedimentary deposits, however, do not unambiguously discriminate between a deltaic or purely riverine origin for the feature. By using a numerical model describing fan construction solely by river channels, we estimate a minimum formation time of several decades to centuries. A minimum value for the total volume of transporting fluid required to construct the fan is modest, 900 km^3, and may not have required precipitation.

[4] From Jerolmack, D.J., D. Mohrig, M.T. Zuber, and S. Byrne, A minimum time for the formation of Holden Northeast Fan, Mars, *Geophys. Res. Lett.*, *31*, L21701, doi:10.1029/2004GL021326, 2005.

7.1. Introduction

With few exceptions, putative fluvial features identified on Mars have been erosional in nature (e.g. Mars Channel Working Group, 1983; Aharonson et al., 2002, and references therein). The recent discovery of a large, partially eroded fan deposit in a crater northeast of Holden Crater (hereafter called Holden NE Crater, Malin and Edgett, 2003; also assigned the provisional IAU name Eberswalde) has, therefore, significant implications for both the history of flowing water in the region, and the persistence of liquid water on Mars during Noachian (~ 3.7 Ga) time (Moore et al., 2003). Moore et al. (2003) interpreted the Holden NE fan as a delta, i.e. building out into a standing body of water. Herein we argue that the fan may have been constructed without a standing body of water present at its distal end, but acknowledge that remote imaging of the sedimentary deposits is not sufficient to unambiguously distinguish between these depositional origins. We quantitatively assess the evidence for water recorded by the sedimentary deposits at Holden NE Crater, using data from Mars Orbiter Laser Altimeter (MOLA), Thermal Emission Imaging System (Themis) and Mars Orbiter Camera (MOC). In particular, we use a numerical model of riverine fan construction (Parker et al., 1998) to invert topographic and volumetric data from MOLA, producing an estimate of the time required to build the fan out of channel and overbank deposits. This analysis provides a minimum estimate of formation time, as there is no way to assess how long or how frequently the fan was active, and construction of the fan as a delta would require more time due to the reduced transport efficiency in lacustrine versus riverine environments (see, e.g., Paola, 2000). This minimum time is relevant to considerations of whether fan formation required climatic conditions drastically different from the present day.

7.2. Observed features

Holden NE Crater is a severely degraded elliptical depression, with major and minor axes of ~70 km and ~50 km, respectively, and a maximum depth of 1.2 km (Fig. 7.1a). To the west of the crater lies a tributary network of erosional channels (Fig. 7.1a) connecting to two ~0.7 km wide channels on the western rim of Holden NE Crater that define the apex of the depositional fan (Fig. 7.1b, Fig. 7.2, table 7.1). The average longitudinal slope, *S*, of the bed for the longer of the two erosional channels entering the crater is 0.06. This slope drops to a characteristic value of 0.006 upon entering the crater (in agreement with Malin and Edgett, 2003), associated with the approximately radial eastward expansion of the fan. The distal end of the fan is defined by an abrupt increase in surface slope (Fig. 7.3). The deposits most likely represent an ancient delta or riverine fan, depending on interpretation of the amount of post-depositional erosion associated with generation of this terminal surface.

The fan surface is covered by a series of superposed, cross-cutting ridges (Malin and Edgett, 2003; Moore et al., 2003) that we interpret as more resistant, possibly coarser-grained deposits filling paleochannels (Fig. 7.1b, 7.2a, 7.2b). These channel-filling deposits are exposed in plan form on the top of the fan, and in cross section along its terminal surface; they possess relatively low sinuosities (table 7.1) and their branching, radial arrangement is consistent with development either by a distributary network, or via amalgamation of successive deposits from an avulsing channel (Rannie, 1990). Erosion at the distal end of the fan has produced cliffs revealing stratigraphic layers that appear discontinuous over distances of a few hundred meters (Fig. 7.2a),

which we interpret as representing nearly vertical cuts through numerous channel-filling deposits distributed throughout the entire fan package.

7.3. Analysis

The observed superposition of discrete channel-filling deposits with varying flow directions is consistent with stratigraphy produced by a small number of active channels occupying different sites on the fan via relatively abrupt lateral shifts, or avulsions (Mohrig et al., 2000; Rannie, 1990; Slingerland and Smith, 2004). A previously identified meander 'cutoff' (Malin and Edgett, 2003; Moore et al., 2003) is more likely an avulsed channel that reoccupied a former channel course (Fig. 7.2b), as is frequently seen in terrestrial outcrops where old channels may persist as topographic lows (Mohrig et al., 2000). Margins of the 'cutoff' show the channel is superposed on the previous deposit (Fig. 7.2b), and stereo anaglyphs (not shown) show meander scroll-bars progressively increase in elevation (as noted by Moore et al., 2003), implying aggradation-driven channel migration.

The fan considered here is an erosional remnant of a larger depositional feature. Estimating to what degree its shape has been modified is important to our analysis of the time required to build the original deposit. MOC images show that all of the channels which terminate at the distal end correspond to steep slopes at the fan edge, while less resistant material between channels grades into the crater bottom at shallow slopes (Fig. 7.2a). Also, remnant 'stringer' channels, sinuous ridges similar in morphology to those on the fan, extend across the floor of Holden NE Crater, beyond the fan (Fig. 7.2c). Taken together, these observations suggest that the original fan was more extensive, and

point to the abrupt termination of the fan being an erosional artifact, most likely produced by wind. We propose that the entire fan may have been constructed from river-like channels traversing its entire length.

Themis night-time infrared data show a correlation between temperature and degree of rock exposure (Fig. 7.1b), resulting in exhumed features having higher thermal inertia than surrounding terrain (Chistensen et al., 2003), which is mantled with loose sediment. MOC data from the fan record no evidence of talus (rubble piles) or scree at the base of steep slopes, suggesting that material eroded off of the fan deposit by wind abrasion is also transported away from the site by wind, and implying the channel deposits are composed of weakly lithified sand or finer-grained material.

We explore the conditions required to construct the observed deposit by a purely riverine system. Our goal is to provide a reasonable minimum bound on the time that freely flowing water persisted in Holden NE Crater, as this is the only constraint we can deduce from the current data. To do this we use the numerical model *Acronym6*, based on the theory of Parker et al. (1998), for the equilibrium shape of channelized alluvial fans (code freely available at: *http://www.safl.umn.edu/publications/software/srmsgf.shtml*). This semi-analytical formulation computes bed slope and elevation of a fan experiencing frequent avulsions, which act to distribute water and sediment across the fan surface. A significant advantage of this sediment transport formulation is that model equations are dimensionless. Martian gravity (g = 3.7 m/s^2) is then directly accounted for in determining the dimensional, system-wide values.

The model takes advantage of the following simplified conditions. Dimensionless formative shear stress, τ^*_a, is treated as constant for the length of the fan, as observed in

terrestrial environments (Parker et al. 1998; Paola et al., 1999). Steady and uniform flow is assumed, and the relationship between shear stress, τ, and sediment discharge, Q_s, follows $Q_s \sim \tau^n$, where n is 1.5 for gravel and 2.5 for sand. The result of this formulation is an equation relating fan slope along the profile to sediment and fluid discharge (equation (29) in Parker et al. (1998)):

$$S = \left[R^{-1/2} \alpha_s^{-1} \alpha_b^{(3+2p)/2} \alpha_r \left(\frac{\alpha_b}{R} - \tau^*_c \right)^{-n} \frac{Q_s (1-\hat{r}^2)}{Q_w} \right]^{1/(1+p)}, \qquad (1)$$

where R, τ^*_c, $\hat{r}$ and Q_w are submerged specific density of grains, critical dimensionless Shields stress, dimensionless down-fan distance (ranging from 0 to 1) and fluid discharge, respectively. The coefficients α_s, α_b and α_r, and the exponent p are dependent on the form of the sediment transport and flow resistance relationships. The numerical model solves eq. (1) to obtain the slope along the profile for a given sediment/water discharge ratio; all other parameters are treated as constant, though values of some constants are different for sand and gravel. Elevation along the profile is found by integrating eq. (1) subject to the proper boundary conditions (see Parker et al., 1998). As grain size is an unconstrained parameter, all computations are performed for both medium sand (D = 0.3 mm) and gravel (D = 20 mm), with values for all constants as reported in table 1 of Parker et al. (1998) for simplicity.

The top surface of the present day fan is taken to represent the equilibrium profile. While some erosion has occurred, the fact that large channels may be traced over the entire fan top implies differential eolian weathering on this surface is less than one

channel-depth in magnitude, and so the present surface slope is taken as a reasonable approximation of the original fan gradient. The ratio Q_s/Q_w in the model is varied in an iterative manner to find the theoretical fan profile that best matches the observed slope and elevation (Fig. 7.3). This surface fit implies that the fan was significantly more extensive than now (table 7.1), having a total length, L = 45 km. We assume one active channel with a measured width, B = 100 m. To estimate channel depth, H, we use the observed relationship for terrestrial alluvial rivers, $3 < BS^{0.2}/H < 10$ (Fukuoka, 1989). Finally, Q_w can be obtained by calculating mean fluid velocity, u, using a Chezy flow resistance relation:

$$u = (\tau^*_a R g D \alpha_r^2)^{1/2}, \qquad (2)$$

where all parameters are the same as table 1 of Parker et al. (1998). A similarity closure based on the Froude number yields a velocity estimate similar to that of eq. (2). Fluid discharge is computed as $Q_w = uBH$, using combinations of parameter values specified above to obtain a minimum, maximum, and 'preferred' value, where the preferred value uses $BS^{0.2}/H = 7$, the middle range of terrestrial values. The time scale of formation, t_{eq}, can be estimated directly from fan volume (corrected for assumed porosity, $\lambda = 0.35$) and sediment discharge as $t_{eq} = (1-\lambda)V/Q_s$, assuming that all sediment input at the apex is captured by the fan. A reconstructed volume for the fan, V = 30 km^3, was calculated by fitting the analytical profile with parabolic cross sections assuming a radially symmetric fan of L = 45 km and opening angle $\theta = 81°$.

7.4. Implications and Conclusions

Frequently avulsing terrestrial channels on alluvial fans produce deposits consistent with those seen in the martian fan deposit. Abundant stratigraphic evidence for vertical accretion and channel avulsion clearly demonstrates that the top of the fan was a free surface, not confined by an overlying rigid boundary such as a glacier. We cannot determine, however, whether channels formed in a completely riverine environment or on top of a delta draining into a (possibly ice-covered) crater lake. On Earth, rivers often build alluvial fans at abrupt transitions in slope (Rannie, 1990). Ancient avulsing channels and their associated alluvial fans have been found as inverted sandstone ridges in Oman (Maizels, 1990) and Spain (Mohrig et al., 2000), with gradients and channel sinuosities similar to the Holden NE fan (Maizels, 1990).

The preferred water discharge for a sandy fan, $Q_w = 410$ m^3/s (table 7.2), is close to the value of 700 m^3/s proposed by Moore et al. (2003), who used empirical terrestrial relations between discharge and meander wavelength, channel width and drainage area. Our approach, however, takes advantage of the time-integrated deposit and thus allows estimation of time scales and sediment yields associated with construction of Holden NE fan. Unconstrained variables having the greatest influence on calculated discharges and fan formation time are grain size and channel depth. Calculations have been performed for reasonable ranges of these values (table 7.2). The analysis shows that Holden NE fan could have been constructed in decades to centuries, with a preferred minimum formation time of 50 years for medium sand. Calculated times, reported in terrestrial years, assume continuous flow at calculated discharge values, consistent with the minimum time formulation. If flow had a typical terrestrial intermittency value of 0.05 (Parker et al.,

1998), which means channel-forming flow conditions were present 5% of the time, fan formation times reported in table 7.2 would increase by a factor of 20.

If the deposit in Holden NE Crater is in fact an alluvial fan, the original structure must have occupied a large portion of the crater floor (Fig. 7.3). While there is no definitive evidence for a fan of such extent, there are indeed sedimentary deposits of similar morphology extending across the floor of Holden NE Crater (Fig. 7.2c). Inspection of the crater rim does not reveal any outlet through which water flowed, so inflowing water was either contained within the crater or infiltrated into the ground, as observed in some terrestrial desert environments (McCarthy et al., 1988). Estimates of water discharge and duration vary depending on choice of channel depth (table 7.2), but the total volume of water necessary to build the fan is only affected by grain size, which changes sediment discharge (eq. (1)) and hence fan formation time. We estimate this water volume to be 900 km^3 for sand, and 5000 km^3 for gravel. The absence of talus on exposed steep slopes suggests that the fan material is weakly lithified sand.

We present an internally consistent, quantitative method (Parker et al., 1998) showing that the observed fan could have been built in a rapidly aggrading riverine environment in less than 100 years. The modest estimated quantity of water necessary for alluvial fan construction does not require precipitation (e.g. Moore et al., 2003) if a local source of water was present. If the martian soil contained significant water ice, groundwater could have been delivered to the surface by heat generated from the impact formation (Jach et al., 1999) of nearby Holden Crater to the south. We are currently evaluating the adequacy of shock heating to deliver the fluid and sediment discharges required for fan formation.

Acknowledgements

Support for our research was provided in part by the STC Program of the National Science Foundation under Agreement Number EAR-0120914. We thank John Grotzinger for stimulating discussions that refined the focus of this work.

References

Aharonson, O., M.T. Zuber, D.H. Rothman, N. Schorghofer, and K.X. Whipple, Drainage basins and channel incision on Mars, *Proc. Nat. Acad. Sci.*, *99*(4), 1780-1783, 2002.

Christensen, P. R., et al., Morphology and composition of the surface of Mars: Mars Odyssey THEMIS results, *Science*, *300*, 2056– 2061, 2003.

Fukuoka, S., Finite amplitude development of alternate bars, in *River Meandering*, edited by S. Ikeda and G. Parker, pp. 237-265, AGU Water Resources Monograph 12, 1989.

Jach, K., et al., Modifications of martian ice-saturated regolith due to meteoroid impact, *Adv. Space. Res.*, *23*(11), 1933-1937, 1999.

Maizels, J., Long-term paleochannel evolution during episodic growth of an exhumed Plio-Pleistocene Alluvial Fan, Oman, in *Alluvial Fans: A Field Approach*, edited by A.H Rachocki and M. Church, pp. 271-304, Wiley, New York, 1990.

Malin, M.C. and K.S., Edgett, Evidence for persistent flow and aqueous sedimentation on early Mars, *Science*, *302*, 1931-1934, 2003.

Mars Channel Working Group, Channels and valleys on Mars, *Geol. Soc. Amer. Bull.*, *94*, 1035-1054, 1983.

McCarthy, T.S., et al., Incremental aggradation on the Okavango delta-fan, Botswana, *Geomorphology*, *1*, 267-278, 1988.

Mohrig, D., P.H. Heller, C. Paola, and W.J. Lyons, Interpreting avulsion process from ancient alluvial sequences: Guadalope-Matarranya system (northern Spain) and Wasatch Formation (western Colorado), *Geol. Soc. Amer. Bull.*, *112*(12), 1787-1803, 2000.

Moore, J.M., A.D. Howard, W.E. Dietrich., and P.M. Schenk, Martian layered fluvial deposits: implications for Noachian Climate Scenarios, *Geophys. Res. Lett.*, *30*(24), 2292, doi:10.1029/2003GL019002, 2003.

Paola, C., G. Parker, D.C. Mohrig, and K.X. Whipple, The influence of transport fluctuations on spatially averaged topography on a sandy, braided fluvial fan, in *Numerical Experiments in Stratigraphy:Recent Advances in Statigraphic and Sedimentologic Computer Simulations*, edited by J. Harbaugh, L. Watney, G. Rankey, R. Slingerland, R. Goldstein, and E. Franseen, *Spec. Publ. SEPM*, *62*, 211-218, 1999.

Paola, C., Quantitative models of sedimentary basin filling, *Sedimentology*, *47*, 121-178, 2000.

Parker, G., C. Paola, K.X. Whipple, and D. Mohrig, Alluvial fans formed by channelized fluvial and sheet flow. I: Theory, *J. Hydraul. Eng.*, *124*(10), 985-995, 1998.

Rannie, W.F., The Portage La Prairie 'Floodplain Fan', in *Alluvial Fans: A Field Approach*, edited by A.H Rachocki and M. Church, pp. 180-193, Wiley, New York, 1990.

Slingerland, R., and N.D. Smith, River avulsions and their deposits, *Ann. Rev. Earth Planet. Sci.*, *32*, 257–285, 2004.

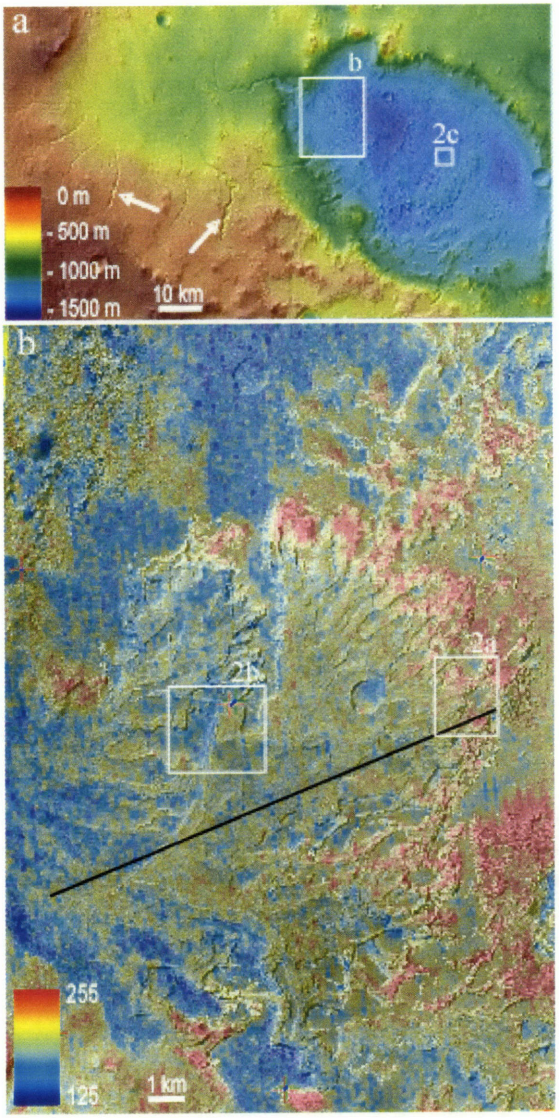

Figure 7.1. (Color) (a) Interpolated 500 m resolution MOLA topography draped on Themis daytime image mosaic (100 m/pixel, images I01737002, I01762002, I02461003, I03185002, I03210002, I03572002, I03597002, I04733002 and I04758002). White boxes indicate locations of other figures. Arrows point to large erosional channels. The mosaic is centered on 26°S, 34°W. (b) Themis night-time infrared image (100 m/pixel, image I04327002) superposed on MOC image mosaic (< 5 m/pixel, images M18-00020, E14-01039, E17-01341, E18-00401, E21-01153, E21-00454, E22-01159, E23-00003, R06-00726, R08-01104 and R09-01067). Night-time temperature (indicated in legend) is strongly correlated to exposure of outcrop, and so reflects degree of exhumation rather than compositional changes of the material from fan formation. Black line indicates location of profile shown in Fig. 7.3. North is up for all figures.

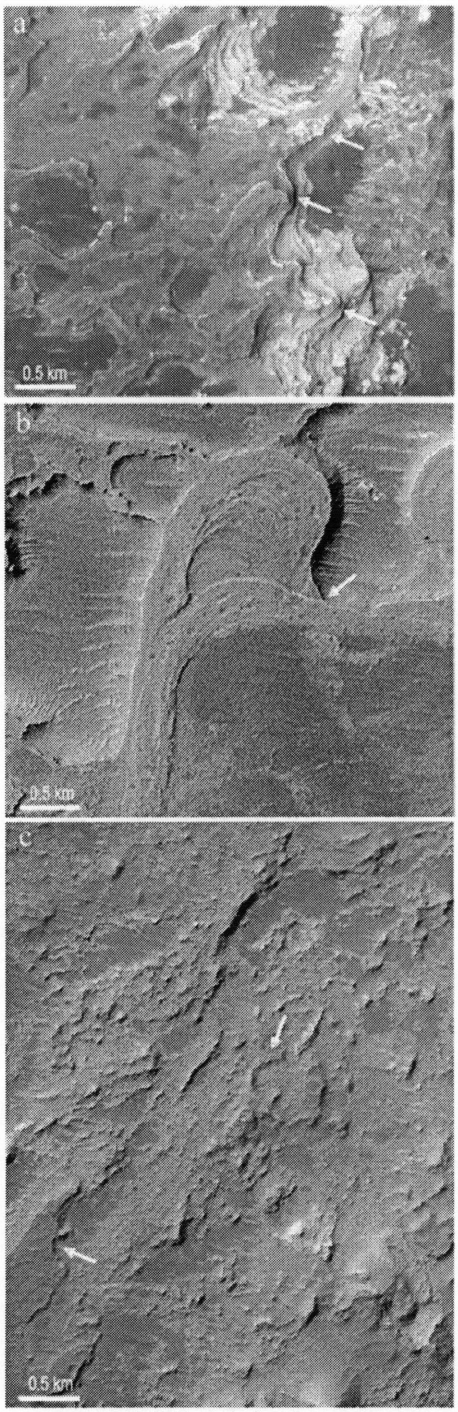

Figure 7.2. MOC sub-images of (a), distal end of the fan with resistant channel ridges corresponding to steep slopes, indicated by arrows (image E14-01039); (b), aggrading, migrating meander bend and a superposed avulsed channel denoted by arrow (image E18-00401); and (c), remnant sedimentary deposits (indicated by arrows), including stringer channels, found in the middle of Holden NE crater (image E20-01420) – see Fig. 7.1 for locations of all images.

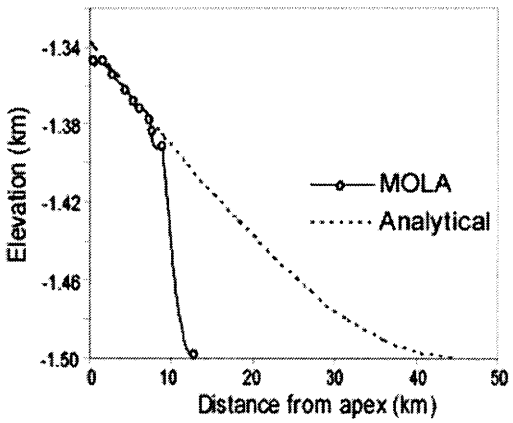

Figure 7.3. Interpolated MOLA longitudinal profile across Holden NE fan, with circles representing actual MOLA shots. Dotted line is the numerical solution of *Parker et al.* (1998) fit to the profile of the top fan surface. Location is shown in Fig. 7.1b.

Table 7.1. Characteristics of present and proposed pre-erosion Holden NE fan.

Fan	L (km)	R_{max} (km)	θ (°)	A (km^2)	V (km^3)	S (km/km)	K_{ave} (km/km)
Present	12.6	0.15	81	90	6	0.006	1.19
Proposed	45	~ 0.15	81	1400	30	~0.006	~ 1.19

R_{max}, A, and K_{ave} are maximum relief, fan area and average channel sinuosity (for channels longer than 1 km) – all other parameters defined in text. S is reported for top fan surface.

Table 7.2. Minimum, maximum and preferred discharges (units (m^3/s)), and the corresponding formation times (units (year)), associated with construction of Holden NE fan.

Parameter	Min. Q_w	Max. Q_w	Pref.
Q_w - sand	280	950	**410**
Q_s - sand	8.5	28	**12**
t_{eq} - sand	70	20	**50**
Q_w - gravel	240	790	340
Q_s - gravel	1.3	4.3	1.8
t_{eq} - gravel	480	140	340

Values of Q_w correspond to: Min. - $BS^{0.2}/H = 3$; Max - $BS^{0.2}/H = 10$; Pref. - $BS^{0.2}/H = 7$.

Chapter 8

Conclusions

In the Introduction, I posed two questions to be addressed in the body of work presented here: (1) which physical processes are most important in determining pattern at a certain scale?; and (2) how are patterns at one scale coupled (or not) to patterns at larger and smaller scales? Question 1 has been answered in part for sandy river systems by modeling the evolution of patterns at several specific scales: at the smallest scale of bed roughness on river bottoms (Chapters 2-4), at the intermediate scale of channel planform geometry and the causes and consequences of river avulsions (Chapters 5 and 6), and at the largest scale of depositional fans constructed by channels on Mars (Chapter 7). Question 2 has also been partially answered, if indirectly. To the extent that we are able to explicitly model the behavior of large-scale patterns, such as deltas, with little or no information about the smaller-scale dynamics, such as channel behavior, it appears that patterns at different scales may be dynamically decoupled (e.g., Werner, 1999). Evidence for this decoupling of scales was presented in Chapter 6 where I showed that dramatic spatial variations in river planform geometry had little effect on the routing of fluid and sediment through the lower Niobrara River.

To make the relationships among scales more concrete, we return to the example of the lower Mississippi River introduced in Chapter 1. Figure 8.1 illustrates the patterns of interest, from smallest to largest scale. The formation of sand dunes on the bottom of

the Mississippi may be understood as a consequence of the local fluid and sediment transport processes. While the detailed fluid flow structure undoubtedly influences sediment transport (e.g., Nelson et al., 1995), I have demonstrated that it is not necessary to explicitly model the flow field in order to understand the emergence of bedforms (Chapter 3). River dunes are generally limited in amplitude by water depth, a parameter that is determined by processes at larger scales. Hence, it is possible to model the dynamics of bedforms by parameterizing the smaller-scale processes of fluid transport, while the channel size acts as a boundary condition. At the scale of planform pattern, the lower Mississippi exhibits several distributary channels formed by avulsions. In modeling the spatially-averaged sediment transport at this scale, bedforms do not need to be explicitly considered. Their main effect is flow resistance, and to first order the complex evolution of bedforms may be collapsed to a constant friction factor (Chapters 5 and 6). Channel geometry is determined by a combination of time- and space-averaged flow and sediment transport conditions. In particular, the formation of multiple channels depends on the time-averaged dynamical quantities of bank erosion rate and channel deposition rate (Chapter 5), of which the latter depends strongly on the boundary condition of base level (e.g., relative sea level for deltas). At the scale of the Mississippi Delta, the overall system slope and extent may be understood without detailed knowledge of channel dynamics. At long times, sedimentation on the delta is driven by the downstream boundary condition of relative sea-level rise. The width-averaged delta profile may be modeled using a diffusive transport model (Parker et al., 1998) that averages over many river avulsion events (Chapter 7).

Modeling the evolution of river channel patterns using detailed calculations of instantaneous fluid and sediment transport may be effective for short-range prediction of channel adjustment. Extending these simulations to longer timescales, however, is not trivial because the governing equations are nonlinear and errors associated with inevitable parameterizations attenuate as we consider longer durations and larger spatial domains (e.g., Murray, 2003). For instance, sediment flux in a sandy river may not be strongly coupled to the distribution of bed stresses (Chapter 6), such that even detailed knowledge of fluid flow is not sufficient to accurately model sediment transport. In problems of a geological nature, we are concerned with the evolution of patterns over time periods in which boundary conditions themselves may be highly dynamic. The challenge and enjoyment then derives from finding compact descriptions of pattern formation that are flexible and provide fundamental physical insight, albeit at the expense of accuracy (and occasionally rigor). In this thesis I have used very simple mathematical modeling to describe the behavior of the sediment-fluid interface of sandy rivers over a large range of scales. Such simplifications are often possible when pattern formation is robust, and become necessary to model phenomena over time and space scales relevant to river management and landscape evolution.

Whether or not we can explicitly segregate patterns at different scales depends, of course, on the nature of the question being asked. Sun et al. (2002) demonstrated a model that reproduces the dynamics of channel avulsion in a depositional basin, and showed that the width-averaged elevation profile of the fan constructed by these channels asymptotically approached the profile produced from a diffusive transport model. Other aspects of this fan, however – notably surface and shoreline roughness – were quite

different from the diffusive model. While capturing the spatial and temporal variability of roughness is not necessary to model the long profile of a delta, it becomes important to understand this variability when interpreting the stratigraphic record. Errors associated with a simplified model of river evolution may average out for the instantaneous surface morphology, but they accumulate in the preserved record of these surfaces. The history of these stacked, rough surfaces may in fact be dominated by the variability of topography rather than the mean (Chapter 4; Lyons, 2004; Pelletier and Turcotte, 1997). At present, our ability to resolve climate signals in sedimentary deposits is limited by our understanding of the internal variability generated by depositional mechanics even in steady flows, such as bedforms and river avulsions. Characterizing the internal dynamics of sedimentary systems has been one goal of the present work. Incorporating this variability into long-term models of basin filling, while maintaining the simplicity in approach presented in this thesis, is a challenge that will be taken up in future work.

References

Lyons, W.J., 2004, Quantifying channelized submarine depositional systems from bed to basin scale (Ph. D. thesis): Massachusetts Institute of Technology, 252 p.

Murray, A.B., 2003, Contrasting the goals, strategies, and predictions associated with simplified numerical models and detailed simulations. In: Wilcock, P.R., and Iverson, R.M., *Prediction in Geomorphology*: Geophysical Monograph 135. American Geophysical Union, 151-168.

Nelson, J.M, R.L. Shreve, S.R. McLean and T.G. Drake, 1995, Role of near-bed turbulence structure in bed load transport and bed form mechanics: *Water Resources Res., 31*(8), 2071-2086.

Parker, G., C. Paola, K.X. Whipple, and D. Mohrig, 1998, Alluvial fans formed by channelized fluvial and sheet flow. I: Theory: *J. Hydraul. Eng., 124*(10), 985-995.

Pelletier, J. D., and Turcotte, D. L., 1997, Synthetic stratigraphy with a stochastic diffusion model of fluvial sedimentation, *J. Sedimentary Res., 67*, 1060-1067.

Sun, T., C. Paola, G. Parker, and P. Meakin, 2002, Fluvial fan deltas: Linking channel processes with large-scale morphodynamics: *Water Resources Res., 38*(8), 1151, 10.1029/2001WR000284.

Werner, B.T., Complexity in natural landform patterns, *Science, 284*, 102-104, 1999.

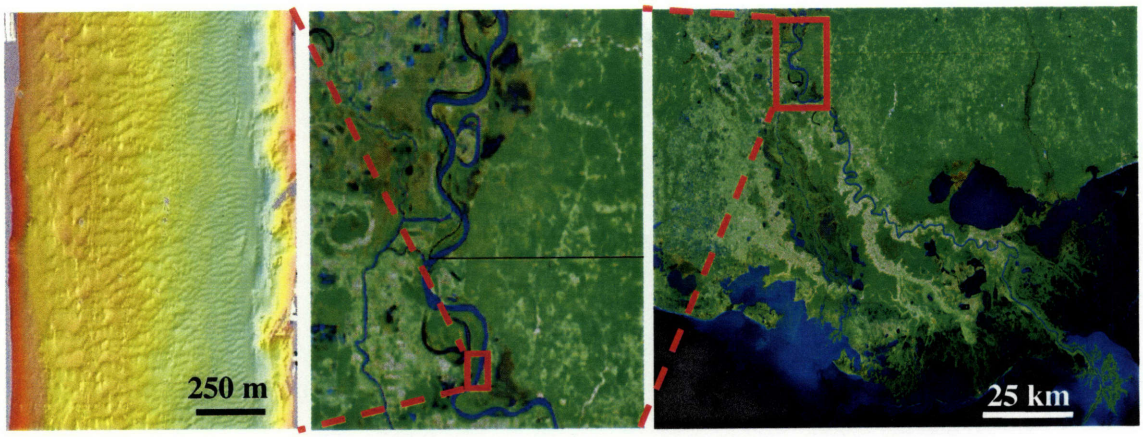

Figure 8.1. (Color) Depositional patterns on the lower Mississippi River, from dunes (left) to distributary channels (center) to the entire delta (right).